DESIGN AND CHARACTERIZATION OF AXIAL-LIGAND MUTANTS OF OUTER MITOCHONDRIAL CYTOCHROME b_5 WITH HIGHLY EFFICIENT HEME OXYGENATION ACTIVITY

By

JUAN CARLOS RODRIGUEZ-QUINTERO

Bachelor of Science

Universidad Autonoma de Guadalajara

Guadalajara, Mexico

1990

Submitted to the Faculty of the
Graduate College of the
Oklahoma State University
in partial fulfillment of
the requirements for
the Degree of
DOCTOR OF PHILOSOPHY
December, 1999

ACKNOWLEDGMENTS

I wish to express my gratitude to all those who, with work, advise, or words of encouragement, have made an important and invaluable contribution to this dissertation.

My most sincere appreciation goes to Dr. Tetsuya Ogura, whose wisdom and unselfish advice has influenced my life in so many ways, and inspires my most profound admiration.

I would like to thank my parents, Jose Rodriguez and Esther Quintero, and my brothers, Fernando and Jorge, for their unconditional support and continuous encouragement. Even in the most difficult days, they have always been there for me.

Finally, I would like to thank my graduate adviser, Dr. Mario Rivera, the Department of Chemistry, and the Phillips Petroleum Fellowship for financial support throughout these years of postgraduate education.

TABLE OF CONTENTS

Chapter Page

Chapter Page

LIST OF TABLES

Table Page

Chapter I

Chapter III

LIST OF FIGURES

Figure Page

Chapter I

Chapter II

Figure Page

Figure Page

Chapter III

LIST OF SYMBOLS AND ABBREVIATIONS

Ala	Alanine
ALA	δ-Amino levulinic acid
a.m.u.	Atomic mass units
Arg	Arginine
Asp	Aspartic acid
Cys	Cysteine
DMF	Dimethyl formamide
ϵ	Extinction coefficient
E°	Standard reduction potential
EDTA	Ethylenediamine-tetraacetic acid
EPR	Electron paramagnetic resonance
ESI	Electrospray ionization
GC	Gas chromatography
His	Histidine
HMQC	Heteronuclear correlation multiple quantum coherence
HO	Heme oxygenase
HPLC	High performance liquid chromatography
IPTG	Isopropyl-β-thiogalactoside
J	Coupling constant
KHz	Kilohertz
μ	ionic strength

Met	Methionine
MHz	Megahertz
MOPS	3-[N-Morpholino]propane sulfonic acid
MS	Mass spectrometry
mW	Miliwatts
MW	Molecular weight
MWCO	Molecular weight cutoff
m/z	mass to charge ratio
NADPH	Nicotinamide adenine dinucleotide phospate
NHE	Normal hydrogen electrode
NMR	Nuclear magnetic resonance
NOESY	Nuclear Overhauser effect spectroscopy
OD	Optical density
OM	Outer mitochondrial membrane
Ox	Oxidized
ppm	Parts per million
Red	Reduced
rpm	revolutions per minute
Ser	Serine
SPME	Solid phase micro extraction
Thr	Threonine
TRIS	Tris-hydroxymethyl aminomethane
UV-Vis	Ultraviolet-visible
Val	Valine
WT	Wild-type

CHAPTER I

INTRODUCTION

Iron-protoporphyrin IX (heme) (Fig 1) is ubiquitous in nature, and constitutes the prosthetic group of numerous proteins of high biological significance. The wide variety of reactions supported by heme-containing proteins underscores the great versatility exhibited by the heme molecule. For example, heme proteins carry out functions such as oxygen transport (e.g. hemoglobin), electron transfer (e.g. cytochrome b_5), catalysis of redox reactions (e.g. cytochrome P450, oxygenases), etc. Interestingly, despite the differences in the chemistry they support, all of these proteins have heme as their prosthetic group. Therefore, it is evident that their different functions stem from specific interactions between the heme and the polypeptide [1].

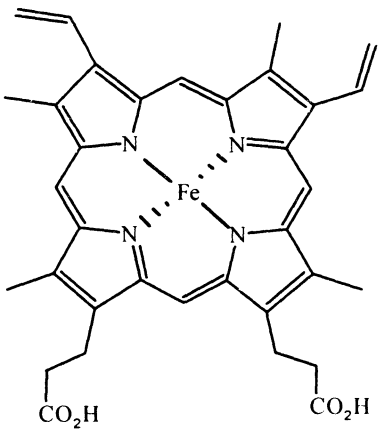

Figure 1. Structure of iron-protoporphyrin IX (Heme).

The prosthetic group in heme proteins is embodied within a cavity composed of amino acid residues in the polypeptide backbone. For a given hemoprotein, this cavity possesses unique structural elements that to a large extent determine the function and properties of the protein. The central metal atom, iron, is coordinated to the pyrrole nitrogens of the heme macrocycle forming a complex with square planar geometry. In hexacoordinated heme proteins, the inner coordination sphere of the metal center is typically completed by ligands that originate from protein amino acid side chains (endogenous ligands), and/or by small ligands that do not belong to the protein (exogenous) (Table I). Despite the presence of potential ligands such as water in the heme crevice, the sixth coordination site of a few heme proteins can remain vacant, thus producing pentacoordinated heme proteins.

Protein function is also correlated to the nature of the axial ligands. Heme in electron-transfer proteins typically possesses two strongly coordinated axial ligands bound to iron, and generally these proteins do not bind exogenous ligands. In contrast, the heme in oxygen transport enzymes has the sixth coordination site (distal site) accessible for coordination by an exogenous sixth ligand (Fig 2). In fact, the accessibility to the sixth coordination site constitutes a fundamental structural difference between proteins that function exclusively as electron-transport proteins and those that may carry out reactions with substrates.

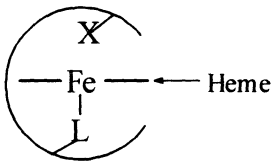

Figure 2. Schematic representation of the structural arrangement of axial ligands in proteins possessing an accessible sixth coordination site. L and X represent the proximal and distal ligands, respectively. The semicircle represents the protein backbone.

Table I. Examples of coordinating groups in endogenous and exogenous ligands.

Endogenous Ligands

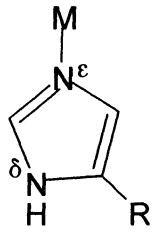

Imidazolyl
e.g. His

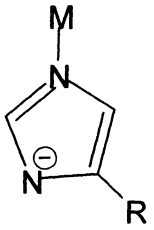

Imidazolate
e.g. His

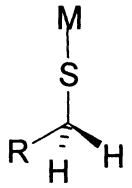

Thiolate
e.g. Cys

Thioether
e.g. Met

Exogenous Ligands

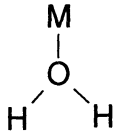

Aquo

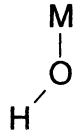

Hydroxo

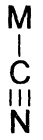

Cyano

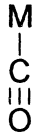

Carbonmonoxy

i). Brief History and General Aspects of Cytochrome b_5

In the 1880s MacMunn discovered spectroscopically that a wide range of tissues posses hemes, which in the reduced state have characteristic visible absorption spectra that disappear when the hemes are oxidized [2]. Years later he proposed a respiratory function for the pigments and named them "histohematins". Work in this area remained unexplored until 1925 when Keilin introduced the name cytochromes. Keilin classified the cytochromes into three main categories (a, b, and c) according to the different rates at which the bands in the absorption spectrum appeared and disappeared [2]. It was eventually proved that there are more than three different types of cytochromes and that they are respiratory enzymes acting as electron carriers between other proteins and oxygen. At present it is known that the cytochromes constitute a diverse group of proteins found in nearly all forms of life, including bacteria, protozoa, yeasts and all higher organisms, and that most cytochromes are involved in energy transduction to produce ATP from the oxidation of metabolites or by photosynthesis.

The first b-type cytochrome to be well characterized is the microsomal cytochrome b_5, which is functionally quite distinct from the mitochondrial cytochrome b_5. Microsomal cytochrome b_5 is located in the smooth endoplasmic reticulum of liver cells of a variety of mammals and avian species. The native protein is a monomer of 15 kDa, and is essential in a variety of electron-transfer reactions related to fatty acid desaturation. The polypeptide chain is folded into two domains of unequal size. The larger domain, hydrophilic in nature, contains the heme group and extends into the aqueous environment of the cellular cytoplasm. The smaller domain is hydrophobic in nature and is used to anchor the protein to the microsomal membrane. The heme-containing fragment can be solubilized by treatment of microsomes with proteases. By

comparison, mitochondrial cytochrome b_5 is of similar size to its microsomal counterpart, and is composed of a hydrophobic and a hydrophilic heme-containing domain. The water-soluble domain of this enzyme has been isolated from the outer mitochondrial membrane (OM) of rat liver hepatocytes by proteolytic cleavage and by detergent solubilization. The amino acid sequence of the water-soluble fragment of rat outer mitochondrial membrane cytochrome b_5 is approximately 58% homologous to its microsomal counterpart. This high degree of sequence homology between the microsomal and outer mitochondrial membrane proteins is consistent with the fact that their three-dimensional structures are very similar [3]. Although the function of mitochondrial cytochrome b_5 is still uncertain [5], OM cytochrome b_5 has been shown to have NADH-cytochrome c reductase activity, which is insensitive to rotenone and therefore it is not part of the oxidative phosphorylation electron transport chain [3, 5]. Such activity involves a pathway in which the electrons flow from NADH to NADH cytochrome b_5 reductase, which in turn reduces cytochrome b_5 in the outer mitochondrial membrane. OM cytochrome b_5 subsequently reduces cytochrome c, which shuttles the electron across the intermembrane space in order to reduce cytochrome c oxidase in the inner mitochondrial membrane.

Modulation of Function by Protein Structural Motifs

i). Electron Transfer Heme Proteins

The reduction potential of cytochromes provides the driving force necessary for electron-transfer processes. The modulation of the reduction potential of a particular cytochrome is one of the major functional roles carried out by the polypeptide moiety and

is important for regulation of electron flow among physiological redox partners [4]. There are three relatively independent, additive factors which govern the reduction potential of the heme group: (a) the nature of the axial ligation to the heme-iron, (b) the inductive effect of the peripheral heme group substituents, and (c) the effects of the protein heme environment [4]. The quantitative measurement of the contribution of each of these factors is associated with the intrinsic difficulty of designing reliable experiments aimed at measuring the contribution of one factor while holding the others constant.

One approach to this problem has been to study the effect of each factor individually by using model compounds. From such experiments it has been possible to examine the effect of substituting one of the axial ligands in a hexacoordinated heme complex. For example, it has been found that the net effect of replacing one imidazole ligand by methionine is to raise the redox potential of the parent bis-imidazole coordinated molecule. The observed effect has been attributed to the electron-withdrawing power of the methionine thioether relative to the strong donor power of the histidine imidazole ring [5]. Withdrawal of electron density from the heme iron destabilizes the positive charge in ferric heme, thus favoring the ferrous heme species. In the absence of other contributing factors, a general trend of redox potentials can be expected for heme proteins according to the electron withdrawing and electron donor capabilities of their axial ligands.

Cytochromes exhibit two modes of attachment of the heme to the polypeptide. The heme in cytochrome c, for example, is covalently bound to the polypeptide via thioether linkages between the heme vinyl groups and cysteine side chains [6]. By comparison, the heme in cytochrome b_5 conserves the unsaturated vinyl groups while its heme is held by the polypeptide through bis-histidine axial coordination bonds. The

individual contribution of the heme substituents to the reduction potential has been probed by replacing the vinyl groups for ethyl side chains in model compounds. The overall contribution of this factor, however, appears to be small in relation to other effects [5].

The effect of histidine as axial ligand in electron transfer heme proteins was discussed previously. The presence of this amino acid, however, may affect the reduction potential in various ways. For example, histidine coordinates to the heme-iron via the N^{ε}-atom of its imidazole side chain (see Table I). Since the N^{δ}-atom is normally protonated, histidine may interact with neighboring amino acids via hydrogen bonding. In fact, hydrogen bonds of this sort were found to be responsible for the shifts to more negative potentials observed when the reduction potential of a heme derivative was measured in the presence of imidazole and 1,10-phenantrolene [7]. This effect has been attributed to the increased anionic character of the imidazole ring, which brings about a decreased positive charge on the ferric heme, thus causing destabilization of the reduced form [6].

The third factor determining the reduction potential of cytochromes involves the degree of solvent exposure, the polarity of the heme pocket, and the nature and distribution of charged groups about the heme as well as other perturbations of electric field surrounding the heme group [6, 8-15]. Participation of these factors in changes of the reduction potential of heme proteins have been traditionally examined by performing point mutations of recombinant heme proteins and determining the effects by measuring their reduction potentials [16-20]. In a recent related study [20], the exposed heme edge of mitochondrial cytochrome b_5 was found to play an active role in modulating the reduction potential. The results of this investigation indicated that the neutralization of

the charge on one of the heme propionates, combined with the exclusion of water from the heme crevice, are important contributors to the anodic shifts observed when the reduction potential is measured in the presence of polylysine [20]. The conclusions drawn from this study serve to illustrate that a wide variety of different factors may operate under different circumstances; consequently, no single factor is always dominant. Nevertheless, it is highly desirable to understand, at a fundamental level, how these factors modulate the reduction potential of heme containing proteins.

ii). Oxygen Binding Heme Proteins

Dioxygen (O_2) serves two essential functions in aerobic life; it is both a terminal electron acceptor and a biosynthetic reagent. Heme proteins that have an accessible coordination site play an active role in the biological chemistry of this molecule. The function of these proteins varies from case to case depending on the nature of the axial ligands and the heme environment. Heme proteins that require molecular oxygen to perform their normal function may be classified into two main categories. (1) Proteins that reversibly bind dioxygen and preserve the integrity of the O_2 molecule and (2) proteins that bind dioxygen and utilize it in reactions with substrates by facilitating oxygen-oxygen bond cleavage of the O_2 molecule. The ubiquitous involvement of heme proteins in the preservation and cleavage of the oxygen-oxygen bond highlights the significance of the role played by the polypeptide moiety in modulating protein function. Such exquisite control of the protein heme environment over the reactivity is superbly illustrated by considering the fact that, with the exception of the cysteine-ligated cytochrome P450 enzymes, all proteins that react with O_2 possess histidine as a proximal

ligand.

The species typically produced in the general reaction of dioxygen with heme proteins are shown schematically in Fig 3. The reversible binding of molecular oxygen and the formation of reactive oxygen species in the heme microenvironment are initiated by the one-electron reduction of ferric heme to produce its ferrous counterpart (Reaction 1, Fig 3). This step is followed by the binding of O_2 to the ferrous heme, thus producing the six-coordinate Fe^{2+}-O_2 complex. Further differentiation into the reactions depicted in Fig 3 distinguishes the two types of reactivity, and is under the strong influence of the protein environment.

a). Reaction of O_2 with Myoglobin. The physiological function of myoglobin is that of storing oxygen in the muscles until it is required for metabolic action. The reaction between myoglobin and O_2 is reversible and occurs exclusively when its heme-iron is present in the reduced state (i.e. Fe^{2+}). It is interesting that O_2 and Fe^{2+} are able to coexist despite the fact that the oxidation of the metal by the coordinated dioxygen molecule is thermodynamically favorable. A series of studies involving recombinant DNA methodology [19, 21, 22], X-ray crystallography [21], and electrochemical [19, 23] techniques have provided information that allows one to explain how the three dimensional arrangement of atoms in the heme environment overcomes the potentially disastrous oxidation of the ferrous heme by O_2. Data obtained from X-ray crystallographic, and site directed mutagenesis experiments have clearly established the role of the distal His64 residue in assisting the binding of O_2 to Fe^{2+} by forming a hydrogen bond to the protonated N^{δ}-atom of its imidazole ring. In addition, electrochemical studies of wild-type and myoglobin mutants have provided conclusive

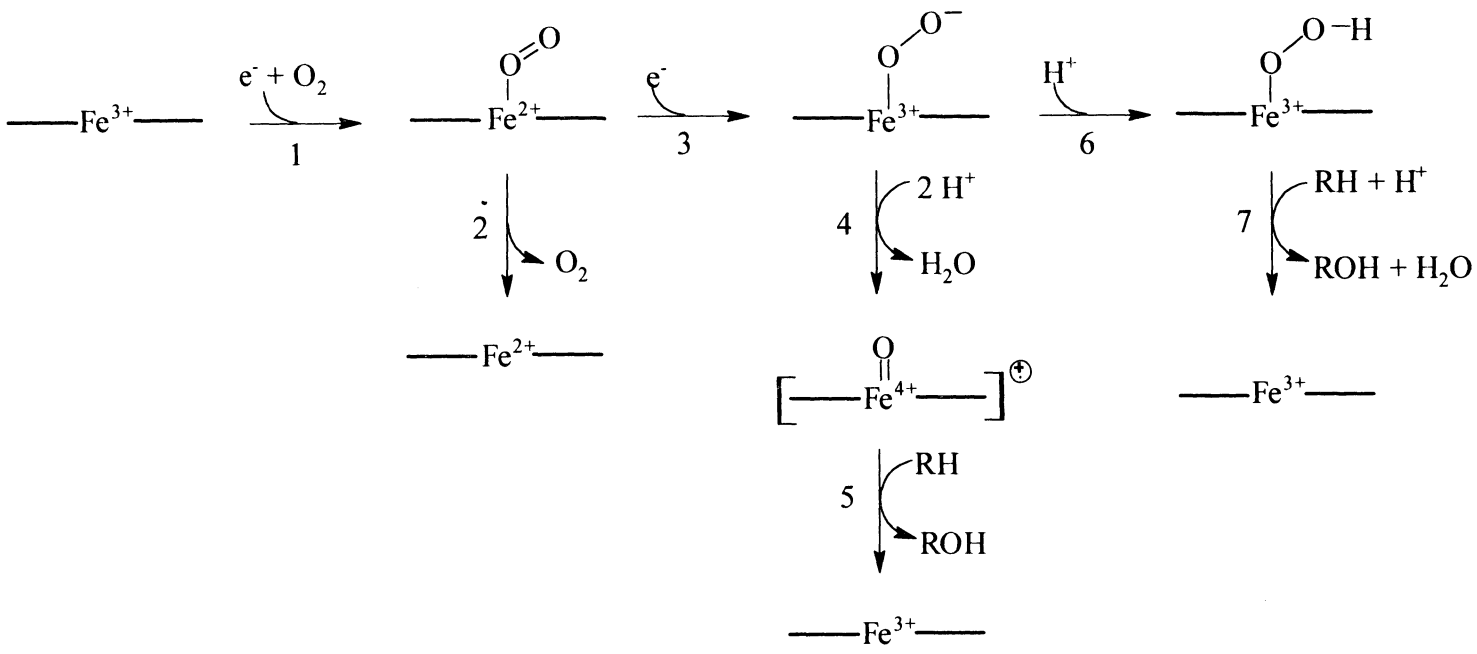

Figure 3. Species produced during the general reaction between heme proteins, O_2, and two reducing equivalents.

evidence that demonstrates that the stability of the ferrous heme in the presence of O_2 is the result of slow kinetics of oxidation. Such kinetic barrier results from the reorganization of structured water in the heme crevice of myoglobin [11, 13, 19]. In summary, the stability of the ferrous heme is accomplished by kinetic control of the oxidation reaction. This kinetic control, in turn, results from the structural properties of the heme environment.

The body of experimental evidence just described is consistent with the ability of myoglobin to carry out the reversible O_2 binding process. A more profound analysis of spectroscopic data, however, indicates that electron-transfer in the Fe^{2+}-O_2 complex is not completely abolished. Early work on the magnetic properties of myoglobin has shown that oxymyoglobin is diamagnetic, result that contradicts the expected paramagnetic properties of a complex formed with triplet dioxygen [24]. This finding indicated that the oxygen molecule undergoes a change of its electronic structure upon binding to the protein [25]. To account for the diamagnetic characteristics of oxymyoglobin, the following possibilities can be envisioned: (a) Singlet (diamagnetic) O_2 is coordinated to a low-spin Fe^{2+} species (diamagnetic), (b) The complex exists as a Fe^{3+}-$O_2\cdot$ species in which the two S = 1/2 entities (Fe^{3+} and $:O_2\cdot$) are antiferromagnetically coupled (*i.e.* interacting with antiparallel spins) [26]. Magnetic moment measurements of model compounds seem to support the latter picture [26]. The manner in which dioxygen is bound to myoglobin (and hemoglobin) is of considerable interest in light of the applicability of the reversible binding of dioxygen in the production of blood substitutes.

b). Reaction of O_2 with Heme-containing Oxygenases. Oxygenases are enzymes that incorporate oxygen atoms from dioxygen into organic substrates. Although the name

"oxygenases" applies to non-heme enzymes as well, the term "oxygenases" will be used here only in reference to those that possess heme as prosthetic group. The oxygenases can be classified into two categories, monooxygenases and dioxygenases, depending on whether one or both oxygen atoms are incorporated into the substrate. In view of their relevance to the present subject, the discussions included here will deal exclusively with monooxygenases.

The general reaction that describes the function of the monoxygenases is shown schematically in Fig 3. Akin to myoglobin, the monooxygenases go through the Fe^{2+}-O_2 complex as a key intermediate of the reaction (Reaction 2, Fig 3). The latter, however, requires the input of a second electron for continuation of the catalytic cycle (Reaction 3, Fig 3). The nature of the protein oxo-complex in these proteins is still a matter of debate (see above) [27], however, the proven existence of a ferric peroxo complex as catalytic intermediate in several reactions of heme proteins argues in favor of the Fe^{3+}-O_2· species [28]. The sequence of events leading to the formation of the ferric peroxo complex may occur as follows. (1) An electron is donated to the heme protein to produce the ferrous species. (2) Dioxygen binds to ferrous iron and an electron is transferred in intramolecular fashion from Fe^{2+} to the bound O_2 to yield the ferric-superoxo (Fe^{3+}-O_2·) intermediate. (3) Finally, a second electron is donated to this intermediate, thus producing the ferric peroxo (Fe^{3+}-O_2^{-}) species. It is interesting that, in a few cases, the catalytic reaction may be initiated by substituting reducing equivalents and dioxygen for the direct addition of H_2O_2 or other peroxides to the ferric protein [28].

Studies of the catalytic mechanisms of heme proteins that employ either oxygen or H_2O_2 (e.g. peroxidases) as a cosubstrate have provided evidence for two types of oxygen reactivity. The most common mode of operation involves the oxidative

intermediate ferryl species ($O=Fe^{4+}$), which has been observed spectroscopically in reactions catalyzed by cytochrome P450 and the peroxidases [30, 31]. A less common reactive species is the ferric peroxo anion ($^{-}OO-Fe^{3+}$), or alternatively, its protonated form, the hydroperoxo species ($HOO-Fe^{3+}$) [32], which is presumably the active oxygen species in the reaction catalyzed by the enzyme heme oxygenase [32-34].

As already emphasized previously, the various mechanisms through which heme proteins accomplish their oxygenation reactions are testament to the versatility of the heme group, and a direct consequence of the control exercised by the polypeptide moiety. Cytochrome P450 and the peroxidases share the common ability of catalyzing the heterolytic O-O bond cleavage with formation of the ferryl intermediate. Nevertheless, cytochrome P450 is cysteine ligated (see Table I), whereas the peroxidases have histidine as axial ligand (See Table I). X-ray crystallographic and sprectroscopic studies of cytochrome P450cam and cytochrome c peroxidase has provided important structural information that accounts for their similar activity in spite of their having different heme environments.

The mechanistically relevant amino acid side chains in the heme pocket of cytochrome P450 and cytochrome c peroxidase are shown schematically in Fig 4. For cytochrome c peroxidase a "push-pull" mechanism has been proposed to account for the O-O bond cleavage upon formation of the ferric-peroxo complex [28]. The "push" is provided by the proximal histidine ligand whose electron donor capability is enhanced via hydrogen bonding to a neighboring carboxylate group, thereby increasing its imidazolate character relative to the corresponding non-hydrogen-bonded histidine in myoglobin and heme oxygenase (see below). At the same time, the distal histidine accepts a proton, and an appropriately positioned protonated arginine donates a proton,

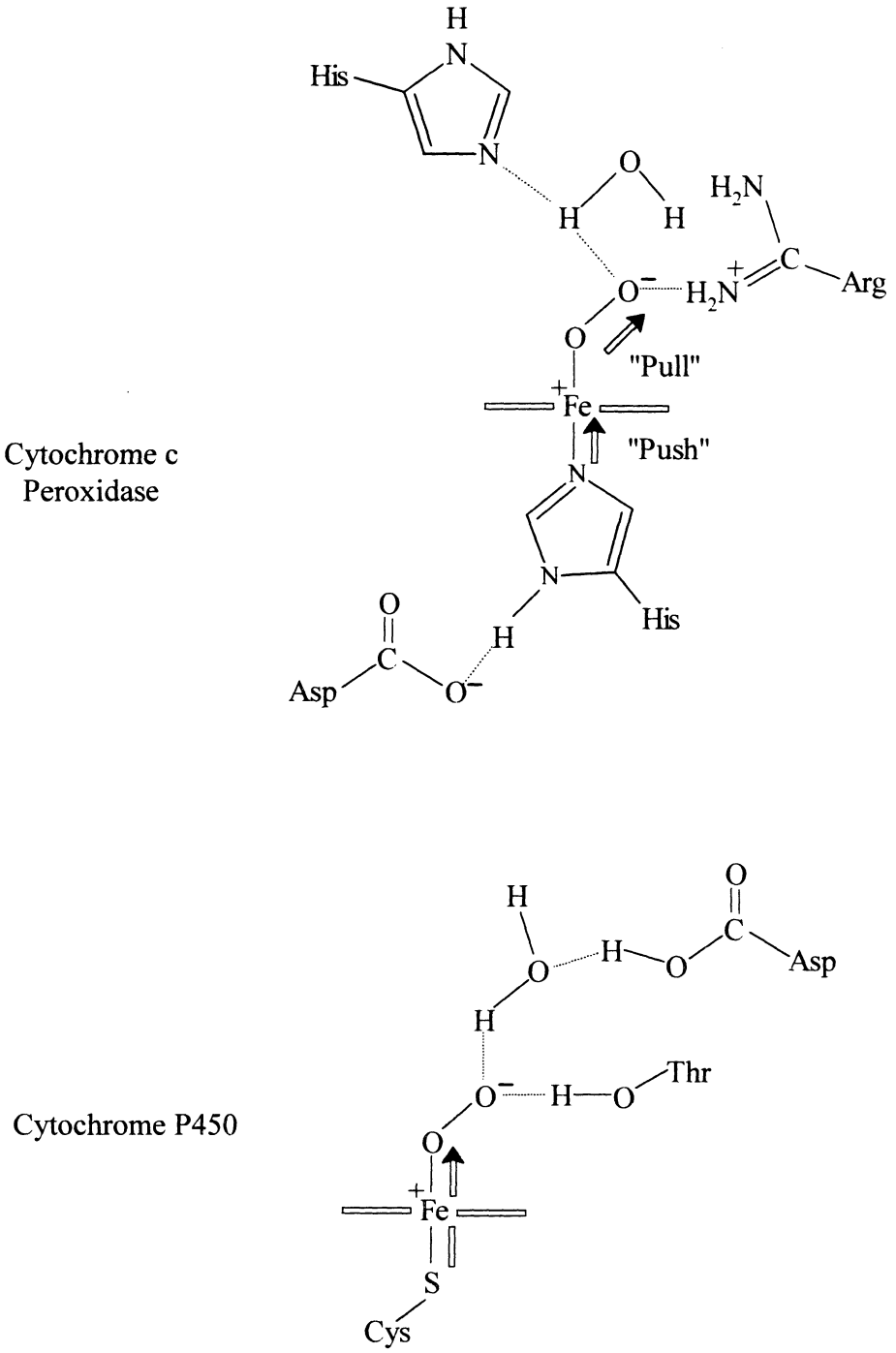

Figure 4. Schematic representation of the role of amino acid residues on the catalytic mechanism of histidine- (cytochrome c peroxidase) and thiolate-ligated (cytochrome P450) systems. Adapted from reference 26.

which weakens the O-O bond due to hydrogen bonding to the bound peroxo species (Fig 4). The combined participation of the distal histidine and arginine provides the "pull" effect.

On the other hand, the O-O bond cleavage catalyzed by cytochrome P450 likely follows a different mechanistic pathway. Since the heme crevice in cytochrome P450 lacks the spatial distribution of amino acids in the distal side present in cytochrome c peroxidase, the heterolytic bond cleavage of dioxygen has been proposed to be mainly facilitated by the strong electron-releasing character of the proximal thiolate ligand [28]. Several lines of evidence have been reported that support the idea of the "big push" (strong electron-releasing character) of the proximal cysteinate ligand. For example, amino acid residues located in the distal side of the pocket in thiolate ligated myoglobin mutants show enhanced basicity relative to the parent molecule. In addition, significant differences have been reported for the affinities of anionic ligands to ferricytochrome P450 and myoglobin, with anionic ligands having much lower affinity for cytochrome P450, presumably due to the electron-releasing character of the proximal thiolate ligand [28].

During the monooxygenation of organic compounds, one of the oxygen atoms is incorporated into the substrate while the other is released as a water molecule (Reactions 4 and 7, Fig 3). Undoubtedly, the formation of water upon reduction of dioxygen requires the presence of hydrogen ion sources in the distal pocket of the oxygenases. As a consequence, the strong electron-releasing character of the cysteinate proximal ligand cannot, by itself, accomplish the O-O bond cleavage. Sligar et al. proposed that the presence of two distal side amino acids in P450cam (Thr-252 and Asp-251) carries out the proton donation (Fig 4) [35]. Ishimura and coworkers, on the other hand, have

claimed that the role of Thr-252 in cytochrome P450cam is that of positioning a water molecule in close proximity to the iron-bound peroxo group, rather than serving as a direct proton donor [36]. To date, the true role of the amino acids in the distal pocket of cytochrome P450cam has not been yet clarified, however, it is quite certain that they do not provide the "pull" effect described for the peroxidases.

Heme oxygenase catalyzes the regioespecific ring cleavage of the heme macrocycle to produce biliverdin [37, 38]. The enzyme exists in its native state as a polypeptide devoid of heme, which justifies that the protein is not considered a heme protein *per se*. However, the apopeptide is readily reconstituted with heme to form a stable 1:1 complex, which displays spectroscopic characteristics similar to those of myoglobin. The heme in heme oxygenase is coordinated by a histidine and a water molecule [39-42]. It has already been established that the catalytic turnover of heme oxygenase requires the presence of O_2 and reducing equivalents provided by NADPH-cytochrome P450 reductase. Furthermore, it is also known that the reaction proceeds via the formation of a ferric peroxo intermediate, without producing the ferryl ($O=Fe^{4+}$) species observed in oxygenases and peroxidases [33].

The fact that heme oxygenase does not require formation of the ferryl intermediate to perform the monooxygenation reaction is highly unusual and unique. As mentioned above, the formation of a ferric peroxo intermediate in most monooxygenases is followed by the formation of ferryl species. This process is facilitated by the presence of a proximal ligand with strong electron-releasing capability, or by the synergistic contribution of a histidinate ligand ("push") and hydrogen bonds in the distal side of the pocket ("pull"). Heme oxygenase, on the other hand, is coordinated by a neutral histidine [39, 42], thus biasing against the formation of the ferryl intermediate.

Rationale and Purpose of the Studies

The ultimate investigative goal of any biological process is the understanding of function as an inseparable consequence of molecular structure. One need only consider the examples given above to recognize that the modulation of protein function is most likely conceived at the molecular level. Furthermore, inasmuch as the presence of the heme prosthetic group is common to the heme proteins, one must ponder the achievement of high levels of function refinement as a result of a continuous evolutionary process. Thus, nature has created propitious environments around the heme group by taking advantage of intrinsic physical and chemical properties of amino acids, likely with the sole purpose of achieving function optimization. The advent of recombinant DNA methodologies has provided researchers with convenient tools to redesign those heme environments created and optimized by nature. For example, conversion of electron-transfer proteins into oxygen-activating species, and *viceversa*, has been attempted with the purpose of deciphering the individual and collective role of amino acid residues in determining function [16, 43-49]. To date, however, only mutants that exhibit novel properties, albeit with poor reaction efficiencies, have been obtained.

Investigating the effects that structural elements have on both, the protein function and the properties of heme proteins, requires the application of experimental methods that allow for the structure of the protein under study to be modified, while their altered properties are scrutinized through the use of the appropriate analytical techniques. Along these lines, a strategy has been design to convert mitochondrial cytochrome b_5 into a species that exhibits oxygen-activating capabilities. Chapters II and III of the present dissertation describe the detailed characterization of a novel function and spectroscopic

properties exhibited by mutants of mitochondrial cytochrome b_5 produced upon replacement of one of the axial ligands. The conversion of cytochrome b_5 into a mutant displaying oxygen-activating properties is the first example of a mutation that confers "efficient" new reactivity to a protein optimized by nature to carry out electron-transfer reactions. In addition, the work described here provides important new, as well as complementary, information regarding the participation of protein structural motifs in reactions that lead to heme breakdown. Such information is relevant to achieve a better understanding of heme catabolism, a vital physiological process that takes place in organisms to maintain iron homeostasis and to dispose of unwanted heme generated under normal and pathological conditions. The study of enzymatic heme catabolism has recently gained considerable interest in light of the potential role of CO (a heme catabolyte) in molecular signaling, and also due to the strong antioxidant characteristics of bilirrubin produced upon reduction of the product of heme catabolism biliverdin.

In view of early reports claiming the ability of hexacoordinated heme proteins to perform reductive dehalogenation reactions in the presence of sodium dithionite as primary electron donor [50], experiments were carried out to test such ability in mitochondrial cytochrome b_5. Our studies on this subject indicated that, contrary to the findings reported by Castro and coworkers [50], cytochrome b_5 is not capable of carrying out the reduction of halogenated alkyl compounds. Furthermore, the results also showed that sodium dithionite itself, used in the experiments as the initial electron donor, efficiently dehalogenates carbon tetrachloride, thus raising important questions as to the claimed ability of other hexacoordinated proteins to perform these types of reactions. Because sodium dithionite is a readily available and inexpensive reducing agent, its potential application in reductive dehalogenation of water pollutants was explored.

Studies that lead to the identification of trichloromethyl sulfinate anion produced in the reductive dehalogenation of carbon tetrachloride by sodium dithionite are the subject of Chapter IV.

References

1. Ortiz de Montellano, P. A. (1987) *Acc. Chem. Res.* 20, 289.

2. Dickerson, R. E., Kopka, M. L., Weinzierl, J. E., Varnum, J. C., Eisenberg, D., and Margoliash, E. In *Structure and Function of Cytochromes*; Okunuky, K., Kamen, M. D., and Sekuzu, I., Ed.; University Park: Baltimore, Maryland, 1968; pp 225.

3. Rodriguez-Marañon, M. J., Qiu, F., Stark, R. E., White, S. P., Zhang, X., Foundling, S. I., Rodriguez, V., Scilling, III, C. L., Bunce, R. A., and Rivera, M. (1996) *Biochemistry* 35, 16378.

4. Marchon, J. -C., Mashiko, T., and Reed, C. A. In *Electron Transport and Oxygen Utilization*; Ho, C., Ed.; Elsevier: North Holland, New York, 1982; pp 67-73.

5. Mathews, F. S. (1985) *Prog. Biophys. Molec. Biol.* 45, 1.

6. Moore, G. R. and Williams, R. J. P. (1977) *FEBS Lett.* 79, 229.

7. Doeff, M. M., Sweigart, D. A., and O'Brien, P. (1983) *Inorg. Chem.* 22, 851.

8. Sligar, S. G. and Gunsalus, I. C. (1976) *Proc. Nat. Acad. Sci., USA.* 73, 1078.

9. Reid, L. S., Mauk, M. R., and Mauk. A. G. (1984) *J. Am. Chem. Soc.* 106, 2182.

10. Fisher, M. T. and Sligar, S. G. (1985) *J. Am. Chem. Soc.* 107, 5018.

11. Mayo, S. L., Ellis, Jr., W. R., Crutchley, R. J., and Gray, H. B. (1986) *Science* 233, 948.

12. Lieber, C. M., Karas, J. L., and Gray, H. B. (1987) *J. Am. Chem. Soc.* 109, 3778.

13. King, B. C., Hawkridge, F. M., and Hoffman, B. M. (1992) *J. Am. Chem. Soc.* 114, 10603.

14. Rusling, J. F. and Nassar, A. -E. F. (1993) *J. Am. Chem. Soc.* 115, 11891.

15. Karlsson, J. J., Rostrup, T. E., and Ulstrup, J. (1996) *Acta Chem. Scand.* 50, 284.

16. Sligar, S. G., Egeberg, K. D., Sage, J. T., Morikis, D., and Champion, P. M. (1987) *J. Am. Chem. Soc.* 109, 7896.

17. Zhou, H. -X. (1994) *J. Am. Chem. Soc.* 116, 10362.

18. Guillemette, J. G., Barker, P. D., Ellis, L. D., Lo, T. P., Smith, M., Brayer, G. D., and Mauk, A. G. (1994) *Biochimie* 76, 592.

19. Van Dyke, B. R., Saltman, P., and Armstrong, F. A. (1996) *J. Am. Chem. Soc.* 118, 3490.

20. Rivera, M., Seetharaman, R., Girdhar, D., Wirtz, M., Zhang, X., Wang, X., and White, S. (1998) *Biochemistry* 37, 1485.

21. Quillin, M. L., Ardrini, R. M., Olson, J. S., and Phillips, Jr., G. N. (1993) *J. Mol. Biol.* 234, 140.

22. Brantley, Jr., R. E., Smerdon, S. J., Wilkinson, A. J., Singleton, E. W., and Olson, J. S. (1993) *J. Biol. Chem.* 268, 6995.

23. Chou, J., Zhou, H., Lu, T., Wu, Y., and Cotton, T. (1996) *Bioelectrochemistry and Bioenergetics* 41, 217.

24. Pauling, L. and Coryell, C. D. (1936) *Proc. Nat. Acad. Sci.*, USA 22, 210.

25. Summerville, D. A., Jones, R. D., Hoffman, B. M., and Bassolo, F. (1979) *J. Chem. Ed.* 56, 157.

26. Cotton, F. A. and Wilkinson, G. *Advanced Inorganic Chemistry*; John Wiley & Sons: New York, 1988; pp 1344-1345.

27. Holm, R. H., Kennepohl, P., and Solomon, E. I. (1996) *Chem. Rev.* 96, 2239.

28. Sono, M., Roach, M. P., Coulter, E. D., and Dawson, J. H. (1996) *Chem. Rev.* 96, 2841.

29. Ortiz de Montellano, P. R. *Cytochrome P450*, 2nd. ed.; Ortiz de Montellano, P. R. Ed.; Plenum: New York, 1995.

30. George, P., Irvine, D. H. (1952) *Biochem. J.* 52, 511.

31. Davies, M. J. (1991) *Biochem. Biophys. Acta* 1077, 86.

32. Ortiz de Montellano, P. R. (1998) *Acc. Chem. Res.* 31, 543.

33. Wilks, A. and Ortiz de Montellano, P. R. (1993) *J. Biol. Chem.* 268, 22357.

34. Wilks, A., Torpey, J., and Ortiz de Montellano, P. R. (1994) *J. Biol. Chem.* 269, 29553.

35. Gerber, N. C. and Sligar, S. G. (1992) *J. Am. Chem. Soc.* 114, 8742.

36. Kimata, Y., Shimada, H., Hirose, T., and Ishimura, Y. (1995) *Biochem. Biophys. Res. Commun.* 208, 96.

37. Tenhunen, R., Marver, H. S., and Schmid, R. (1969) *J. Biol. Chem.* 244, 6388.

38. Yoshida, T. and Kikuchi, G. (1978) *J. Biol. Chem.* 253, 4224.

39. Sun, J., Wilks, A., Ortiz de Montellano, P. R., and Loehr, T. M. (1993) *Biochemistry* 32, 14151.

40. Ito-Maki, M., Kazunobu, I., Mansfield-Matera, K., Sato, M., Ikeda-Saito, M., and Yoshida, T. (1995) *Arch. Biochem. Biophys.* 317, 253.

41. Takahashi, S., Wang, J., Rousseau, D. L., Ishikawa, K., Yoshida, T., Host, J. R., and Ikeda-Saito, M. (1994) *J. Biol. Chem.* 269, 1010.

42. Takahashi, S., Wang, J., Rousseau, D. L., Ishikawa, K., Yoshida, T., Takeuchi, N., and Ikeda-Saito, M. (1994) *Biochemistry* 33, 5531.

43. Egeberg, K. D., Springer, B. A., Martinis, S. A., Sligar, S. G., Morikis, D., and Champion, P. (1990) *Biochemistry* 29, 9783.

44. Adachi, S., Nagano, S., Watanabe, Y., Ishimori, K., and Morishima, I. (1991)

Biochem. Biophys. Res. Commun. 180, 138.

45. Adachi, S., Nagano, S., Ishimori, K., Watanabe, Y., Morishima, I., Egawa, T., Kitagawa, T., and Makino, R. (1993) *Biochemistry* 32, 241.

46. Hildebrand, D. P., Ferrer, J. C., Tang, H., Smith, M., and Mauk, A.G. (1995) *Biochemistry* 34, 11598.

47. Decatur, S. M., DePillis, G. D., and Boxer, S. G. (1996) *Biochemistry* 35, 3925.

48. Hildebrand, D. P., Tang, H., Luo, Y., Hunter, C. L., Smith, M., Brayer, G. D., and Mauk, A. G. (1996) *J. Am. Chem. Soc.* 118, 12909.

49. Ozaki, S., Matsui, T., and Watanabe, Y. (1997) *J. Am. Chem. Soc.* 119, 6666.

50. Bartnicki, E. W., Belser, N. O., and Castro, C. E. (1978) *Biochemistry* 17, 5582.

CHAPTER II

CONVERSION OF CYTOCHROME b_5 INTO A SPECIES CAPABLE OF PERFORMING THE EFFICIENT COUPLED OXIDATION OF HEME

Introduction

Heme-containing proteins play a crucial role in maintaining life in essentially all living organisms. Examples of these proteins include the oxygen-carriers hemoglobin and myoglobin, in which the heme active center is used by the protein as an oxygen-binding site. Cytochromes, on the other hand, are electron-transfer heme proteins in which the heme active site is shuttled between different oxidation states in order to accept or donate electrons (cytochrome b_5, cytochrome c). Heme-containing enzymes are also capable of reacting with molecular oxygen to perform monooxygenation reactions (cytochrome P450) or react with peroxides to carry out peroxidase reactions (horseradish peroxidase, cytochrome c peroxidase). It is remarkable that despite the wide range of chemical functions displayed by heme containing enzymes and proteins, they all share the same prosthetic group, iron-protoporphyrin IX. Important properties such as the reduction potential and reactivity exhibited by the heme active site in several different heme proteins are modulated by the structural characteristics encountered in their heme

binding cavities. One of the most significant structural characteristics governing the activity of hemoproteins is the coordination environment of the heme iron. For example, the heme in electron-transfer proteins is coordinated by two strongly coordinated axial ligands, and in general, these proteins do not bind molecular oxygen or peroxides. On the other hand, the heme in most other types of heme containing proteins is coordinated by a proximal axial ligand, therefore, providing an accessible vacant distal site where molecular oxygen, peroxides, and other exogenous ligands, can bind.

A large effort has been directed to understand the effect that changes in axial ligation have on the properties of heme proteins [1-13]. Protein semisynthesis and, in particular, site-directed mutagenesis, have been exploited to generate heme proteins with novel heme-axial ligation. For example, Raphael and Gray reported that replacement of methionine-80, a heme axial ligand in cytochrome c with a histidine [2], or with a cysteine [3] results in heme proteins with reduction potentials similar to those displayed by microsomal cytochrome b_5 and cytochrome $P450_{cam}$, respectively. Horse heart myoglobin has been converted into an electron-transfer protein upon replacement of the distal valine-68 residue with a histidine. This resulted in a bis-histidine coordinated species with spectroscopic characteristics similar to those of cytochrome b_5 [4]. Replacement of the proximal axial ligand of human myoglobin with cysteine resulted in a ferric species whose heme is coordinated by a proximal thiolate and whose spectroscopic characteristics are similar to those of cytochrome P450. In addition, the monooxygenase activity of the mutant was modestly increased [7, 8].

Evidence is presented here that demonstrates that upon replacement of histidine-63 for methionine in the electron transfer protein outer mitochondrial membrane (OM) cytochrome b_5, a mutant is produced that is capable of performing the efficient coupled

oxidation of heme. The coupled oxidation of the heme in the H63M mutant is arrested at the verdoheme stage and proceeds with >90% regioselectivity for the α-meso position. The only other example of a mutant protein capable of performing the efficient and regioselective coupled oxidation of heme is that reported for the Val67Ala-Val68Ser double mutant of horse heart myoglobin [14].

Experimental Procedures

i). Site-directed mutagenesis, Protein Expression and Purification.

The transformer site-directed mutagenesis kit (Clonetech) and the recombinant plasmid MRL1 [29] were used to construct the mutants following a protocol outlined previously [21]. The sequences corresponding to the mutagenic primers designed to introduce mutations H63M, H39M, and that corresponding to the selection primer (*Afl*III to *Bgl*II) are 5'-CCGAATCTTTCGAAGATGTTGGCATGTCTCCGGATGCGCG-3', 5'-CCCGTTTCCTGTCTGAAATGCCGGGCGGCGAAGA-AGTTCTGC-3', 5'-GGGGA-TAACGCAGG-AAAGAAGATCTGAGCAAAAGGCC-3', respectively. The underlined codons represent mismatches introduced to generate the mutations. The mutated gene was subcloned into the pET 11a vector and expressed in *E. coli* B834(DE3), a methionine auxotroph [15]. Expression of the H63M mutant was carried out following a procedure similar to that described by Rivera *et al.* [16]. In brief, 1.0 L of M9 minimal media supplemented with essential metals [17] was inoculated with 5 mL of an *E. coli* B834(DE3) culture grown overnight. When the OD_{600} reached a value of 0.80-1.0, biosynthesis of the polypeptide was induced by adding IPTG (isopropyl-β-thiogalactoside) to a final concentration of 1.0 mM, and the culture supplemented with 40

mg of L-methionine per L of fermenting cells. Approximately 10 min after induction of protein synthesis, 17 mg of δ-aminolevulinic acid, and 100 mg of $FeSO_4 \cdot 7H_2O$ were added to each liter of cell culture. The cells were harvested by centrifugation 3 h after induction of protein synthesis. Longer incubation times after induction of protein synthesis resulted in the formation of green color on otherwise reddish cells. The harvested cells were subsequently resuspended and lysed as described previously [18]. Cell debris was separated by ultracentrifugation, the supernatant made 3 mM in $K_3Fe(CN)_6$, and 1 mM in imidazole, and then dialyzed (Spectrapor; 6-8000 MWCO) at 4.0 C against ion exchange buffer (10 mM EDTA, 50 mM TRIS and 1.0 mM imidazole, pH 7.8). The desalted solution was then loaded onto an anion exchange resin (DE52, Whatman) previously equilibrated with ion exchange buffer, and eluted with a linear salt gradient (0.0-0.50 M NaCl) containing 1.0 mM imidazole. Fractions with purity ratio (A_{280nm}/A_{412nm}) < 1.5 were pooled, dialyzed against gel filtration buffer (100 mM NaCl, 20 mM Tris and 1.0 mM EDTA, pH 7.4), concentrated by ultrafiltration (Y3 Diaflo ultrafiltration membranes, Amicon), and purified by size exclusion chromatography [18]. Fractions with a purity ratio (A_{280}/A_{410}) < 0.5 were pooled, dialyzed exhaustively against 50 mM phosphate buffer, pH 7.0, and concentrated by ultrafiltration to approximately 4-5 mL. Protein concentrations were determined using the molar absorptivity coefficient determined by the pyridine hemochrome method ($\epsilon_{410} = 108\ mM^{-1}\ cm^{-1}$) [19].

ii). UV-Vis Absorption and EPR Spectroscopy.

UV-Vis spectra of the H63M mutant were collected on a Hewlett Packard 8452A diode array spectrophotometer equipped with a jacketed cuvette holder connected to a

thermostated water bath. EPR spectra of samples containing the H63M mutant in the presence and in the absence of imidazole (1.0 mM) were acquired using a Bruker EPR spectrometer operating at 9.35 GHz. The samples were analyzed at 4.1 K under the following conditions: receiver gain, 1.0 x 10^5; microwave power, 0.200 mW; modulation frequency, 100 kHz; modulation amplitude, 5.69 G.

iii). NMR Spectroscopy

Expression and purification of the H63M mutant enriched with L-^{13}C-methyl methionine ($^{13}CH_3SCH_2CH_2CH(NH_2)CO_2H$, Aldrich) was carried out as described above. Proton decoupled ^{13}C-NMR spectra of the H63M mutant were obtained at 15 °C with the aid of a *Unity Innova* NMR spectrometer operating at a ^{13}C spectrometer frequency of 150.57 MHz. The protein solutions (typically 1.5 mM) were exchanged with perdeuterated sodium phosphate buffer (μ = 0.10 M; pH 7.0, not corrected for the isotope effect). In a separate experiment, 1.0 μL of a concentrated imidazole solution was added to the solution containing the mutant to achieve a final concentration of 1.0 mM. Typically 3200 scans were collected over a 33 kHz spectral width, with an acquisition time of 0.5 sec and a relaxation delay of 1.5 s. The spectra were referenced against an external reference solution consisting of 35 % (v/v) of dioxane in D_2O, and processed with a line broadening of 1.5 Hz. The heterocorrelated multiple-quantum coherence (HMQC) [20a] spectrum of the H63M mutant in the absence of imidazole was acquired with spectral widths of 18 kHz for ^{1}H and 7 kHz for ^{13}C, a $^1J_{CH}$ set to 140 Hz, water presaturation during the relaxation delay (1.5 s), and WURST decoupling on the ^{13}C channel. [20b]. The data were collected as an array of 4K x 1K points, which after

linear prediction in the t_1 dimension and zero filling in both dimensions produced a 4K x 4K data matrix.

iv). Electrochemistry

Cyclic voltammetry experiments were carried out with a BAS 50W computer-controlled potentiostat. Materials, experimental setup and methods used in the voltammetric determination of the reduction potentials of the H63M mutant were identical to those described by Rivera *et al.* [21]. The voltammetric experiments were typically carried out with solutions consisting of 90 μM protein, 0.20 mM polylysine, in a total volume of 250 μL of MOPS (100 mM, pH 7.0). Transmission mode spectroelectrochemical titrations were carried out in cell bodies constructed of polyacrylate that had an optically transparent gold minigrid (200 wires/in, 70% transmittance, Buckbee Mears Co., St. Paul, MN), quartz windows, a gold minigrid counter electrode and a compartment for the Ag/AgCl reference electrode. The details of the spectroelectrochemical cell and titrations have been reported elsewhere [22]. Typical solutions used for these experiments contained 64 μM H63M mutant, 50 mM imidazole, 50 mM phosphate buffer, pH 7.0. Methyl viologen (3.0 mM) and $[Ru(NH_3)_6]Cl_3$ (0.80 mM) were added as mediators. Absorption spectra were taken every 20 mV in the range of -200 to -280 mV vs a Ag/AgCl reference electrode. The spectrum of completely oxidized and completely reduced species were obtained at -100 mV and -500 mV, respectively.

v). Coupled oxidation assays

Coupled oxidation reactions were carried out at 35 °C with solutions containing 14 μM of the H63M mutant in 1.0 mL of 50.0 mM phosphate buffer, pH 7.0. The reaction was initiated by addition of a concentrated solution of sodium ascorbate to achieve a final concentration of 2.0 mM in the reaction mixture, and the reaction was stopped after 7.0 h by cooling to 4.0 °C. An 800 μL aliquot of the resultant solution was extracted with a mixture of pyridine (0.10 mL) and $CHCl_3$ (1.0 mL), and the chloroformic phase transferred to a test tube, dried over anhydrous Na_2SO_4, concentrated with a gentle stream of nitrogen to approximately 500 μL, and analyzed by UV-vis spectrophotometry.

vi). Mass Spectrometry

The coupled oxidation reaction (10 mL) was performed as described above and stopped after 10 h by cooling to 4 °C. The resultant solution was dialyzed against 40 mM NH_4HCO_3 and subsequently concentrated by ultrafiltration to approximately 600 μL. One hundred μL of the resultant solution was diluted with 100 μL of 10 mM amonium acetate and then injected (5 μL/min) into a Sciex API III triple quadrupole mass spectrometer equipped with an atmospheric pressure ion source. Sampling of the positive ions was achieved in the first quadrupole using a voltage difference of 125 V. Increments of 0.1 a.m.u were collected in the range of 500 to 750 a.m.u.

vii). HPLC Analysis

The regiospecificity of the reaction was assessed by analysis of biliverdin dimethyl-ester isomers with the aid of a Beckman System Gold HPLC chromatograph

equipped with a diode array UV-Vis detector. Samples (dissolved in chloroform) were prepared as follows: A solution containing the reaction product (10 mL) was extracted with a mixture of 2-picoline (2.0 ml) and $CHCl_3$ (5.0 mL). The conversion of verdoheme to biliverdin was accomplished by addition of KOH followed by the addition of HCl to the chloroformic phase, as described by Saito and Itano [23]. Synthesis of the dimethyl esters was carried out as described by O'Carra and Colleran [24]. Coupled oxidation of the pyridine hemochrome was carried out as described previously [25]. Samples were injected into a Beckman Ultrasphere ODS C18 column (4.6 mm x 25 cm) and separated by isocratic elution with a mixture 20:80 consisting of methanol:methanol/water (75/25). The retention time of the product generated from the coupled oxidation of the heme in the H63M mutant was compared to those obtained from samples of authentic α-bliliverdin (Sigma), and from samples obtained by coupled oxidation of iron protoporphyrin-IX in the presence of pyridine.

Results

i). Protein Purification and Absorption spectra

Centrifugation of the B834(DE3) cells three hours after induction of protein synthesis produces a red pellet due to the overexpression of the OM cytochrome b_5 mutant. After lysis and ultracentrifugation, the mutant is in the reduced state, as indicated by its visible spectrum (Fig 1a), and it oxidizes upon dialysis. When the H63M mutant is oxidized during the dialysis process, its electronic spectrum (Fig 1b) displays a band at 660 nm. On the other hand, when the protein is oxidized with an excess of potassium ferricyanide in the presence of imidazole, immediately after

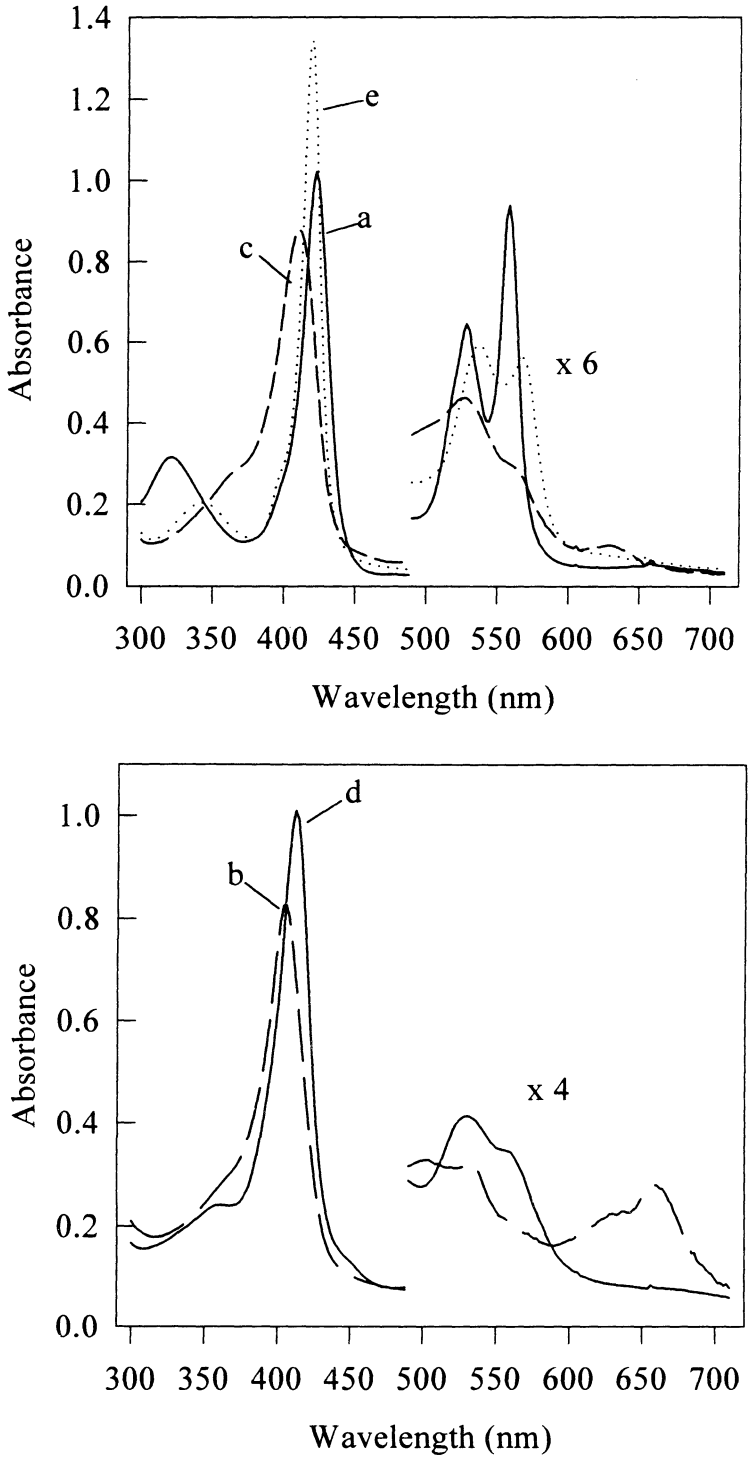

Figure 1. UV-Vis absorption spectra of the H63M mutant of OM cytochrome b_5. (a) Fe(II); (b) Fe(III) species obtained by dialyzing a solution containing the ferrous mutant, dithionite (0.10 mM), and dithiothreitol (1.0 mM); (c) Fe(III) species obtained by oxidizing the Fe(II) species with ferricyanide; (d) Fe(III)-imidazole complex; (e) Fe(II)–CO complex. Adapted from reference 27.

ultracentrifugation, the spectrum of the resultant ferric protein is devoid of the band at 660 nm (Fig 1c). These results provided the first indication that the ferrous H63M mutant reacts with oxygen to produce a derivative whose electronic spectrum displays a peak at 660 nm. The UV-Vis absorption spectrum of the ferric mutant displays a charge-transfer transition at 630 nm (Fig 1c) indicative of a high-spin state. The spin state of the ferric mutant was corroborated by its EPR spectrum (Fig 2a) which displays signals with *g* values at 6.45 and 2.16 [26], typical of high spin ferric hemes with heme as the proximal ligand. On the other hand, the ferrous protein appears to be in the low-spin state, as indicated by the resolved α and β bands (558 and 528 nm, respectively) observed in its electronic spectrum (Fig 1a) [27]. Furthermore, when CO is bubbled through a solution of the ferrous mutant, a stable Fe^{2+}-CO species is formed, as indicated by its electronic spectrum (Fig 1e).

When a solution containing the ferric protein was loaded onto an ion-exchange column, a red band was formed at the top of the column, as expected. However, when the salt gradient was started, the characteristic red color of the holo-protein disappeared gradually, leaving behind a green color characteristic of heme devoid of axial ligands. This indicated that the ferric mutant loses its heme during the elution process, presumably due to electrostatic interactions between the heme propionates and the anion-exchange resin. This suggests that the heme-H63M complex is significantly weaker than the heme-wild-type cytochrome b_5 complex. To purify the holoprotein by ion-exchange chromatography, the solution containing the ferric H63M mutant was made 1.0 mM in imidazole and then loaded onto an ion-exchange column, previously equilibrated with ion-exchange buffer containing 1.0 mM imidazole. The holoprotein was eluted, subsequently dialyzed in order to remove the imidazole and then purified by size-

exclusion chromatography. The electronic spectrum of the ferric H63M-imidazole complex (Soret band at 412 nm and a visible peak at 530 nm) (Fig 1d) is similar to that obtained from wild-type OM cytochrome b_5, hence suggesting that the heme becomes hexacoordinated in the presence of imidazole. The incorporation of imidazole as the sixth ligand was corroborated from the EPR spectrum of the H63M-imidazole complex, which displays signals with g values characteristic of low-spin ferric hemoproteins, g = 3.04, 2.22, and 1.45 (Fig 2b).

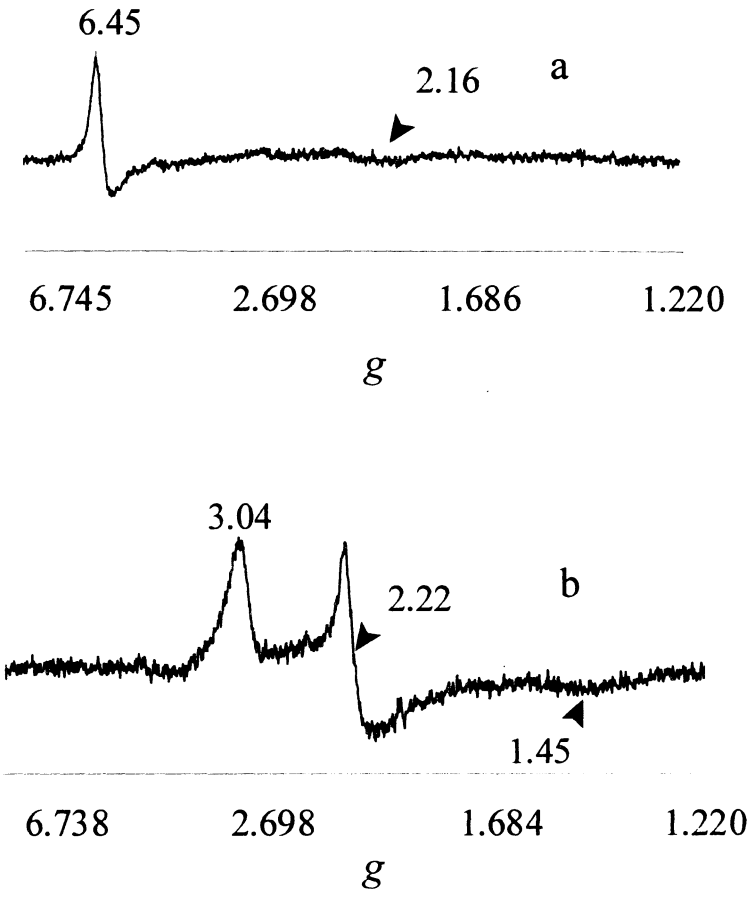

Figure 2. EPR spectra of the H63M mutant of OM cytochrome b_5. (a) Fe(III); and (b) Fe(III)-imidazole complex.

ii). NMR Spectroscopy

To determine whether Met-63 binds to the ferric heme, the H63M mutant was expressed in *E. coli* B834(DE3), a methionine auxotroph. This strategy permitted the labeling of the mutant with ^{13}C-methyl methionine ($^{13}CH_3SCH_2CH_2CH(NH_2)COOH$). The ^{13}C-NMR spectrum of the labeled mutant (Fig 3a) displays eight resonances between 13.90 and 16.50 ppm. These resonances arise from Met-1, Met-23, Met-63 and Met-70. On the basis of ^{1}H-NMR spectroscopic studies, it has been previously demonstrated that cytochrome b_5 is a mixture of two interconvertible isomers that differ by a 180° rotation about the α-γ-meso axis of the heme [28]. The ratio of isomeric populations A:B in the case of OM cytochrome b_5 is 1:1 [29]. It is also known from the crystal structure of OM cytochrome b_5 [16] that the side chain of Met-23 is in van der Waals contact with the heme substituents on pyrrole I, and that Met-70 is in van der Waals contact with the heme substituents on pyrrole III. On this basis it is possible to propose that the intense signal at 14.06 ppm (Fig 3a) arises from Met-1, while the two sets or resonances at 14.11, 14.45, and 14.64, 14.82 ppm originate from Met-23 and -70. Each set consists of two resonances of almost equal intensity due to the heme isomeric mixture A:B = 1:1. The three resonances between 15.40 and 16.50 ppm appear to arise from Met-63. The relatively larger width of these resonances seems to indicate that their corresponding methyl groups are in relative close proximity to the ferric ion, hence favoring dipolar interactions with the unpaired electron on the ferric heme. It is noteworthy, however, that the chemical shift range observed for the methyl carbons in all methionine residues is typical of methyl carbons in diamagnetic molecules. This implies that the sulfur atom in Met-63 is not coordinated to the ferric heme iron.

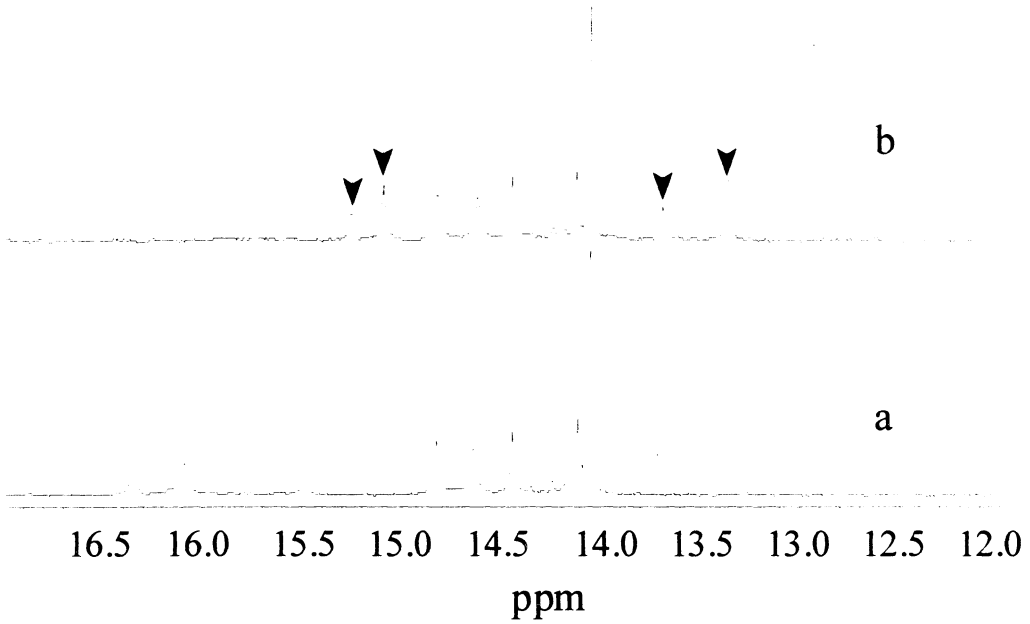

Figure 3. ^{13}C-NMR spectrum of the H63M mutant labeled with L-^{13}C-methyl methionine. (a) Fe(III); (b) Fe(III)-imidazole complex. Resonances not arising from Met-63 in spectrum (a), *i.e.* those observed in the range between 14.00 and 14.90 ppm, do not shift upon formation of the Fe(III)-imidazole complex. Resonances highlighted with arrows shift upon formation of the Fe(III)-imidazole complex. Adapted from reference 27.

Addition of imidazole to a solution of the mutant results in large shifts for the resonances arising from Met-63, as depicted by the peaks highlighted by arrows in Fig 3b. There are four resonances arising from Met-63 in the H63M-imidazole complex because there are two orientations of the methionine and two orientations of the heme active site. Furthermore, these resonances become narrower upon binding of exogenous imidazole, hence suggesting a weaker dipolar interaction between the methyl carbons and the unpaired electron on the heme iron. This indicates that the methyl group in Met-63 is displaced further away from the heme iron upon biding of imidazole. In contrast, the resonances between 13.90 and 14.80, which are thought to arise from Met-1, Met-23 and

Met-70, are not affected (Fig 3b). Additional evidence that Met-63 is not bound to the ferric heme was obtained from the ^{1}H chemical shifts arising from the methyl groups in the H63M mutant. These ^{1}H chemical shifts, which were obtained with the aid of an HMQC experiment (Fig 4), are characteristic of methyl groups in diamagnetic environments, thus clearly indicating that Met-63 is not bound to the ferric heme.

iii). Electrochemistry

The reduction potential of the H63M mutant was measured by spectroelectrochemistry and by cyclic voltammetry in the presence and in the absence of imidazole. A family of spectra obtained during the spectroelectrochemical titration of the mutant in the presence of imidazole is shown in Fig 5, along with the Nernst plot (inset). The reduction potential of the imidazole-H63M complex, which was shown to exist as a low-spin Fe(III) species, was found to be -92 mV *vs* NHE. The reduction potential of this species measured by cyclic voltammetry was found to be -80 mV *vs* NHE (Fig 6a). By comparison, the reduction potential of OM cytochrome b_5 (a bis-histidine-coordinated species) under similar conditions is -102 mV *vs* NHE [30]. The spectroelectrochemical measurement of the reduction potential exhibited by the H63M mutant in the absence of imidazole was more difficult to obtain due to the gradual decomposition of the protein during the course of the potentiometric titration. The reduction potential obtained from several potentiometric measurements is 110 mV *vs* NHE. In order to substantiate this value, the reduction potential of the mutant was measured by cyclic voltammetry (Fig 6b) and found to be +130 mV *vs* NHE. It has been previously reported that when electrodes modified with poly-electrolytes are utilized for voltammetric measurements of the

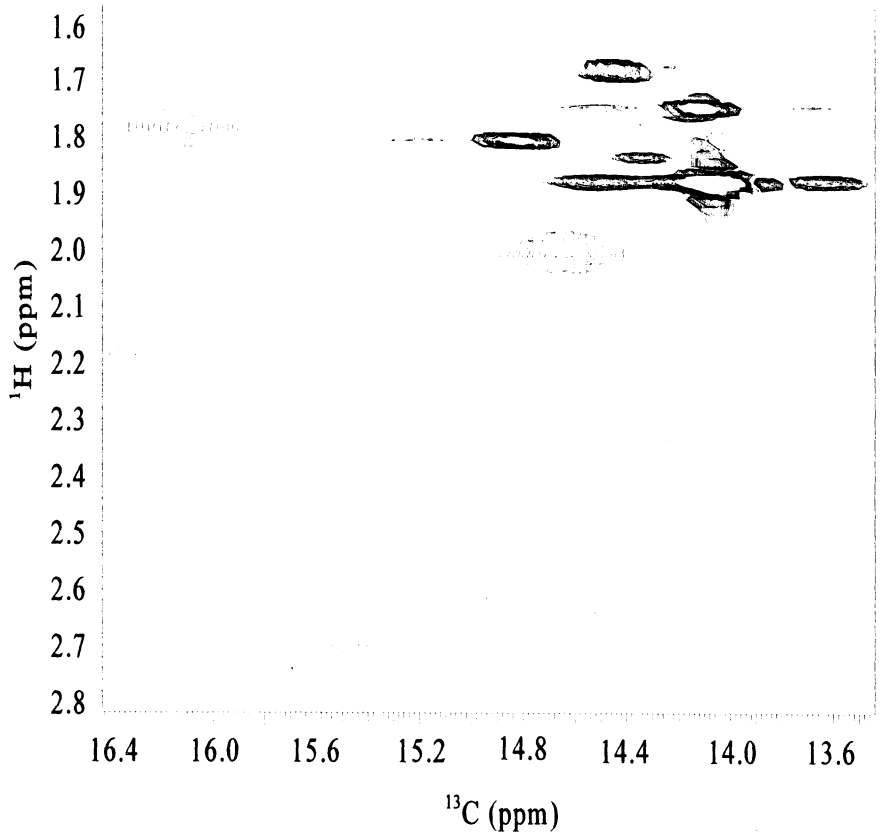

Figure 4. HMQC spectrum of the H63M mutant labeled with L-[^{13}C]-methionine.

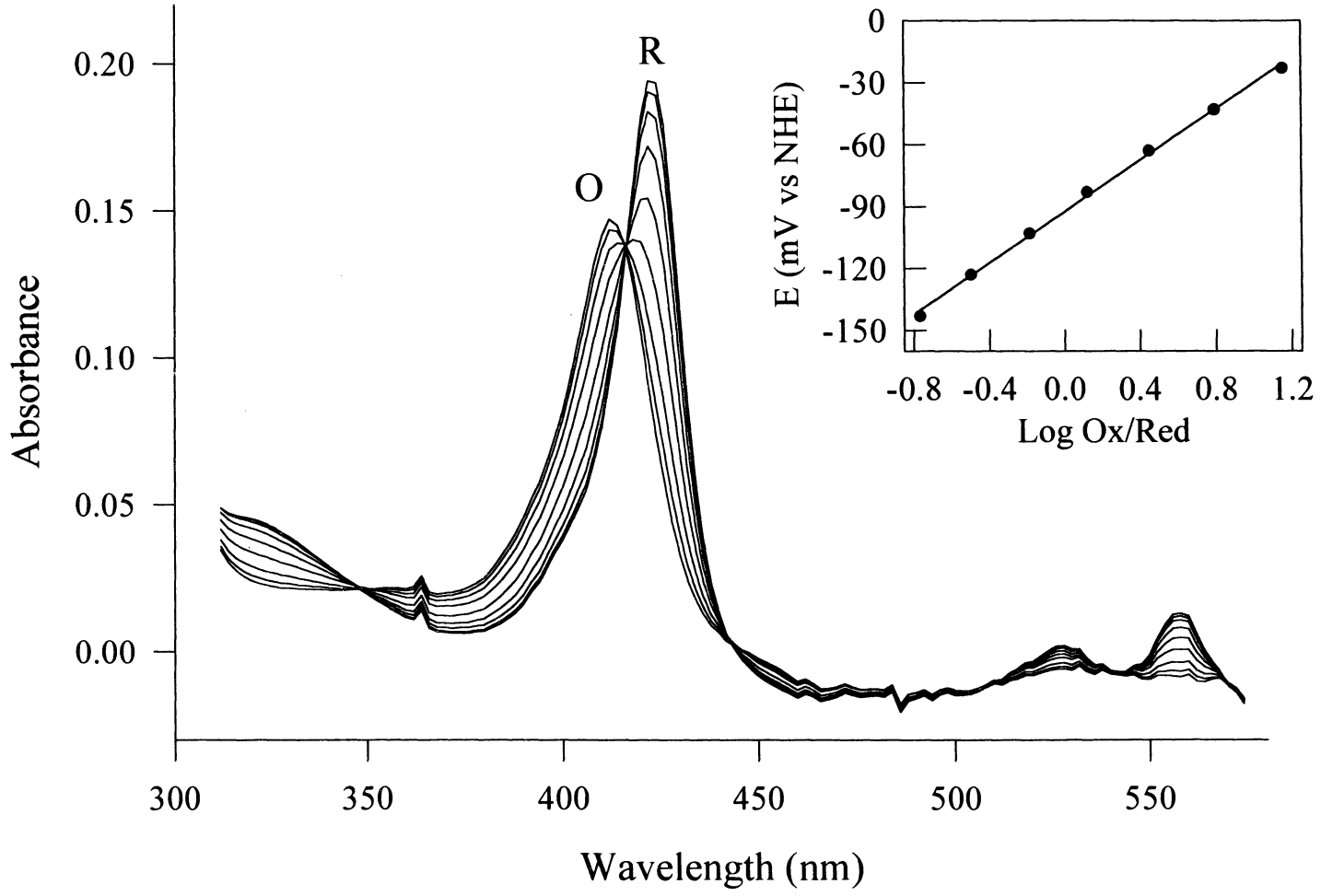

Figure 5. Spectroelectrochemical titration of solutions containing the H63M mutant (65 μM) in the presence of imidazole (50 mM). (Inset) Nernst plot constructed from the dependence of the absorbance at 424 nm on the applied potential. The Nernst slope is 62 mV. Adapted from reference 27.

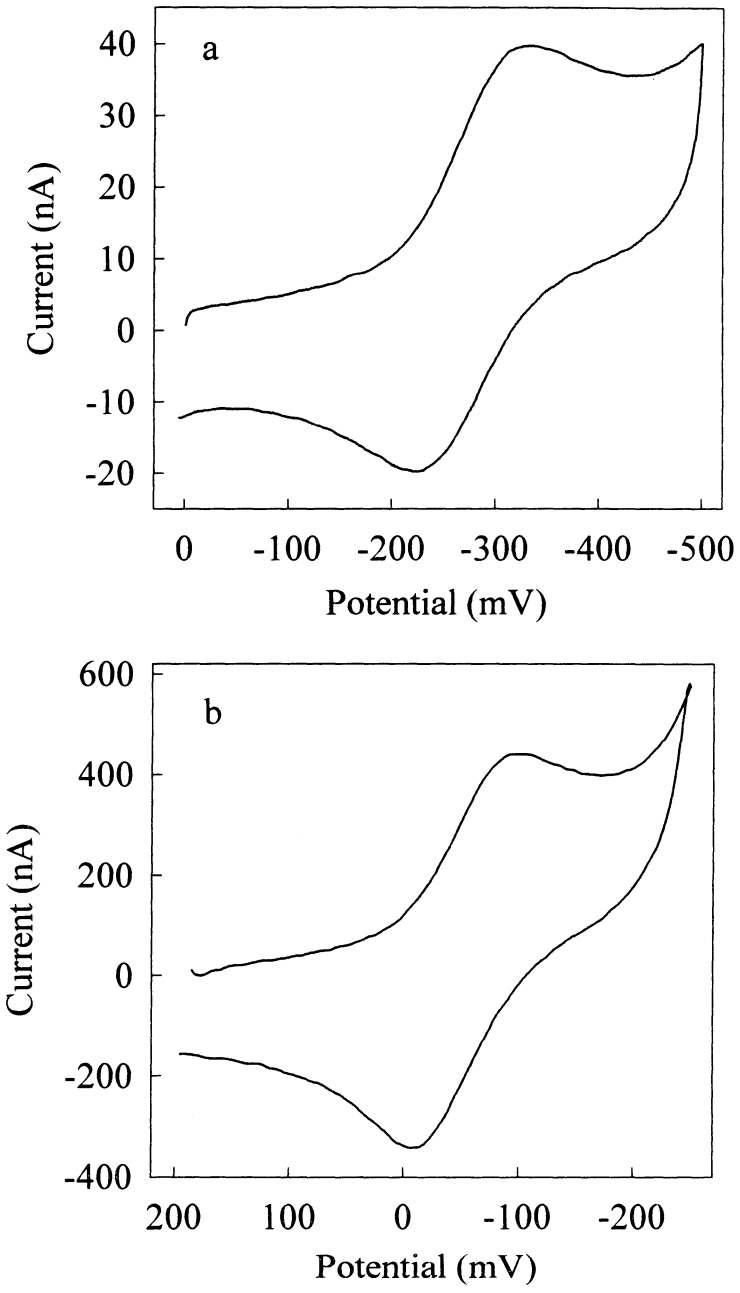

Figure 6. Cyclic voltammograms obtained from solutions containing the H63M mutant of OM cytochrome b_5 (90 μM), in the presence (a) and in the absence (b) of imidazole (50 mM). A gold disk electrode was modified with β-mercaptopropionate and the voltammograms were obtained in the presence of 0.20 mM polylysine (MW = 3970), with a scan rate of 20 mV/sec. The potential axis shown is with respect to the Ag/AgCl reference electrode but the reduction potentials in the text are given with respect to the NHE. Adapted from reference 27.

reduction potential of cytochrome b_5, these values are consistently more positive than those measured potententiometrically [21, 30]. An explanation for the observed anodic shifts has been proposed recently [30]. Consequently, the value of the reduction potential measured potentiometrically for the H63M mutant (110 mV) appears to be reasonably close to the true value. It is also noteworthy that this value compares well with the reduction potential displayed by horse heart myoglobin, 45 mV [31], sperm whale myoglobin, 55 mV [32], and human myoglobin, 50 mV [32], consistent with a species in which heme is axially ligated by a proximal histidine.

iv). Coupled Oxidation of Heme

The spectral change produced upon addition of excess ascorbate to a solution of the H63M mutant previously equilibrated with air was monitored spectrophotometrically (Fig 7). The electronic spectrum of the ferric H63M mutant before addition of ascorbate was identical to that shown in Fig 1c. Addition of ascorbate results in reduction of the mutant, as demonstrated by the Soret band (420 nm) and visible peaks at 558 and 528 nm that are characteristic of a hexacoordinated low-spin ferrous heme. As the coupled oxidation reaction proceeds, the intensity of the Soret band at 420 nm decreases with the concomitant increase of a peak at 402 nm. The peaks at 528 and 558 nm also disappear, giving rise to a peak with absorption maxima at 534 nm. It is also evident from Fig 7 that as the reaction progresses, a peak with absorption maxima at 660 nm is formed, whose intensity increases as the reaction proceeds. The electronic spectrum obtained after 7.0 h of reaction (Fig 8a) is very similar to the spectrum reported for the pyridine hemochrome of verdoheme [33], therefore implying that verdoheme is the product of the coupled

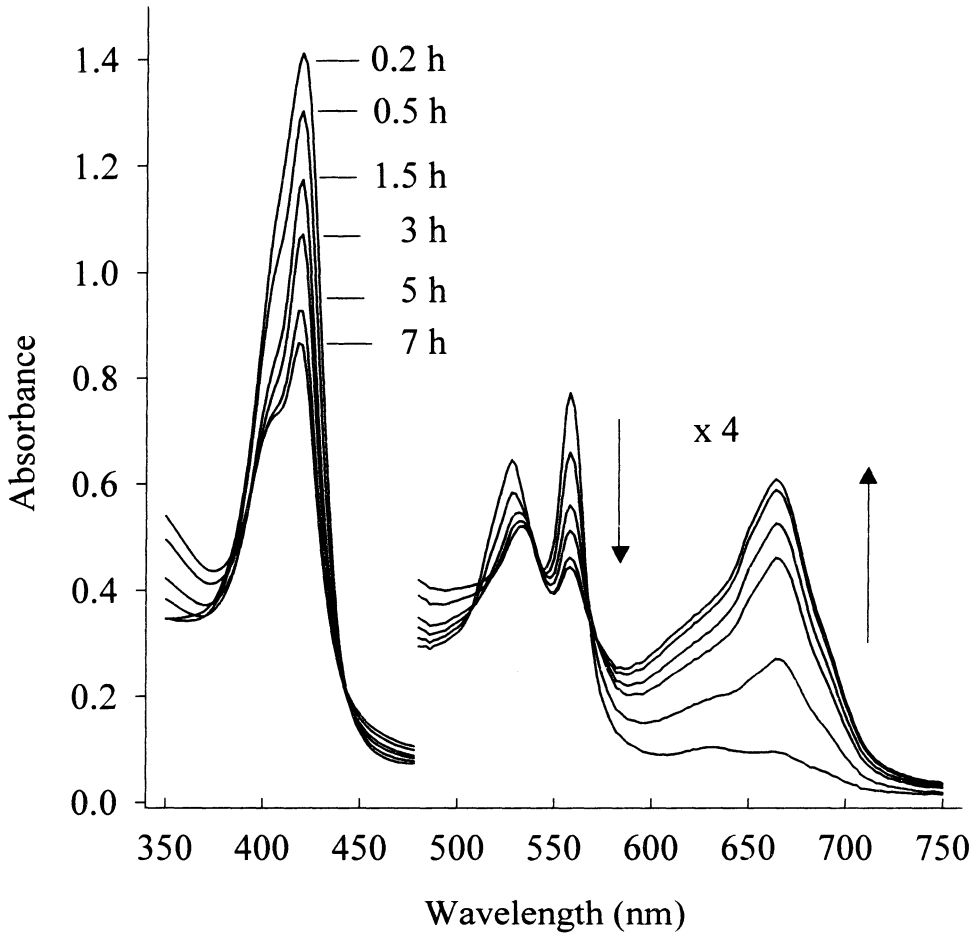

Figure 7. Changes in the UV-Vis absorption spectrum of the H63M mutant of OM cytochrome b_5 during the coupled oxidation of heme in the presence of ascorbate. Adapted from reference 27.

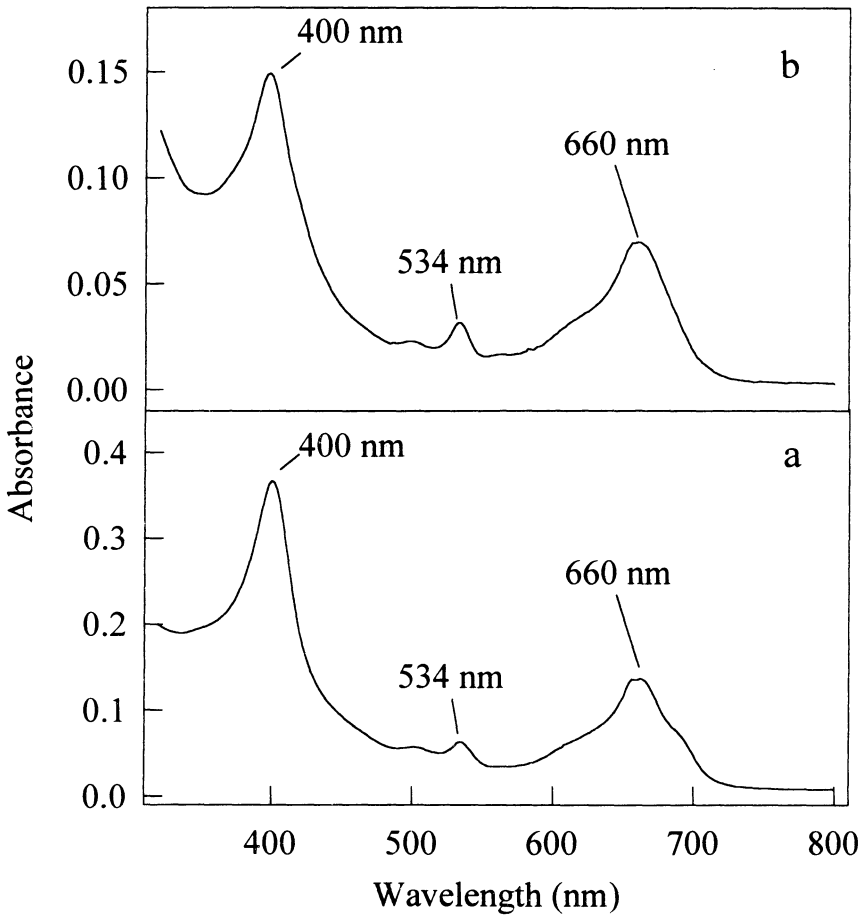

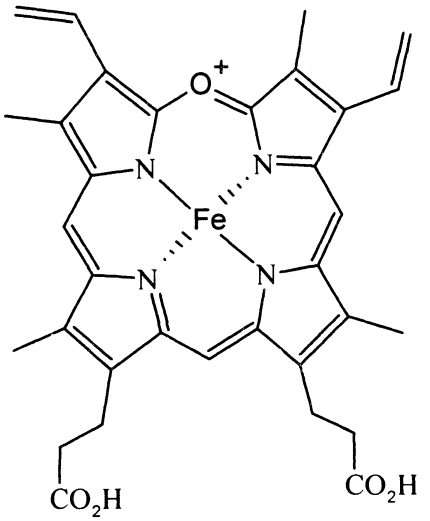

Verdoheme

Figure 8. (a) UV-Vis absorption spectrum of a solution containing the H63M-verdoheme complex obtained after 7 h of reaction with ascorbate. (b) UV-Vis absorption spectrum of the verdohemochrome obtained by extracting the verdoheme in solution (a) with 10% pyridine in chloroform. Adapted from reference 27.

oxidation reaction performed by the H63M mutant of OM cytochrome b_5.

Additional evidence corroborating that verdoheme is the product of the coupled oxidation of the heme in the H63M mutant of OM cytochrome b_5 was obtained by incubating a more concentrated solution of the mutant with ascorbate. The reaction was stopped after approximately 10 h and the reaction product extracted as the pyridine hemochrome into chloroform. The electronic spectrum obtained from the resultant chloroform solution (Fig 8b) is identical to the spectrum reported by Lagarias [33] for the pyridine hemochrome of verdoheme. Moreover, in a separate experiment, the coupled oxidation reaction was quenched by cooling the reaction mixture to 4.0 °C. The ascorbate-containing solution of the mutant was subsequently dialyzed *vs* a 40 mM solution of ammonium bicarbonate at 4 °C. The resultant solution was concentrated by ultrafiltration, diluted with ammonium acetate and analyzed by electrospray mass spectrometry. The resultant mass spectrum (Fig 9) displays a small peak corresponding to unmodified heme (m/z = 616), and a large peak corresponding to verdoheme (m/z = 619), thus conclusively demonstrating that the product of the coupled oxidation performed by the H63M mutant is verdoheme.

v). Regiospecificity of coupled oxidation

The regiospecificity of the reaction performed by the H63M mutant was assessed by extracting the verdoheme produced upon coupled oxidation into 2-picoline, hydrolyzing it to Fe-biliverdin in basic picoline followed by acidification of the picoline solution in order to produce biliverdin [23]. The biliverdin was then esterified with methanol and the resultant dimethyl ester derivative analyzed by HPLC. The

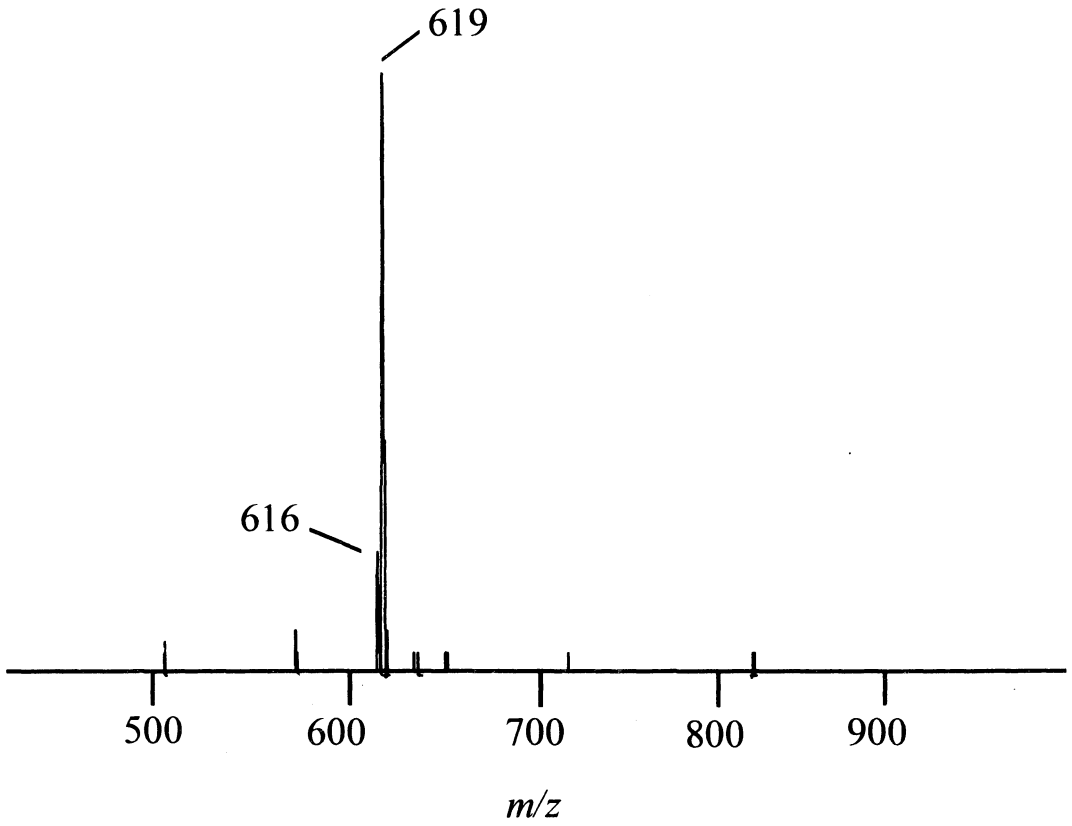

Figure 9. Mass spectrum obtained by ESI-MS analysis of the reaction mixture containing the H63M mutant and L-ascorbate under aerobic conditions. Adapted from reference 26.

chromatogram obtained for the sample derived from the coupled oxidation performed by the H63M mutant (Fig 10a) shows an intense peak with retention time of approximately 8.0 min. A sample of biliverdin dimethyl ester (Fig 10b), which was derived from α-biliverdin, displays a peak with retention time identical to that observed for the product of the coupled oxidation performed by the mutant. This is strong evidence suggesting that the coupled oxidation performed by the mutant is regioselective, with oxygen attacking the α-meso position, as is observed in the case of myoglobin and heme oxygenase. In a separate experiment, the pyridine hemochrome was incubated with ascorbate. It is well known that during the coupled oxidation of the pyridine hemochrome, all four meso positions are attacked by oxygen to produce a random mixture of isomeric biliverdins [34, 35]. The chromatogram obtained from a sample derived from the coupled oxidation of the pyridine hemochrome displays four peaks with retention times ranging from 8.0 to 14.0 min (Fig 10c). This experiment demonstrates that the four isomeric biliverdins can be separated with the conditions utilized in the analysis of the reaction products by HPLC, consequently, it can be concluded that the coupled oxidation of heme performed by the H63M mutant occurs with >90% regioselectivity for the α-meso position.

Discussion

Sligar and Egeberg [36] replaced His-39, a heme axial ligand in rat microsomal cytochrome b_5 for a methionine. On the basis of EPR and resonance Raman spectroscopic studies, these authors reported that the ferric form is a six-coordinated high-spin species. These authors also reported that it was not possible to conclude whether Met-39 or a water molecule acts as the sixth axial ligand in the ferric H39M

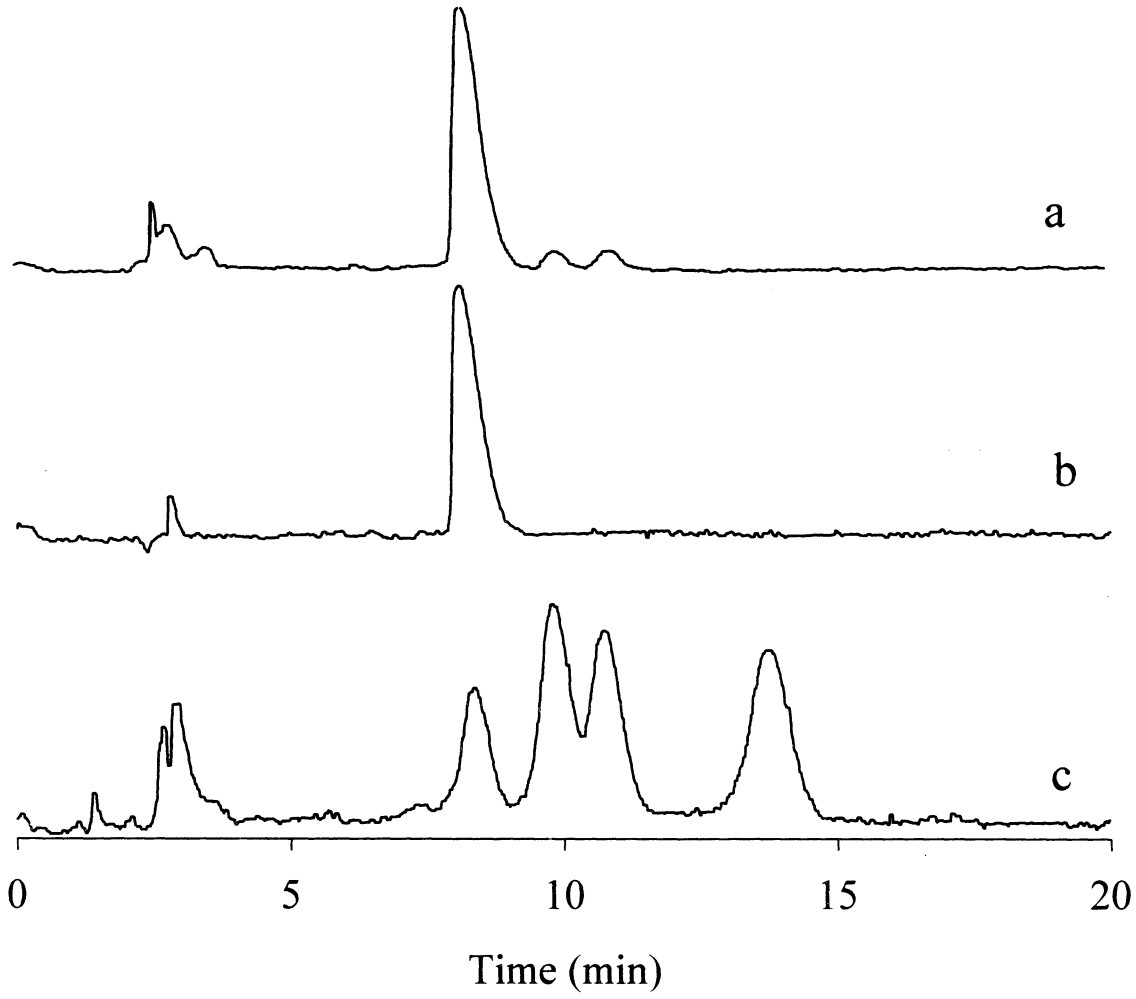

Figure 10. Chromatograms obtained from solutions containing the dimethyl ester derivatives of (a) biliverdin obtained from the verdoheme formed upon coupled oxidation of the heme in the H63M mutant, (b) standard biliverdin, and (c) biliverdin obtained from a coupled oxidation reaction of iron-protoporphyrin IX in aqueous pyridine.

mutant of microsomal cytochrome b_5. The reduction potential of this protein was found to be -240 mV *vs* NHE [36], as compared with 6 mV for the wild type protein [36]. Furthermore, the H39M mutant of rat microsomal cytochrome b_5 was found to catalyze intermolecular oxidative reactions, demonstrated with the hydrogen peroxide dependent oxidative demethylation of N,N-dimethylaniline [36]. On the other hand, when His-63, the other axial ligand in microsomal cytochrome b_5 was mutated to a methionine, the apoprotein failed to incorporate heme during cell fermentation [38].

By comparison, the results presented in this Chapter demonstrate that the H63M mutant of outer mitochondrial membrane (OM) cytochrome b_5 exists as a high spin ferric species coordinated by a proximal histidine residue (His-39), and likely, by a distal water (discussed below). NMR spectroscopic studies provided strong evidence indicating that Met-63 is not coordinated to the ferric heme iron. The reduction potential of the H63M mutant of OM cytochrome b_5 was found to be +110 mV *vs* NHE, a value in close agreement to that displayed by myoglobin. It is also noteworthy that the mitochondrial H63M mutant performs an efficient intramolecular oxidative reaction, the coupled oxidation of heme. On the other hand, the H39M mutant of OM cytochrome b_5 does not incorporate heme during cell fermentation.

i). Heme Axial Ligation

The EPR (Fig 2a) and electronic (Fig 1c) spectra of the ferric H63M mutant of OM cytochrome b_5 are similar to those displayed by met-aquomyoglobin [39], indicating that the heme in the ferric mutant may be coordinated by His-63 in the proximal side and by water in the distal pocket. Coordination of water in the distal pocket of the ferric

mutant can be inferred from the band at 630 nm that is observed in its electronic spectrum. In myoglobin, this band has been assigned to an Fe–O charge transfer transition [39]. When imidazole is added to a solution of the ferric H63M mutant, the resultant electronic spectrum (Fig 1d) is very similar to that displayed by ferric OM cytochrome b_5 [29], with Soret band at 412 nm and visible peaks at 530 and 556 nm. It is therefore possible to suggest that the exogenous imidazole coordinates the heme iron in the distal site, producing a ferric low-spin species, as manifested by the disappearance of the band at 630 nm (Fig 1d). Consistent with coordination of the heme by a proximal histidine, the reduction potential of the H63M mutant in the absence of imidazole was found to be 110 mV *vs* NHE, a value that is in good agreement with the reduction potentials observed for myoglobin. Also consistent with the proposed heme axial ligation, the reduction potential of the mutant measured in the presence of imidazole, is –90 mV *vs* NHE. This value is in good agreement with the E° measured for the bis-histidine coordinated OM cytochrome b_5, –102 mV [30], implying that His-39 coordinates in the proximal site and exogenous imidazole coordinates in the distal pocket. It is important to note, however, that the electronic spectrum of the reduced species (Fig 1a) shows well resolved α- and β-bands at 558 and 528 nm, respectively, and a Soret band at 424 nm. This spectrum is indicative of a low-spin Fe^{2+} species, hence indicating that, upon reduction, the heme is coordinated by His-39 and by Met-63.

Conclusive evidence indicating that Met-63 does not coordinate the heme in the ferric mutant was obtained from NMR spectroscopic studies performed with ^{13}C-methyl methionine- labeled protein. The ^{1}H and ^{13}C chemical shifts arising from the methyl groups in all four Met residues of the ferric H63M mutant resonate in their expected

diamagnetic region, 13.0–17.0 ppm for ^{13}C and 1.80–2.90 ppm for ^{1}H (Figs 3 and 4). Coordination of Met-63 to the ferric ion of the heme should result in the observation of contact shifts for the ^{1}H and ^{13}C nuclei in the methyl group of Met-63. These contact shifts are a consequence of unpaired electron density originating from the ferric ion which is delocalized into the methionine side chain via the S–Fe coordinative bond. In fact, this is observed in the case of cytochrome c, where the Met-70 methyl protons resonate at –21 ppm [30]. In summary, the evidence discussed above indicates that the ferric mutant is coordinated by His-39 in the proximal side and by water in the distal side, whereas the corresponding ferrous species appears to be coordinated by His-39 and Met-63.

ii). Coupled Oxidation of Heme

Heme catabolism is carried out by the enzyme heme oxygenase (HO) via the NADPH-dependent cleavage of heme to biliverdin and carbon monoxide [41]. The heme oxygenase reaction proceeds via a sequential mechanism in which catalytic turnover of HO requires NADPH-cytochrome P450 reductase as a source of reducing equivalents and molecular oxygen [41–44]. The catalytic cycle of heme oxygenase (Fig 11) parallels that of cytochrome P450 in that an oxyferrous complex is formed which accepts a second electron from cytochrome P450 reductase in order to form an activated oxidizing species [45]. The activated oxidizing species in HO adds a hydroxyl to the heme α-meso position, thus producing α-hydroxyheme [46], which undergoes a subsequent O_2-dependent elimination of the hydroxylated α-meso carbon as CO, with the concomitant formation of α-verdoheme (Fig 11). Finally, α-verdoheme is cleaved in an NADPH- and

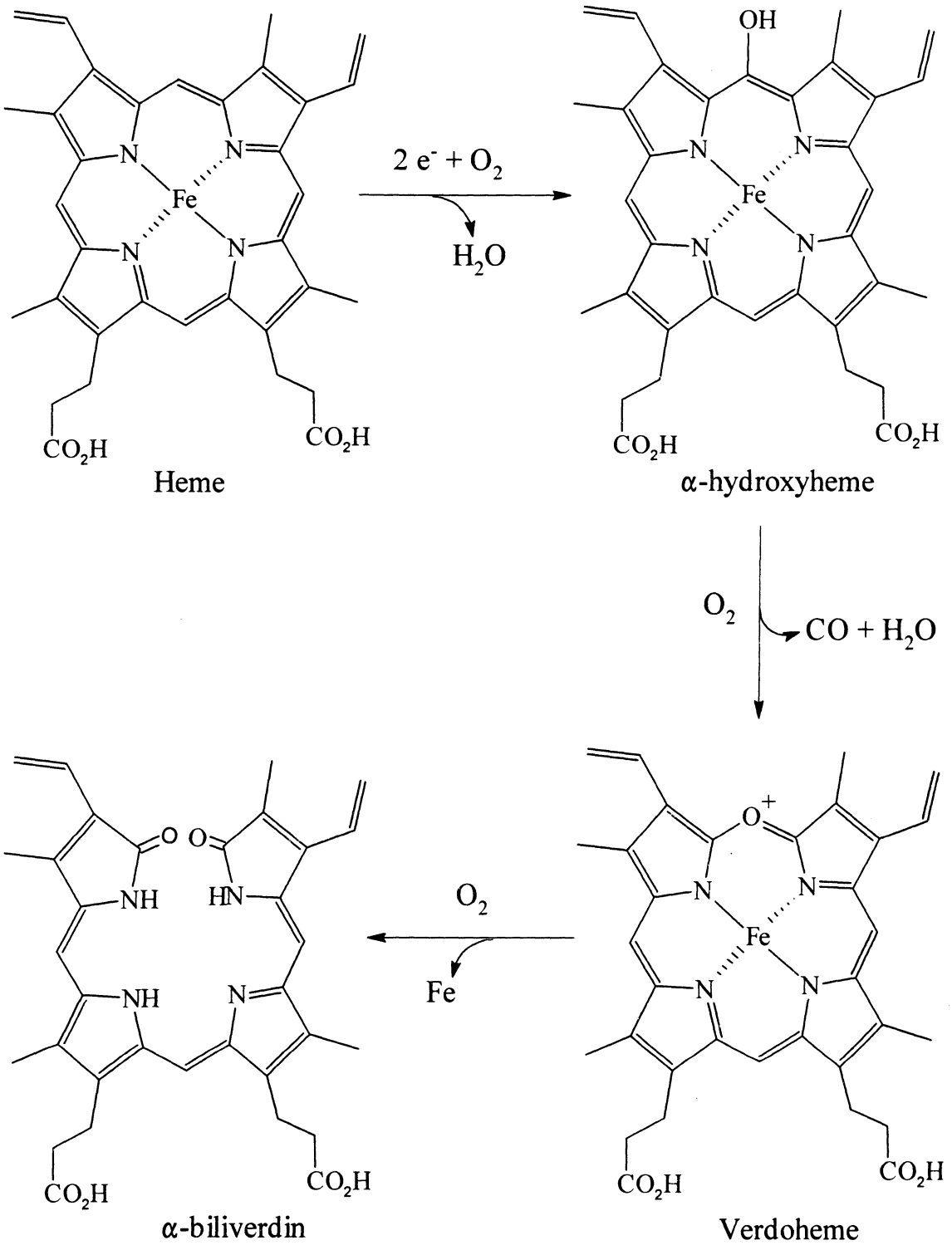

Figure 11. Schematic representation of the reaction pathway for the conversion of iron-protoporphyrin IX into biliverdin by the enzyme heme oxygenase.

O_2-dependent manner to produce α-biliverdin [23, 47]. A related reaction is that of coupled oxidation, in which heme is reacted with a reducing agent, usually ascorbate or hydrazine, and molecular oxygen [48]. The coupled oxidation of heme produces biliverdin via the formation of intermediate species such as α-hydroxyheme and verdoheme, as shown in Fig 11 for the reaction catalyzed by HO. Whereas the coupled oxidation of free heme in aqueous pyridine produces a random mixture of four biliverdin isomers, the coupled oxidation of heme in heme proteins is regioselective. For example, coupled oxidation of heme in myoglobin yields almost exclusively α-biliverdin, whereas human hemoglobin yields 60% α-biliverdin, and 40% β-isomer [14, 35, 49]. Incubation of the H63M mutant of OM cytochrome b_5 with ascorbate results in the formation of >90% α-verdoheme, as demonstrated by its electronic spectrum (Fig 8a), by electrospray mass spectrometry (Fig 9a) and by HPLC analysis (Fig 10a).

It has been established that the activation of oxygen that leads to coupled oxidation or heme oxygenation is initiated by the formation of a ferrous oxy-complex (Fe^{2+}-O_2) [45], in which a molecule of oxygen binds to the heme iron in the distal site of pentacoordinated proteins such as myoglobin, hemoglobin and the enzyme heme oxygenase. It is therefore noteworthy that although the ferrous H63M mutant is coordinated by two axial ligands (His-39 and Met-63), it is still capable of activating oxygen to perform the coupled oxidation of heme. The formation of an oxy-ferrous species in the H63M mutant can be envisioned to occur via two possible pathways: (a) reduction of the ferric species followed by the formation of an Fe^{2+}-O_2 complex (Equations 1 and 2) or, (b) reduction of the ferric mutant with the concomitant formation of the His-Met coordinated species (Equations 1 and 3), followed by displacement of Met-63 by O_2 to form the oxy-ferrous complex (Equation 4). The electronic spectrum of

the ferrous mutant, where the heme iron is coordinated by His and Met, or by His and O_2, should display α and β bands. In order to elucidate whether the Fe^{2+}–O_2 species or the His-Met-coordinated ferrous species gives rise to the spectrum observed upon reduction of the mutant with ascorbate under aerobic conditions, the ferric mutant was reduced in the absence of oxygen in a glove box. The electronic spectrum obtained from the sample reduced in the glove box was found to be identical to the spectrum obtained when an air saturated solution of the mutant was reduced with sodium dithionite (Fig 1a). This indicates that the electronic spectrum observed when the mutant is reduced with ascorbate under aerobic conditions corresponds to the His-Met-coordinated species, and not to the Fe^{2+}–O_2 species. Consequently, the formation of the oxy-ferrous species that leads to coupled oxidation of the heme in the H63M mutant may follow the path described by equations 1, 3 and 4, where the displacement of the axial methionine ligand by O_2 (Equation 4) may be the rate limiting step in oxygen activation by the H63M mutant of OM cytochrome b_5.

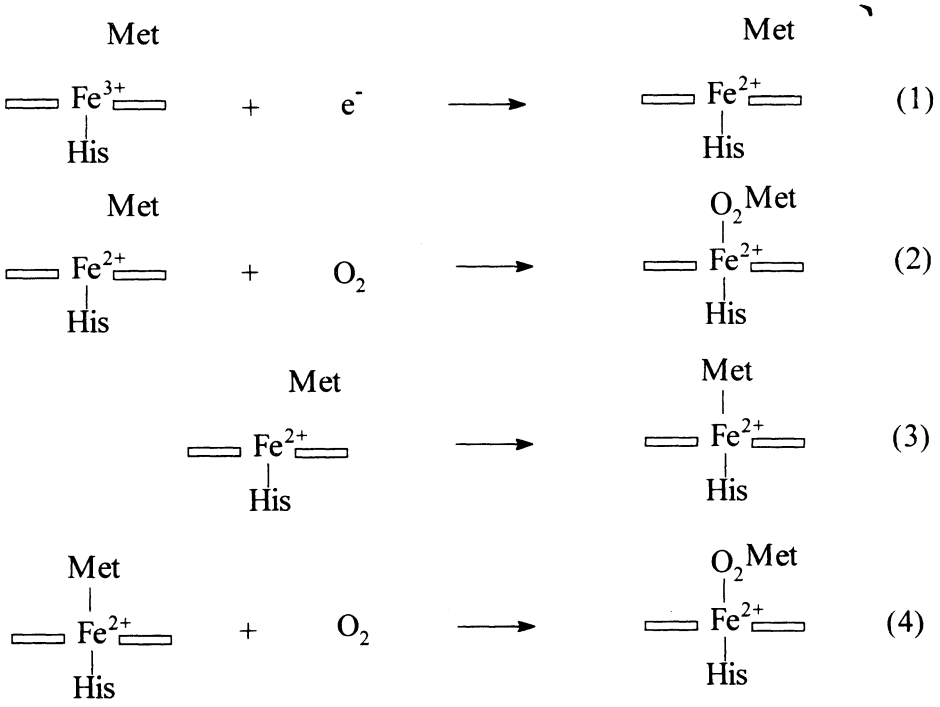

The formation of verdoheme and not iron-biliverdin upon coupled oxidation of the heme in the H63M mutant may arise from the formation of a hexacoordinated (His-Met) ferrous-verdoheme-protein complex. The formation of a hexacoordinated species can be inferred from the electronic spectrum arising from the product obtained by incubating the H63M mutant with a 100-fold excess of ascorbate (Fig 12a). This spectrum displays a band at 660 nm, which is almost identical to the one observed in the electronic spectrum of the ferrous pyridine hemochrome of verdoheme [33]. By comparison, the electronic spectrum of the ferrous pentacoordinated verdoheme in heme oxygenase displays a band at 690 nm [46]. These observations suggest that molecular oxygen cannot readily displace Met-63 from its coordination site on verdoheme, hence arresting the coupled oxidation reaction at the verdoheme stage. Consequently, the mechanism of inhibition for the oxidation of verdoheme to iron-biliverdin in the H63M mutant is similar to that observed for the turnover of the heme-heme oxygenase complex in the presence of carbon monoxide [50, 51], and is consistent with the proposal that further oxygenation of verdohemochrome to iron-biliverdin occurs only with penta-coordinated verdoheme complexes [52]. In a similar fashion, ligands that bind both the fifth- and sixth-coordination sites of verdoheme with relatively high affinity inhibit the formation of biliverdin from verdoheme [47].

Additional evidence for the relatively strong coordination bond formed between Met-63 and the verdoheme iron was obtained from a solution containing the product formed upon incubating the H63M mutant with ascorbate. The electronic spectrum of the reaction product, H63M–verdoheme complex, is shown in Fig 12a. When this solution was saturated with CO, the band at 660 nm decreased in intensity, with a concomitant increase in the intensity of a new band at 635 nm (Fig 12b). The latter arises from

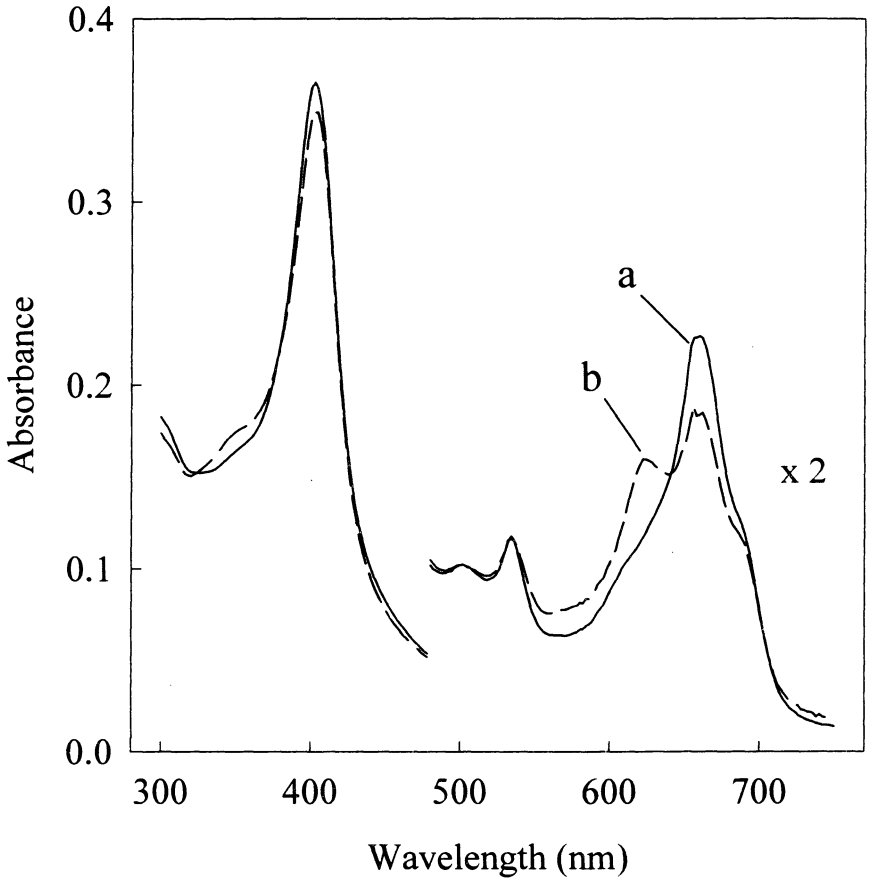

Figure 12. UV-Vis absorption spectra obtained from the product of the coupled oxidation reaction of the heme in the H63M mutant (a) before, and (b) after saturating the solution with carbon monoxide. Adapted from reference 27.

verdoheme coordinated by His-39 and CO [46, 49, 50]. It is noteworthy that the band at 660 does not disappear completely upon saturating the solution with CO for 20 min. However, when air is bubbled to displace the carbon monoxide, the band at 635 disappears and the intensity of the band at 660 nm increases to yield the original spectrum (Fig 12a). By comparison, when a solution of the ferrous H63M mutant (Fig 1a) was bubbled with CO, the carbonmonoxy complex (Fig 1b) is formed immediately. These observations taken together imply that Met-63 can be displaced by O_2 from its coordination site on the ferrous heme, forming the oxy-ferrous complex that leads to coupled oxidation, as shown schematically by equations 1, 3, and 4. On the other hand, Met-63 coordinated to the verdoheme iron in the H63M mutant is not readily displaced by CO. Consequently, it is likely that Met-63 cannot be displaced by O_2 from its coordination site on verdoheme, which is consistent with the fact that the coupled oxidation of heme in the H63M mutant is arrested at the verdoheme stage.

Conclusion

Heme oxygenase catalyzes the NADPH- and cytochrome P450 reductase-dependent oxidation of heme to biliverdin and carbon monoxide [41]. It has been proposed that carbon monoxide generated by the heme oxygenase system functions as an important second-messenger molecule [53, 54]. Therefore, the detailed understanding of the mechanism by which heme oxygenase converts heme to biliverdin is of important physiological relevance. Although several important advances have been made toward the understanding of the mechanism by which heme oxygenase activates heme, important issues such as the details of oxygen activation are not fully resolved yet. Furthermore, it

has been suggested that the mechanism of oxygen activation displayed by heme oxygenase appears to be different from the mechanism displayed by cytochromes P450 and peroxidases [51, 55, 56]. Additional progress in this area has been difficult due to the lack of a three dimensional structure for heme oxygenase. It has also been proposed that understanding the detailed mechanistic aspects of the coupled oxidation reaction performed by myoglobin and other heme-containing proteins is likely to shed light into the details of oxygen activation performed by heme oxygenase [14]. The evidence presented here indicates that further research with the H63M and related mutants of OM cytochrome b_5 may provide important insights related to the mechanistic aspects of heme oxygenation performed by heme oxygenase. In comparison to other heme-containing proteins known to undergo coupled oxidation, the heme in cytochrome b_5 is largely exposed to the aqueous environment. In addition, the heme-binding affinity exhibited by the H63M mutant appears to be lower than that exhibited by the wild type protein. These structural properties compare well with those postulated for the active site of heme oxygenase, which is thought to bind heme with lower affinity and with larger exposure to the aqueous environment than observed for most heme-containing proteins.

References

1. Ortiz de Montellano, P. A. (1987) *Acc. Chem. Res.* 20, 289-294.
2. Raphael, A. L., and Gray, H. B. (1989) *Proteins: Struct. Funct. Genet.* 6, 338-340.
3. Raphael, A. L., and Gray, H. B. (1991) *J. Am. Chem. Soc.* 113, 1038-1040.
4. Lloyd, E., Hildebrand, D. P., Tu, K. M., and Mauk, A. G. (1995) *J. Am. Chem. Soc.* 117, 6434-6438.
5. Barker, P. D., Nerou, E. P., Cheesman, M. R., Thomson, A. J., Oliveira, P., and Hill H. A. O. (1996) *Biochemistry* 35, 13618-13626.
6. Barrick D. (1994) *Biochemistry* 33, 6546-6554.
7. Adachi, S., Nagano, S.. Watanabe, Y., Ishimori, K., and Morishima, I. (1991) *Biochem. Biophys. Res. Commun.* 180, 138-144.
8. Adachi, S., Nagano, S., Ishimori, K., Watanabe, Y., Morishima, I., Egawa, T., Kitagawa, T., and Makino, R. (1993) *Biochemistry* 32, 21-252.
9. Mus, I., Dolla, A., Guerlesquin, F., Payan, F., Czjek, M., Haser, R., Bianco, P., Haladjian, J., Rapp, B. J., Wall, J. D., Voordouw, G., and Bruschi, M. (1992) *J. Biol. Chem.* 267, 16851-16858.
10. Ferrer, J. C., Guillemette, J. G., Bogumil, R., Inglis, S. C., Smith, M., and Mauk, A. G. (1993) *J. Am. Chem. Soc.* 115, 7507-7508.
11. Dolla, A., Florens, L., Bianco, P., Haladjian, J., Voordouw, G., Forest, E., Wall, J., Guerlesquin, F., and Bruschi, M. (1994) *J. Biol. Chem.* 269, 6340-6346.
12. Thodorakis, J. L., Barber, E. A. E., McCracken, J., Peisach, J., Schejter, A., and Margoliash, E. (1995) *Biochim. Biophys. Acta* 1252, 103-113.

13. Schejter, A., Galia, T., Navon, G., Liu, X. J., and Margoliash, E. (1996) *J. Am. Chem. Soc.* 118, 477-478.

14. Hildebrand, D. P., Tang, H., Luo, Y., Hunter, C. L., Smith, M., Brayer, G. D., and Mauk, A. G. (1996) *J. Am. Chem. Soc.* 118, 12909-12915.

15. Doherty, A. J., Ashford, S. R., Brannigan, J. A., and Wigley, D. B. (1995) *Nucl. Acids Res.* 23, 2074-2075.

16. Rodríguez-Marañón, M. J., Qiu, F., Stark, R. E., White, S. P., Zhang, X., Foundling, S. I., Rodríguez, V., Schilling III, C. L., Bunce, R. A., and Rivera, M. (1996) *Biochemistry* 35, 16378-16390.

17. One liter of minimal media consisted of the following: $Na_2HPO_4 \cdot 7H_2O$ (47.7 mM), KH_2PO_4 (22.0 mM), NaCl (8.55 mM), NH_4Cl (18.7 mM), nitrilotriacetic acid (1.00 mM), $MgSO_4$ (2.00 mM), $CaCl_2$ (0.100 mM), $(NH_4)_6Mo_7O_{24} \cdot 4H_2O$ (0.150 μM), $FeSO_4 \cdot 7H_2O$ (40.0 μM), EDTA (17.0 μM), $CuSO_4 \cdot 5H_2O$ (3.00 μM), $Co(NO_3) \cdot 6H_2O$ (2.00 μM), $ZnSO_4 \cdot 7H_2O$ (7.60 μM), $Na_2B_4O_7 \cdot 10H_2O$ (9.40 μM), ampicillin (0.270 mM), D-(+)-glucose (27.7 mM), and L-methionine (0.268 mM).

18. Rivera, M., and Walker, F. A. (1995) *Anal. Biochem.* 230, 295-302.

19. de Duve, C. (1948) *Acta Chem. Scand.* 2, 264-269.

20. (a) Summers, M. F., Marzilli, L. G., and Bax, A. (1986) *J. Am. Chem. Soc.* 108, 4285; (b) Kupće, E., and Freeman, R. (1995) *J. Magn. Reson.* 115A, 273.

21. Rivera M., Seetharaman, R., Girdhar, D., Wirtz, M., Zhang, X., Wang, X., and White, S. (1998) *Biochemistry* 37, 1485-1494.

22. Walker, F. A., Emrick, D., Rivera, J. E., Hanquet, B. J., and Buttlaire, D. H. (1988) *J. Am. Chem. Soc.* 110, 6234-6240.

23. Saito, S., and Itano, H. A. (1982) Proc. *Natl. Acad. Sci.* 79, 1393-1397.

24. O'Carra, P., and Colleran, E. (1970) *J. Chromatog.* 50, 458-468.

25. Torpey, J., and Ortiz de Montellano, P. R. (1996) *J. Biol. Chem.* 271, 26067-26073.

26. Rodríguez, J. C., Desilva, T., and Rivera, M. (1998) *Chem. Lett.* 353.

27. Rodríguez, J. C. and Rivera, M. (1998) *Biochemistry* 37, 13082-13090.

28. (a) Keller, R. M., & Wütrhrich, K. (1980) *Biochim. Biophys. Acta* 621, 204; (b) La Mar, G. N., Burns, P. D., Jackson, J. T., Smith, K. M., Langry, K. C. and Strittmatter, P. (1981) *J. Biol. Chem.* 256, 6075-6079.

29. Rivera, M., Barillas-Mury, C., Christensen, K. A., Little, J. W., Wells, M. A., and Walker, F. A. (1992) *Biochemistry* 31, 12233-12240.

30. Rivera, M., Wells, M. A., and Walker, F. A. (1994) *Biochemistry* 33, 2161-2170.

31. Hildebrand, D. P., Burk, D. L., Maurus, R., Ferrer, J. C., Brayer, G. D., and Mauk, A. G. (1995) *Biochemistry* 34, 1997-2005.

32. Varadarajan, R., Zewert, T. E., Gray, H. B., Boxer, S. G. (1989) *Science* 243, 69-72.

33. Lagarias, J. C. (1982) *Biochim. Biophys. Acta* 717, 12-19.

34. Petryka, Z., Nicholson, D. C., and Gray, C. H. (1962) *Nature* 194, 104.

35. O'Carra, P., and Colleran, E. (1969) *FEBS Lett.* 5, 295-298.

36. Sligar, S. G., and Egeberg, K. (1987) *J. Am. Chem. Soc.* 109, 7896-7897.

37. Rodgers, K. K., and Sligar, S. G. (1991) *J. Am. Chem. Soc.* 113, 9419.

38. Beck von Bodman, S., Schuler, M. A., Jollie, D. R., and Sligar, S. G. (1986) *Proc. Natl. Acad. Sci.* 83, 9443-9447.

39. Antonini, E. and Brunori, M. In *Hemoglobin and Myoglobin in their Reactions with Ligands*; Neuberger, A., and Tatum, E. L., Eds.; North Holland Publishing

Co.: Amsterdam, 1971; pp 13-39.

40. Feng, Y., Roder, H., and Englander, S. W. (1990) *Biophys. J.* 57, 15-22.

41. Tenhunen, R., Marver, H. S., and Schmid, R. (1969) *J. Biol. Chem.*, 244, 6388-6394.

42. Brown, S. B., and King, R. F. G. (1976) *Biochem. Soc. Trans.* 4, 197-201.

43. Yoshida, T. and Kikuchi, G. (1978) *J. Biol. Chem.* 253, 4224-4229.

44. Yoshida, T. and Kikuchi, G. (1978) *J. Biol. Chem.* 253, 4230-4236.

45. Yoshida, T., Noguchi, M., and Kikuchi, G. (1980) *J. Biol. Chem.* 255, 4418-4420.

46. Liu, Y., Moënne-Loccoz, P., Loehr, T. M., and Ortiz de Montellano, P. R. (1997) *J. Biol. Chem.* 272, 6909-6917.

47. Yoshida, T. and Noguchi, M. (1984) *J. Biochem.* 96, 563.

48. Brown, S. B., Chabot, A. A., enderby, E. A., & North, A. C. T. (1981) *Nature* 289, 93-95.

49. Brown, S. B. (1976) *Nature* 159, 23-27.

50. Yoshida, T., Noguchi, M., and Kikuchi, G. (1980) *J. Biochem.* 88, 557-563.

51. Wilks, A., and Ortiz de Montellano, P. R. (1993) *J. Biol. Chem.* 268, 22357-22362.

52. Sano, S., Sano, T. Morishima, I., Shiro, Y., and Maeda, Y. (1986) *Proc. Natl. Acad. Sci. USA* 83, 531-535.

53. Verma, A., Hirsch, D. J., Glatt, C. E., Ronnett, G. V., and Snyder, S. H. (1993) *Science* 259, 381.

54. (a) Maines, M. D. (1997) *Annu. Rev. Pharmacol. Toxicol.* 37, 517-554; (b) Maines, M. D. (1993) *Mol. Cell. Neurosci.* 4, 389-397.

55. Takahasi, S., Ishikawa, K., Takeuchi, N., Ikeda-Saito, M., Yoshida, T. and

Rousseau, D. (1995) *J. Am. Chem. Soc.* 117, 6002-6006.

56. Hernández, G., Wilks, A., Paolesse, R., Smith, K. M., Ortiz de Montellano, P. R., and La Mar, G. (1994) *Biochemistry* 33, 6631-6641.

CHAPTER III

INFLUENCE OF THE POLYPEPTIDE MOIETY ON THE EFFICIENCY AND REGIOSELECTIVITY OF THE COUPLED OXIDATION REACTION PERFORMED BY AXIAL LIGAND MUTANTS OF MITOCHONDRIAL CYTOCHROME b_5

Introduction

In mammalian cells the degradation of heme into biliverdin, CO, and free iron is catalyzed by the enzyme heme oxygenase [1]. Until relatively recently, the products of heme oxygenase (HO) activity were considered to be toxic waste material; more recently, however, CO has been implicated in signal transduction and communication [2], and biliverdin is the source of bilirubin, a powerful antioxidant. Important progress toward the understanding of HO activity has been accomplished by the successful bacterial expression of a soluble fragment of the enzyme [3, 4]. For example, it is now known that the heme environment in the heme complex of HO is similar to the one in myoglobin in that the prosthetic group is coordinated by a proximal non-ionized, non-hydrogen bonded histidine residue, and by a water molecule in the distal site [5, 6]. It is therefore interesting that the proximal site in the heme-HO complex resembles more that of myoglobin than those of oxygen activating species such as peroxidases or cytochrome P450.

It has been proposed that in HO, the ineffectiveness of the neutral histidine ligand as an electron donor may contribute to channeling the activation of oxygen toward heme oxygenation, rather than ferryl formation. In fact, on the basis of the type of reactions exhibited by the heme-HO complex with hydrogen peroxide and alkyl hydroperoxides, a protonated ferric peroxide intermediate (Fe^{3+}-OOH) has been proposed as the species that reacts with the heme prosthetic group [4, 7]. Although important mechanistic aspects regarding the heme oxygenation reaction performed by HO are understood (recently reviewed by Ortiz de Montellano) [8], important factors are still unresolved. For example, it is not clear how the regioselectivity of heme oxygenation is controlled by the enzyme; or what are the detailed structural requirements possessed by HO responsible for channeling oxygen activation toward heme oxygenation, rather than oxyferryl formation. On the basis of resonance Raman spectroscopic studies, it has been suggested that the Fe-O-O angle in the ferric peroxide intermediate of HO is bent, presumably as a consequence of steric interactions in the distal pocket [9]. On the other hand, it has also been proposed, on the basis of EPR spectroscopic studies, that the Fe-O-O tilt originates of the formation of a hydrogen bond with a yet unidentified residue in the distal pocket of HO [10].

A complementary way of gaining insight into the factors channeling oxygen activation toward heme oxygenation is to study the process known as coupled oxidation. It is known that the coupled oxidation of the heme in myoglobin produces almost exclusively α-biliverdin, whereas the coupled oxidation of the heme in human hemoglobin produces 60% and 40% of the α- and β- isomers, respectively [11, 12]. In contrast, the coupled oxidation of the pyridine hemochrome in aqueous solutions produces a random mixture of four biliverdin isomers [13], underscoring the importance

that the polypeptide environment plays in dictating the regioselectivity of the reaction. More recently, it was reported that upon replacement of His-63, an axial ligand in OM cytochrome b_5, the electron transfer protein was converted into a species capable of performing the coupled oxidation of its heme [14]. The coupled oxidation of the heme in the H63M variant of OM cytochrome b_5 is arrested at the verdoheme stage and produces >90% of the α-isomer. In comparison to other heme-containing proteins known to oxygenate their heme, the heme in OM cytochrome b_5 is largely exposed to the aqueous environment [15] and the heme binding affinity exhibited by its H63M variant is lower than that exhibited by the wild-type protein. These properties compare favorably with those postulated for the active site of HO, which is thought to bind heme with lower affinity and with larger exposure to the aqueous environment than observed for most hemoproteins [5, 16].

In the present study, it is demonstrated that the replacement of His-63 for Val in OM cytochrome b_5 produces a species capable of oxygenating its heme approximately 15-fold faster than its H63M counterpart, in order to produce a 50% mixture of α- and γ-verdoheme isomers. The formation of verdoheme as the final product of heme oxygenation is surprising since the H63V variant of OM cytochrome b_5 does not possess a ligand capable of coordinating the verdoheme moiety in order to arrest the coupled oxidation reaction at this step. The results obtained from these studies also indicate that the regioselectivity of the coupled oxidation in OM cytochrome b_5 is controlled by steric interactions between the heme-bound oxygen and side chains in the distal pocket.

Experimental Procedures

i). Site-Directed Mutagenesis, Protein Expression and Purification

The H63V variant was obtained by performing site-directed mutagenesis on the gene coding for wild-type OM cytochrome b_5 utilizing methods described previously [14]. The H63V variant of OM cytochrome b_5 was expressed in *E. coli* BL21-DE3 cells according to the protocol previously described for the WT protein [17, 18]. The *E. coli* cells were incubated for 3 h after inducing polypeptide biosynthesis and subsequently harvested by centrifugation as described previously [17]. The absence of a pink color in the harvested cells indicated that the H63V variant does not incorporate heme during its bacterial expression. Cell debris was separated by ultracentrifugation and the supernatant containing the apoprotein was transferred to a beaker where imidazole and $K_3Fe(CN)_6$ were added to a final concentration 1.0 mM and 2.0 mM, respectively. In order to reconstitute the apo H63V variant with heme, increments (0.5 mL) of a heme-containing solution (1 mg/mL) were added to the solution containing the apo-peptide while the mixture was kept at 4°C with constant but gentle stirring. The formation of the H63V-heme complex was manifested by the gradual increase in the intensity of the Soret band (412 nm), which followed each addition of hemin solution. A total of 1.5 mL, added over a period of 24 h, was typically necessary before the intensity of the Soret band remained constant. Purification by ion-exchange and size exclusion chromatography was carried out as described previously for the H63M variant of OM cytochrome b_5 [14].

ii). Characterization of the Product of Coupled Oxidation

Coupled oxidation reactions were carried out at room temperature with solutions containing 10 μM of the H63V variant (ϵ_{404} = 159 $mM^{-1}cm^{-1}$) in 0.40 mL of 50 mM phosphate buffer, pH 7.0. The reaction was initiated by the addition of less then a mg of sodium dithionite (powder) to a solution of the H63V variant, previously saturated with air. The reaction was monitored by UV-Vis spectrophotometry until the intensity of the Soret band was almost indiscernible in the electronic spectrum. The resultant solution was extracted with a solution of pyridine in chloroform, as described previously [14] and the organic phase was analyzed by UV-Vis spectroscopy and electrospray mass spectrometry. Electrospray mass spectrometric analysis was performed on a Quattro II triple quadrupole mass spectrometer of QhQ geometry (Micromass, Inc. Beverly, MA). The chloroformic solution containing the product of the reaction was introduced into the mass spectrometer via direct infusion (2 μL/min) with the aid of a pneumatically-assisted electrospray interface. Capillary voltages were maintained at 3.3 kV with a nozzle/skimmer voltage drop of 8 eV. Pressure of the argon collision gas was maintained at 5.0 x 10^{-3} mb. Scans were collected in profile mode from 300 to 900 m/z at 1600 points/sec, using 16 points/Da.

iii). Hydrolysis of Verdoheme and Analysis by HPLC

The regioselectivity of the coupled oxidation reaction carried out by the H63V variant of OM cytochrome b_5 was determined by analyzing the reaction products with the aid of HPLC. In brief, verdoheme was extracted from the coupled oxidation reaction mixtures with a solution of pyridine in chloroform. The chloroformic solution was dried over anhydrous sodium sulfate, the solvent evaporated to dryness under a stream of argon, and the resultant solid was immediately redissolved in 2 mL of a

saturated solution of methanolic KOH. The basic solution was allowed to stand for 5 min at room temperature before pouring it into 40 mL of 3.0 M HCl. The resultant solution was then extracted with chloroform, the organic phase dried over anhydrous sodium sulfate, and the solvent evaporated under reduced pressure. Finally, the solid was redissolved in 5 mL of 5% sulfuric acid in methanol, in order to obtain the dimethyl ester derivatives of biliverdin. The solution containing the biliverdin dimethyl ester was injected into a Waters μ Bondapak C18 column (3.9 mm x 300 mm) and separated by isocratic elution with a mixture 20:80 consisting of methanol:methanol/water (75/25).

iv). Preparation of the H63V Variant Containing ^{13}C-Labeled Heme

^{13}C-labeled δ-aminolevulinic acid (ALA) was used to prepare ^{13}C-labeled hemes incorporated into OM cytochrome b_5. Details of the biosynthetic method have been published elsewhere [18, 19]. OM cytochrome b_5 labeled with ^{13}C at the heme active site was purified to homogeneity utilizing the method described by Rivera and Walker [18]. The choice of ALA used as a heme precursor dictates the labeling pattern obtained in the ^{13}C-labeled heme [18, 19]. For the purposes of this investigation [1,2-^{13}C]-ALA was utilized to obtain heme labeled at the four methyl groups, whereas [5-^{13}C]-ALA was utilized to prepare heme labeled at the four meso carbon atoms. The ^{13}C-labeled heme was extracted from the wild-type protein and then used to reconstitute the apo form of the H63V variant. To this end, a solution of wild-type OM cytochrome b_5 in 50 mM phosphate buffer, pH 7.0 was concentrated to a volume of approximately 1.0 mL. Pyridine (1.0 mL) was added to the protein solution and the resultant mixture was extracted with 10.0 mL of chloroform by shaking vigorously until an emulsion was formed. The emulsion was centrifuged at 5,000 rpm for 2 min and the organic phase

(red) was dried over anhydrous sodium sulfate. The extraction procedure was repeated until the resultant organic phase was almost completely devoid of color after the centrifugation step. The solution containing the pyridine hemochrome in chloroform was concentrated under reduced pressure and the solvent evaporated to dryness under a stream of argon. The resultant solid was immediately dissolved in 0.10 M NaOH and the pH adjusted to 8.0 with 0.10 M HCl.

The apo form of the H63V variant was obtained by passing a solution of the holo-H63V variant through an ion-exchange chromatography column previously equilibrated with 10.0 mM potassium phosphate buffer, pH 5.4 at 4 °C. This procedure was based on our previous observations that the heme in the H63M variant of OM cytochrome b_5 releases its heme when eluted from an ion exchange column [14]. This particular behavior was also exhibited by the H63V variant and provided us with an ideal method for preparing the apoprotein in the absence of organic solvents that could compromise the integrity of the apopeptide. Elution of the apoprotein from a DE-52 ion exchange column was accomplished by application of a linear salt gradient (0-0.5 M NaCl). Fractions eluting from the column were monitored spectrophotometrically at 280 nm and 406 nm. All fractions exhibiting absorption exclusively at 280 nm were pooled and then dialyzed against 50 mM potassium phosphate buffer (pH 7.0) containing 1 mM imidazole. The solution containing pure apo-H63V variant was then reconstituted with ^{13}C-labeled heme previously extracted from wild-type cytochrome b_5 by incubating the mixture overnight at 4 °C. The resultant holoprotein was subsequently loaded onto a size-exclusion chromatography column (Sephadex G-50) in order to eliminate excess heme.

v). NMR Spectroscopy

NMR spectra were collected at 4.0 °C on a Varian Unity Innova NMR spectrometer operating at ^{1}H and ^{13}C spectrometer frequencies of 598.71 MHz and 150.55 MHz, respectively. Typically, experiments were carried out on samples containing 1.5–2.0 mM protein and 1 equivalent of imidazole in 600 μL of perdeuterated phosphates buffer (μ = 0.100 M, pH 7.0; not corrected for the isotope effect). One-dimensional ^{1}H spectra were acquired over a 32 kHz spectral width, with an acquisition time of 30 ms and water presaturation during the 400 ms relaxation delay. Proton coupled ^{13}C NMR spectra were acquired over a 53 kHz spectral width, with an acquisition time of 100 ms and a 300 ms relaxation delay. ^{1}H spectra were referenced to the residual HDO peak at 4.70 ppm, whereas ^{13}C spectra were referenced against an external reference solution consisting of 30% of dioxane in D_2O. NOESY spectra were collected using a 60-ms mixing time and a spectral width of 32 kHz, with 156 scans for each of the 320 increments. Data were collected as an array of 320 x 2048 points, which after linear prediction in the t_1 dimension, and zero filling in both dimensions produced a 4096 x 4096 data matrix. Parameters and conditions used to collect the HMQC spectra appear in the corresponding figure caption.

vi). Computational Methods and Molecular Modeling

Computer models of the H63V and H63M mutants were obtained as follows: Coordinates corresponding to the crystal structure of OM cytochrome b_5 were retrieved from the Protein Data Bank (filename 1b5m) [15]. The coordinates were modified by extraction of the heme, deletion of crystallographic water molecules, addition of hydrogen atoms and addition of charges. Formal charges were assigned using the Gasteiger-Hückel method (Fe = +3, pyrrole nitrogens = −1, and each oxygen in the

propionate side chain = −0.5). The corresponding mutation, *i.e.* H63M, or H63V, was performed using the Biopolymer module in Sybyl 6.5. The program Flexidoc was then used in order to dock the heme into the OM cytochrome b_5 apopeptide and to calculate the model structures. In this process, all of the bonds in the peptide and those in the heme were allowed to be flexible, the seed number was chosen at random and the number of generations were set at 30,000, 60,000 and 100,000 in three distinct experiments.

Results

i) Protein Expression and Purification

The overexpression of wild-type OM cytochrome b_5 in *E. coli* BL21-DE3 cells imparts a noticeable pink color to the cells. In contrast, when the H63V variant of cytochrome b_5 was expressed, the pink color was absent from the cells. An UV-Vis spectrum obtained from the supernatant immediately after the *E. coli* cells had been lysed and the cell debris separated by ultracentrifugation displayed a band at 420 nm. The latter was tentatively attributed to originate from the presence of a small concentration of the ferrous-heme complex of the H63V variant. Addition of ferricyanide and imidazole to the supernatant produced a species displaying a band at 412 nm in its electronic spectrum, observations that are similar to those reported previously for the H63M variant of cytochrome b_5 [14, 20]. Subsequent addition of an aqueous solution of hemin, followed by incubation at 4 °C, produced a color change from yellow to red and a steady increase of intensity of the band at 412 nm. These observations clearly indicate that the H63V variant is recovered from the *E. coli* cells predominantly as the apoprotein, but that the holoprotein can be readily obtained by reconstituting the apo form with heme *in vitro*.

ii). Spectroscopic Characterization of the H63V Variant

The electronic absorption spectrum of the homogeneous H63V-heme complex is shown in Fig 1a. In general, the features of the spectrum originating from the ferric variant are very similar to those reported previously for its ferric H63M counterpart [14, 20], *i.e.* a Soret band at 404 nm and the high-spin marker band at 628 nm, characteristic of ferric hemoproteins possessing His as the proximal ligand [21]. The electronic spectrum of the H63V variant reduced with dithionite under anaerobic conditions is shown in Fig 1b. Bubbling CO to the resultant solution affords the spectrum shown in Fig 1d, which is identical to the spectrum originating from the CO complex of the H63M variant of OM cytochrome b_5 [14].

Addition of exogenous imidazole to a solution containing the ferric H63V variant resulted in the formation of a species with electronic (Fig 1c) and EPR spectra (g = 2.97, 2.26, and 1.44) characteristic of low-spin ferric hemoproteins [14].

iii). Coupled Oxidation

The coupled oxidation of the heme in the H63M variant of OM cytochrome b_5 in the presence of ascorbate as the sacrificial reducing agent was reported recently [14, 20]. By comparison, ascorbate cannot reduce the H63V variant, hence this reducing agent cannot be used to carry out the coupled oxidation of the heme in this variant. The addition of sodium dithionite to a solution containing the H63V variant previously saturated with air resulted in a rapid decrease in the intensity of the Soret band and the simultaneous appearance of a band at 660 nm (Fig 2). The appearance and time dependent behavior of the band at 660 nm in the electronic spectrum of the H63V variant

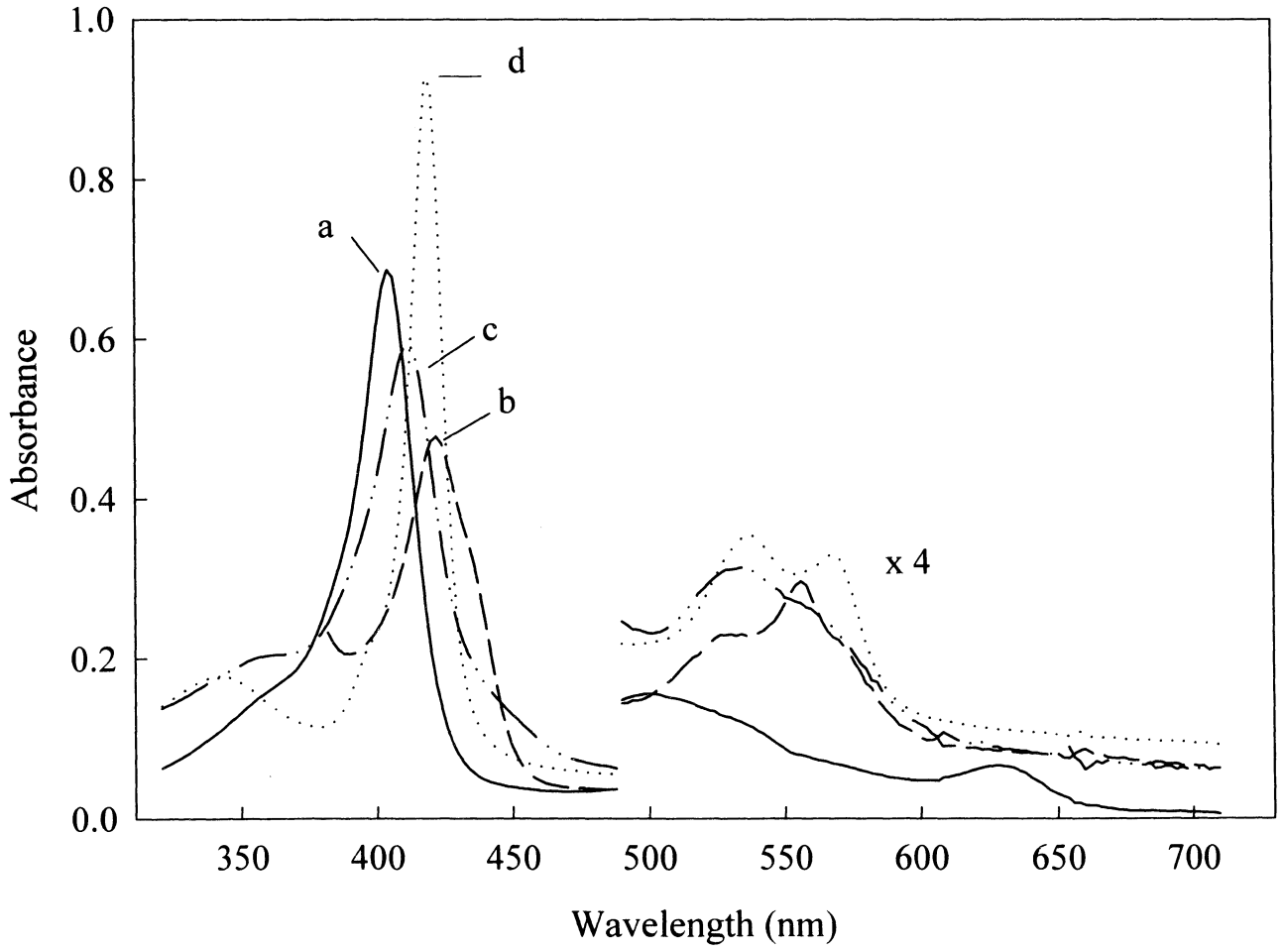

Figure 1. UV-Vis absorption spectra of the H63V mutant of OM cytochrome b_5. (a) Fe(III); (b) Fe(II); (c) Fe(III)-imidazole complex; (e) Fe(II)-CO complex.

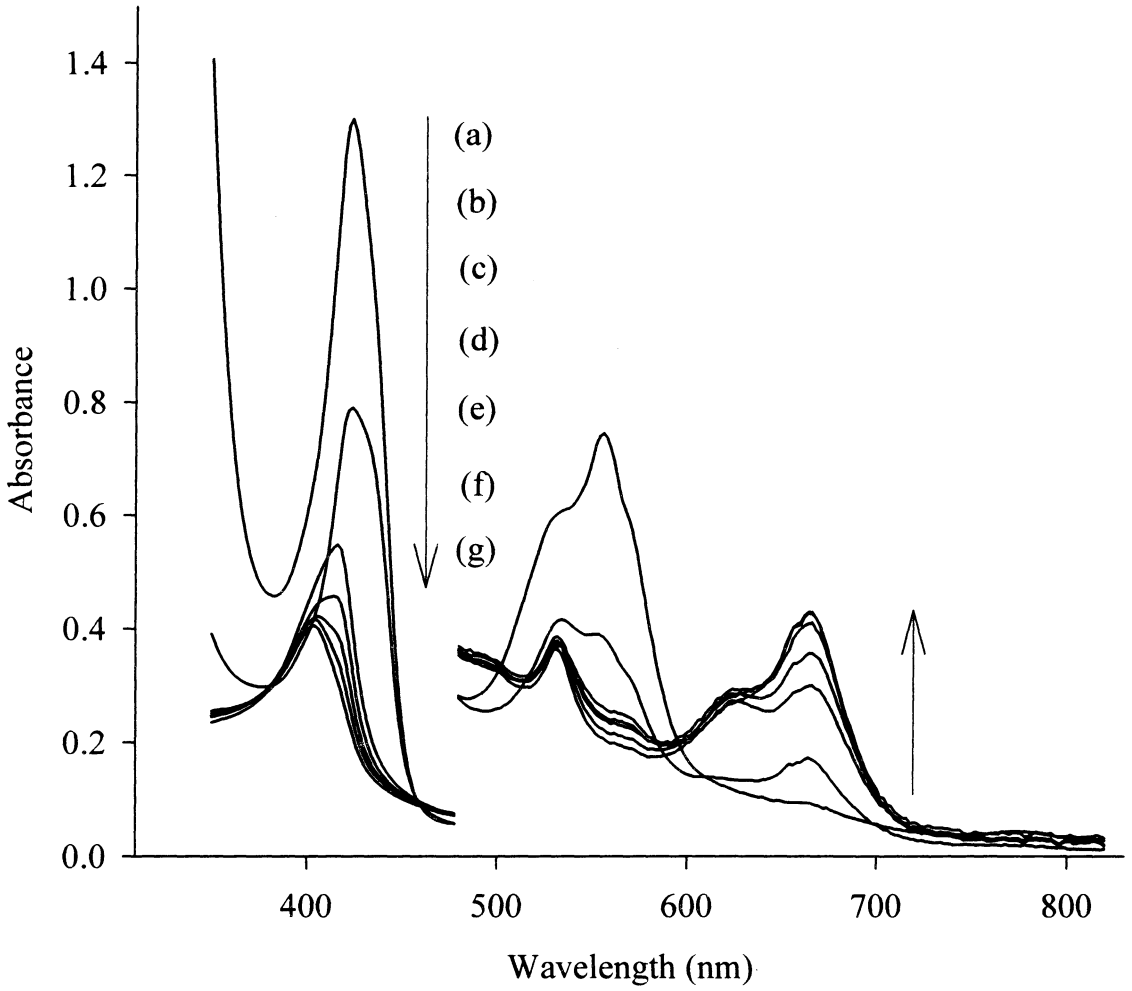

Figure 2. Changes in the UV-Vis absorption spectrum of the H63V mutant of OM cytochrome b_5 during the coupled oxidation of heme in the presence of sodium dithionite. (a) 3; (b) 11; (c) 16; (d) 21; (e) 26; (f) 32; and (g) 37 min after the addition of $Na_2S_2O_4$.

is similar to that reported for the coupled oxidation of the H63M mutant [14]. An important difference between the electronic spectra of the two mutants during the coupled oxidation reaction, however, is the absence of α and β bands in the electronic spectra obtained during the coupled oxidation of the heme in the H63V mutant (Fig 2). The presence of α and β bands in the electronic spectra obtained with the H63M mutant were attributed to the formation of a low-spin (His–Met coordinated) ferrous protein [14]. The distal pocket of the H63V mutant is devoid of side chains that can act as ligands to the heme-iron, hence explaining the absence of α and β bands that are characteristic of low spin ferrous hemes. In fact, the H63V mutant was designed with the expectation that the lack of a distal residue capable of coordinating to the ferrous heme iron would not compete with O_2 for the sixth coordination site, consequently accelerating the coupled oxidation of the heme in the H63V mutant with respect to its H63M counterpart. Evidence corroborating this idea is presented in Fig 3, where the changes in absorbance at 660 nm in the spectra obtained from a solution of protein undergoing the coupled oxidation reaction are plotted against the time course of the reaction. It is evident that the absence of a coordinative group in the distal site, and despite the fact that dithionite is an efficient O_2 scavenger, the coupled oxidation reaction of the heme in the H63V mutant is completed approximately fifteen-fold faster than that of the H63M mutant.

iv). Characterization of Verdoheme as the Product of Coupled Oxidation

The electronic spectrum obtained after the coupled oxidation reaction of the heme in the H63V mutant is complete (Fig 4a) is very similar to the reported for the pyridine hemochrome of verdoheme [22], hence suggesting that verdoheme is the product of the coupled oxidation reaction. Additional evidence corroborating this idea was

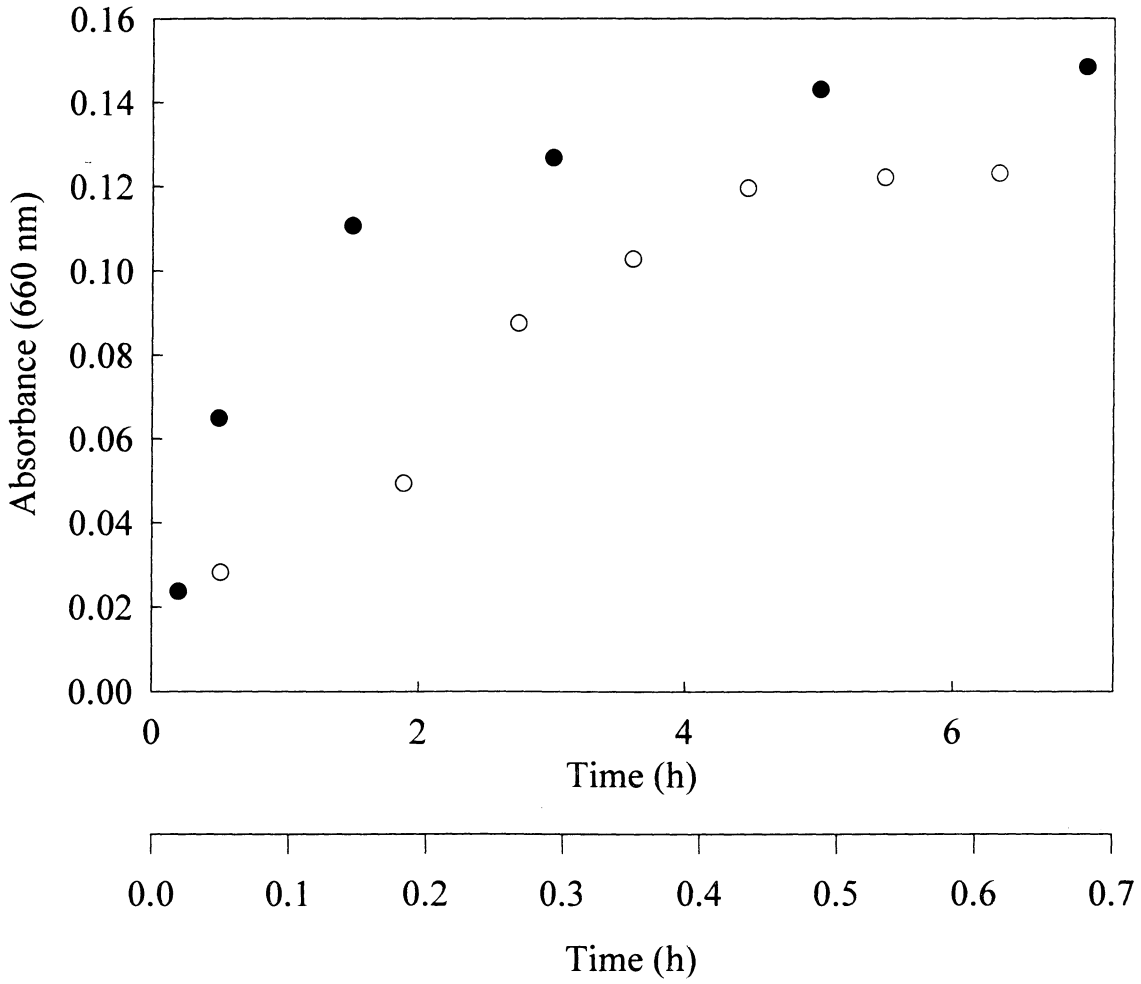

Figure 3. Change in the absorbance monitored at 660 nm for the H63M (solid circles) and H63V (open circles) mutants of OM cytochrome b_5 during the coupled oxidation reaction of their heme. (Additional axis: Reaction times for the reaction carried out with the H63V variant).

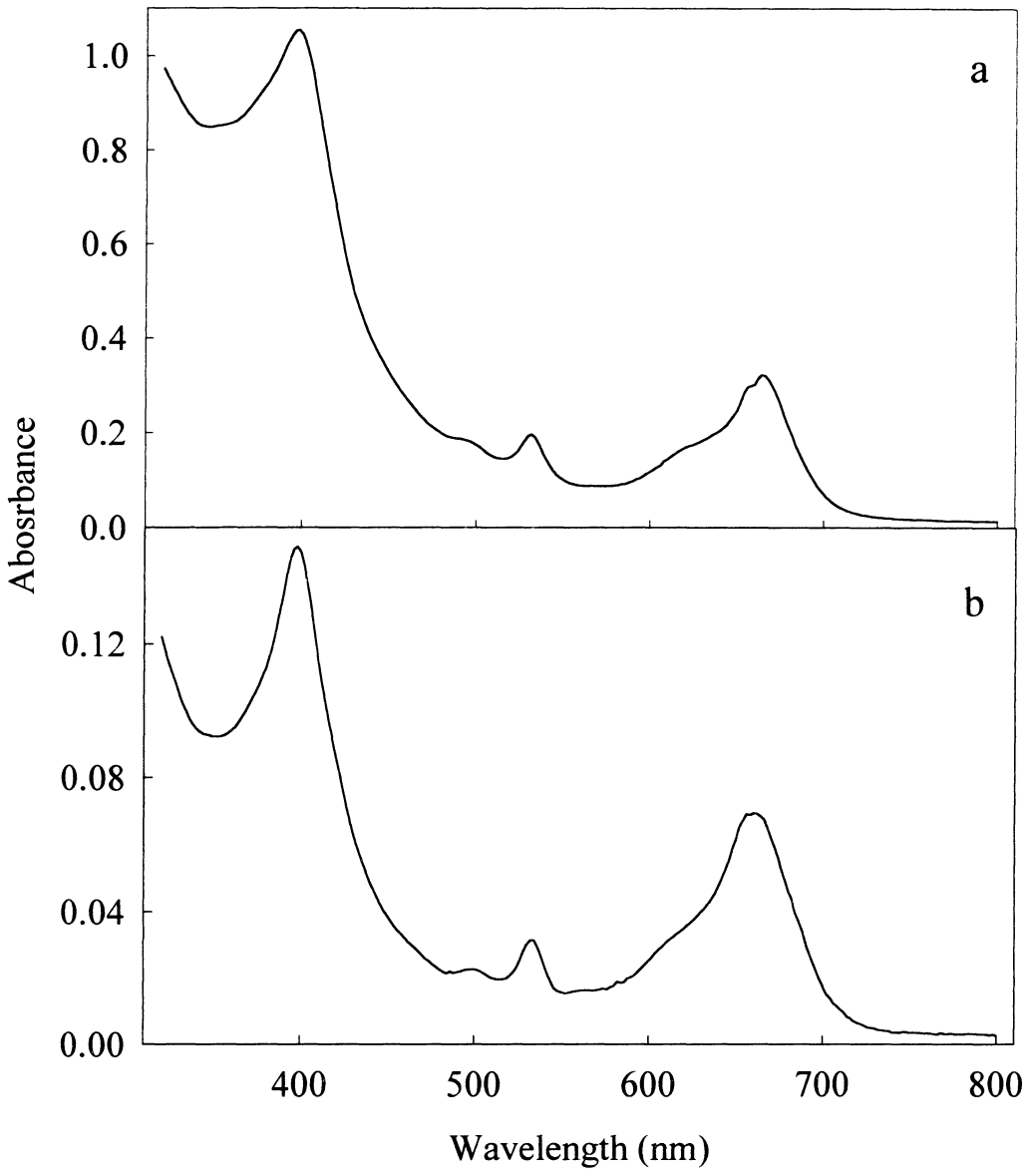

Figure 4. UV-Vis absorption spectrum of (a) the H63V mutant after the coupled oxidation reaction of its heme in the presence of sodium dithionite, and (b) the verdohemochrome obtained by extracting the verdoheme from (a) with 10% pyridine in chloroform.

obtained by extracting the product of the coupled oxidation of the heme in the H63V mutant into a chloroform-pyridine solution. The electronic absorption spectrum of the resultant solution (Fig 4b) is identical to that displayed by authentic verdoheme hemochrome [22]. Furthermore, electrospray mass spectrometric analysis of the pyridine complex of the reaction product showed the presence of species with m/z = 777, indicative of the bis-pyridine complex of verdoheme. Collision-induced dissociation of this species resulted in the loss of pyridine to produce a species with m/z = 698 and 619 a.m.u. (Fig 5). These masses correspond to mono-pyridine and pyridine-free verdoheme, thus confirming the identity of the product resulting from the coupled oxidation of the heme in the H63V mutant.

v). Regiochemistry of the Coupled Oxidation Reaction

Results obtained from the chromatographic analysis of samples containing dimethyl ester derivatives of biliverdin originating from the product of coupled oxidation of the heme in a) H63V OM cytochrome b_5, b) H63M OM cytochrome b_5, c) pyridine hemochrome, and d) standard α-biliverdin, are shown in Fig 6. The retention time of the different biliverdin isomers was determined to be $\alpha < \beta < \delta < \gamma$, on the basis of previously reported analysis [23]. It is evident from Fig 6 that the coupled oxidation of the heme in the H63V mutant produced a 50 % mixture of α- and γ-isomers, finding that is in sharp contrast with the regioselectivity exhibited by the H63M mutant, which typically produces >90% of the α-isomer.

vi). NMR Spectroscopic Studies

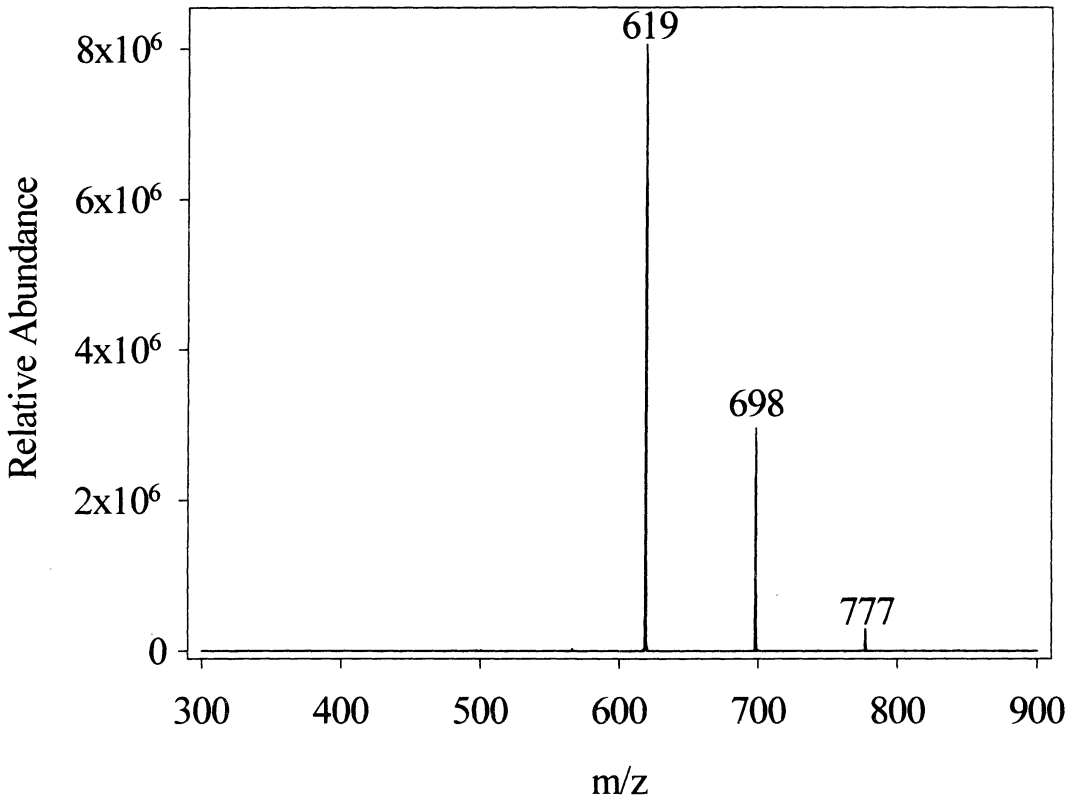

Figure 5. Electrospray mass spectrum obtained by performing collision-induced dissociation on the verdoheme-bis-pyridine complex extracted from coupled oxidation reaction mixtures containing the H63V mutant and sodium dithionite.

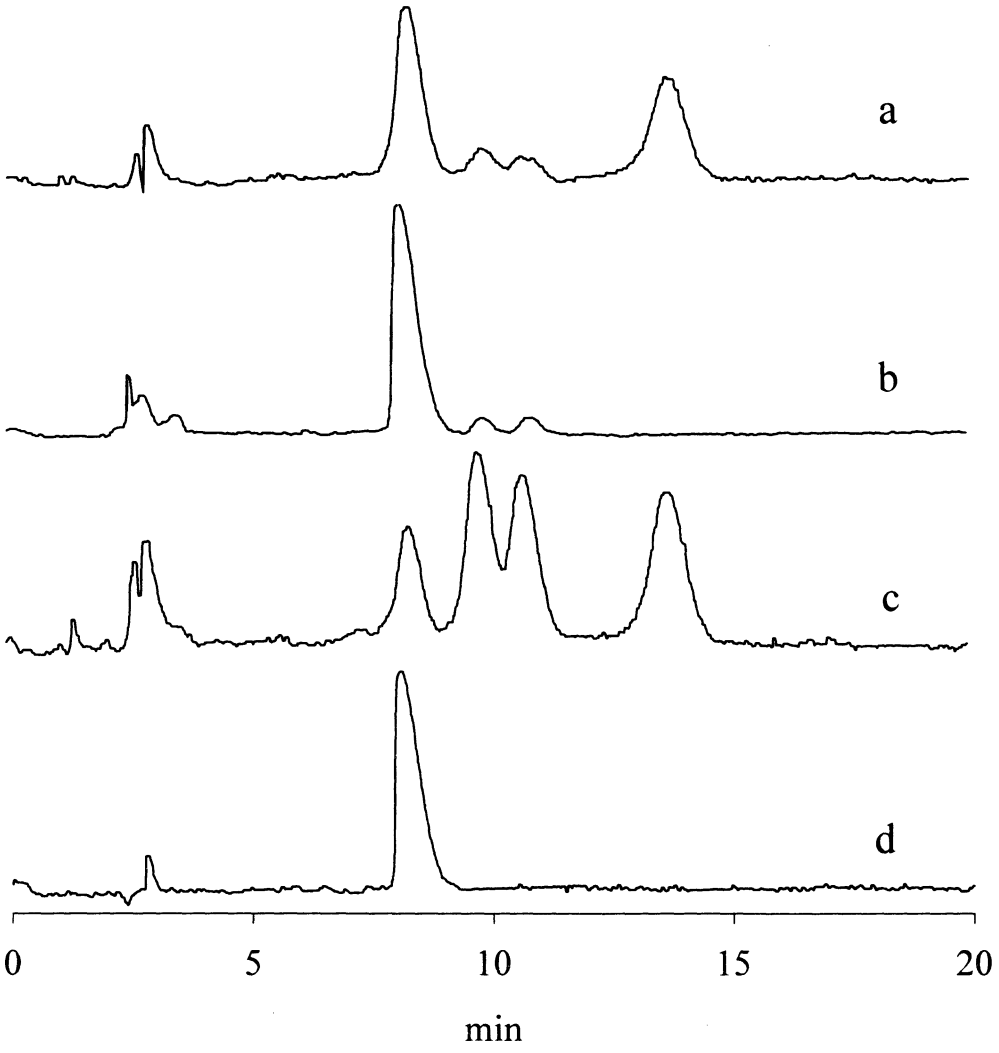

Figure 6. Chromatograms obtained from solutions containing the dimethyl ester derivatives of (a) biliverdin originated from the verdoheme produced by coupled oxidation of the H63V mutant (b) biliverdin originated from the verdoheme produced by coupled oxidation of the H63M mutant, (c) biliverdin originated from the verdoheme produced by coupled oxidation of the pyridine verdohemochrome, and (d) standard biliverdin.

a). Preparation of the H63V Mutant Containing ^{13}C-labeled Heme. A method for the production of cytochrome b_5 containing heme labeled with ^{13}C at distinct positions of the heme macrocycle has been reported [18]. This isotopic labeling strategy has been proven to be a useful tool for NMR spectroscopic studies of structure-function relationships in OM cytochrome b_5 because it facilitates the unambiguous assignment of ^{1}H and ^{13}C heme resonances [15, 19, 24]. The labeling method relies on the efficient expression of the cytochrome b_5 apopeptide, combined with the efficient biosynthesis of heme which is brought about by the addition of suitably labeled δ-aminolevulinic acid to the culture media. The successful production of isotopically labeled hemoproteins is dependent on the ability of the polypeptide to sequester heme. Consequently, attempts to obtain labeled heme by expressing proteins that do not sequester heme during their bacterial expression result in poor yields and isotopic scrambling [18, 25, 26]. Since the H63V mutant was shown not to incorporate heme during its bacterial expression, an alternative method was necessary to prepare H63V containing ^{13}C-labeled heme. In short, ^{13}C-labeled heme was obtained by expressing wild-type OM cytochrome b_5 in the presence of a suitably labeled ALA; labeled heme was subsequently extracted from the wild-type peptide and used to reconstitute the H63V apopeptide, as outlined in experimental procedures. It should be pointed out that this methodology is expected to be applicable to the preparation of a variety of different types of hemoproteins containing isotopically labeled heme.

b). Resonance Assignments. A strategy similar to that employed for the assignment of ^{1}H- and ^{13}C-NMR resonances originating from the heme in wild-type OM cytochrome b_5 [15, 19] was used in the present study. When [1,2-^{13}C]-ALA is used as a

heme precursor, all methyl, β-vinyl, and β-propionate heme carbons in the resultant macrocycle are isotopically labeled (Fig 7). Consequently, the different types of heme-substituents (*i.e.* methyl carbons) can be readily identified on the basis of the multiplicities of their corresponding resonances, as shown in Fig 7. Their corresponding attached hydrogens are subsequently identified from a heterocorrelated (HMQC) experiment, shown in Fig 8, where the one-dimensional ^{1}H spectrum corresponds to the H63V-imidazole complex containing non-labeled heme. Inspection of the HMQC spectrum indicates the presence of four cross peaks originating from methyl groups whose ^{1}H resonances (between 19.0 ppm and 31.0 ppm) are resolved from the diamagnetic envelope (see ^{1}H trace in Fig 8). The peaks at 30.36 and 27.29 ppm are approximately twice as intense as those resonating at 27.03 and 19.06 ppm, hence indicating that each of the two pairs of methyl peaks originate from different heme isomers. In fact, the presence of two interconvertible heme isomers that differ by a 180° rotation about the α-γ-meso axis is a well-known phenomenon occurring in a number of hemoproteins [27, 28]. OM cytochrome b_5 is known to exist in solution as an equimolar mixture of two interconvertible isomers [17]. By comparison, replacement of His-63 for Val in this protein results in the stabilization of one of the two isomers, as evidenced by the different intensities of the two sets of methyl resonances.

Although the resonances originating from vinyl-β and propionate-β carbons are expected to exhibit the same type of multiplicity, the fact that the carbonyl carbon is also labeled in the propionate chains dictates that the resonances originating from the propionate-β carbons must correspond to a doublet of doublets ($^{1}J_{CH}$ = 145 Hz and $^{1}J_{CC}$ = 55 Hz). Inspection of the ^{13}C spectrum in Fig 7 clearly shows the presence of two sets of resonances with the appropriate multiplicity. The set displaying the largest intensity are

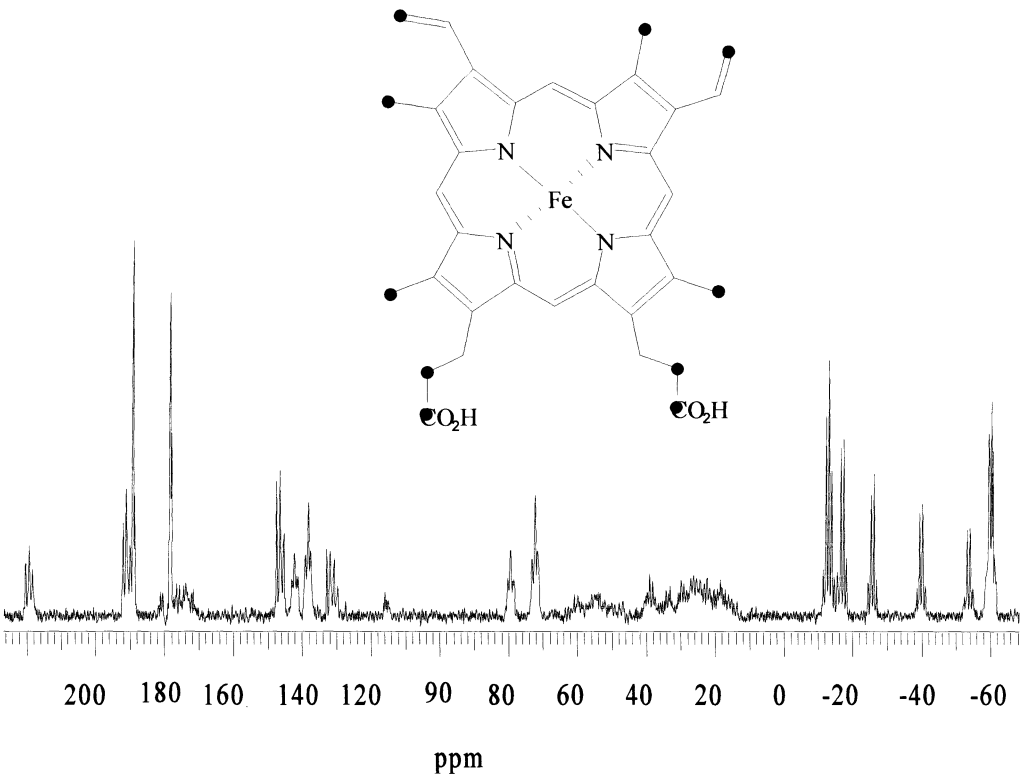

Figure 7. ^{13}C-NMR spectrum of the H63V mutant of OM cytochrome b_5 containing heme derived from [1,2-^{13}C]-ALA. The spectrum was acquired without proton decoupling. The labeled carbon atoms are highlighted in the heme structure by ●.

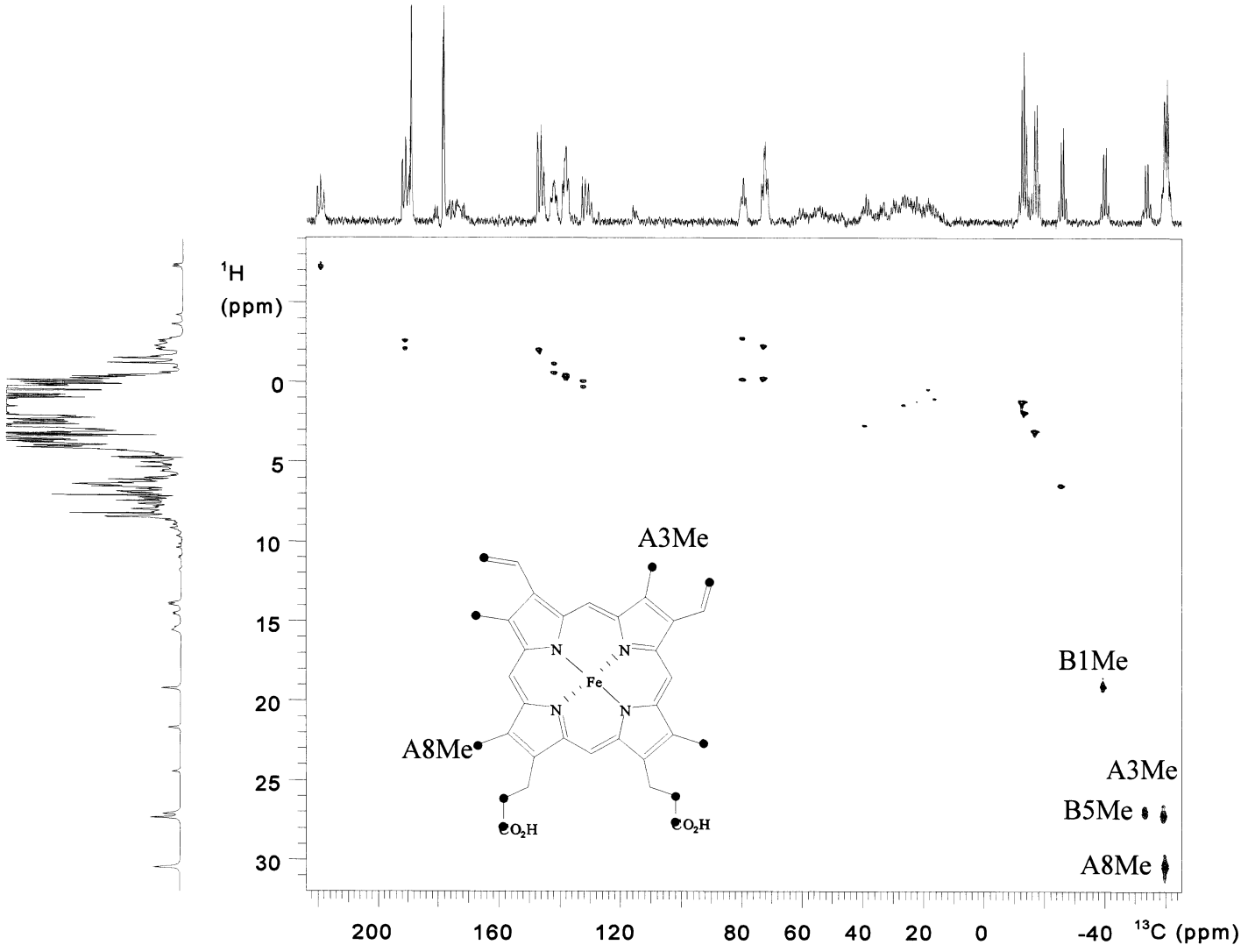

Figure 8. HMQC spectrum of the H63V mutant of OM cytochrome b_5 containing heme derived from [1,2-^{13}C]-ALA. The corresponding one-dimensional spectrum is shown on each axis.

located at 72.5 ppm and 137.8 ppm, whereas the less intense set are located at 79.4 and 141.7 ppm; the chemical shift of their corresponding protons is readily obtained from the cross peaks in the HMQC map. ^{13}C resonances originating from vinyl-β carbons display the expected multiplicity and are therefore readily interpreted.

When [5-^{13}C]-ALA is used as a heme precursor, all meso carbons in the resultant macrocycle are isotopically labeled, as shown in Fig 9, consequently, their corresponding ^{1}H and ^{13}C resonances can be obtained from the most intense cross peaks in the HMQC spectrum shown in Fig 9. It is interesting to note that there are only four intense cross-peaks in the spectrum, although the presence of two heme isomers would suggest that eight cross peaks should be present. This observation strongly suggests that the resonances arising from equivalent meso positions in both heme isomers have almost identical ^{13}C- and ^{1}H-NMR shifts. On the other hand, the one-dimensional ^{13}C-NMR spectrum in Fig 9 displays eight resolved resonances (labeled q); hence indicating that all eight labeled quaternary carbons (four from each isomer) have distinct chemical shifts.

Once the resonances originating from the different types of heme substituents had been identified, the corresponding assignments were performed with the aid of the NOESY spectrum shown in Fig 10. Inspection of the map (Fig 10) reveals correlations between the methyl resonance at 30.36 ppm and the signals at 13.92 and 13.77 ppm, which in turn show correlations to one another. The latter two are devoid of $^{1}J_{CH}$ coupling in the ^{1}H spectrum obtained with a sample containing heme derived from 1,2-[^{13}C]-ALA, hence indicating that these resonances originate from propionate-α hydrogens. This is corroborated from the fact that the hydrogens resonating at 13.92 ppm displays a correlation to the hydrogen at –0.27 ppm, which in turn, is correlated via HMQC to the labeled propionate-β carbon at 72.5 in Fig 8. The other intense methyl

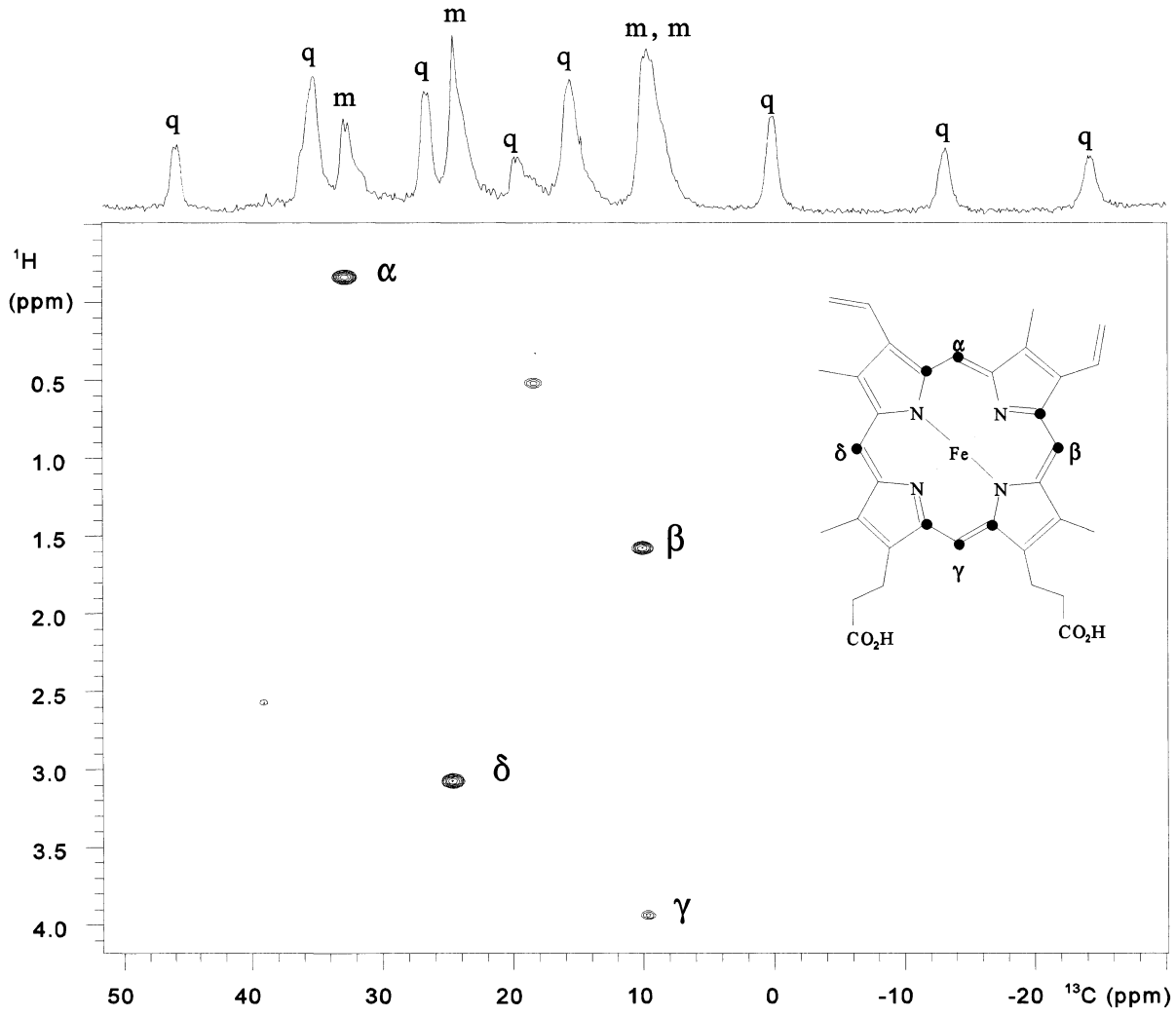

Figure 9. HMQC spectrum of the H63V mutant of OM cytochrome b_5 containing heme derived from [5-^{13}C]-ALA. The parameters used for the acquisition were as follows: spectral width of 9.5 kHz and 45 kHz for ^{1}H and ^{13}C, respectively, $^1J_{CH}$ = 150 Hz. The data were collected as an array of 2K x 300 points which after linear prediction and zero filling in t_1 produced a 2K x 2K data matrix.

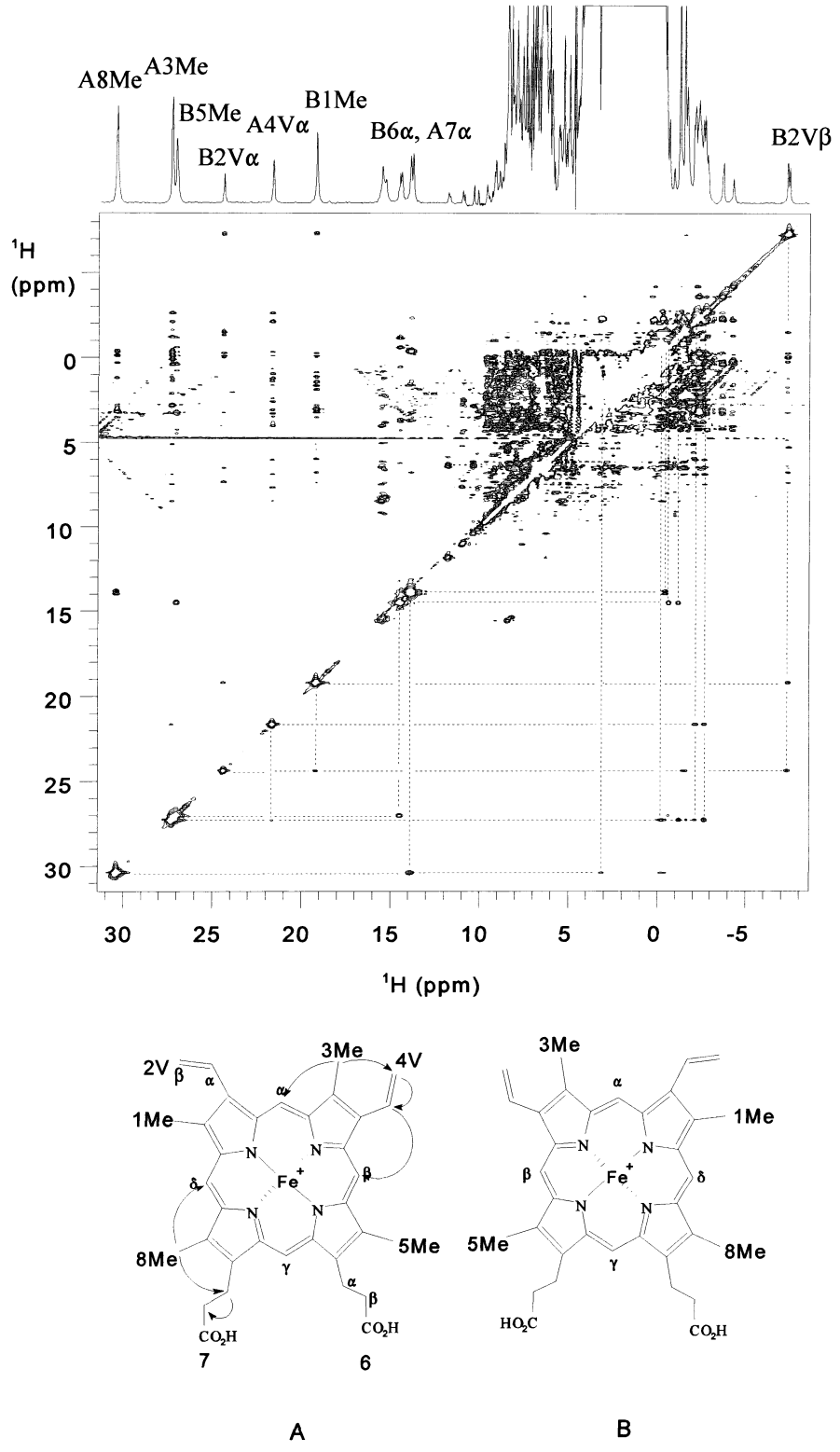

Figure 10. NOESY spectrum for the H63V mutant illustrating the cross-peaks utilized for the assignments. The noesy connectivities of the assigned heme substituents are shown with arrows in the corresponding heme structures.

resonance (27.29 ppm) displays a NOESY correlation to resonances at –2.11 and –2.63 ppm; the latter are correlated via HMQC to a labeled carbon originating from a vinyl-β group at 146.7 ppm (see Fig 8). Consequently, there are only two resolved methyl resonances originating from the more abundant isomer; one of these (30.36 ppm) is located next to propionate substituent and the other (27.29 ppm) is located next to a vinyl group. Because the methyl resonances at 30.36 and 27.03 ppm show correlations to propionate chains, it was determined that these methyl peaks may originate from either of the methyl groups in close proximity to the heme propionates (i.e. A5Me, A8Me, B5Me, B8Me).

The spread and order of the heme methyl isotropic shifts in heme proteins are correlated with the orientation of the planar axial ligand, as demonstrated by the Hückel calculations of Shokhirev and Walker [29]. On the basis of such correlations, these authors reported a plot showing the dependence of the observed shifts on the axial ligand orientation in heme proteins [29]. Because the plot was constructed specifically for heme methyl resonances originating from only one of the heme-isomers, it is possible to infer that methyl heme resonances at 30.36 ppm and 27.03 ppm, arise from A8Me and A3Me, respectively. The definitive assignment of these resonances stems from the premise that there is only one possible assignment that is consistent with the fact that two methyl peaks exhibit large downfield isotropic shifts, with the condition that either 8Me or 5Me should exhibit the largest shift [29]. Consequently, the high-intensity methyl peaks should originate from A8Me, and A3Me, whereas the low-intensity methyl resonances at 27.03 ppm and 19.16 ppm should arise from B8Me, and B3Me, respectively.

Discussion

i). Characterization of the H63V Mutant

Expression of the H63V mutant of OM cytochrome b_5, followed by centrifugation of the bacterial culture produces a bacterial pellet that lacks the characteristic pink color normally observed upon overexpression of the wild-type protein. The H63V mutant can be readily reconstituted with heme in the presence of imidazole; subsequent elimination of imidazole via dialysis results in a stable heme complex. Characterization of this complex by electron paramagnetic resonance spectroscopy, and UV-Vis spectroscopy indicates that the ferric heme in the H63V mutant is high-spin, and it is coordinated by His-39 in the proximal site and likely by water in the distal site. Spectroscopic characterization of the reduced species under anaerobic conditions indicates the presence of a high-spin, pentacoordinated ferrous heme.

ii). Verdoheme as the Product of the Coupled Oxidation Reaction

When the H63V or H63M mutant of OM cytochrome b_5 is incubated with a suitable reducing agent in the presence of air, molecular oxygen is activated at the distal site in order to produce verdoheme. In the case of the H63M mutant, we proposed that the coupled oxidation reaction is arrested at the verdoheme stage because Met-63 binds to the sixth coordination site of the verdoheme [44] hence inhibiting the subsequent oxidation of verdoheme by preventing O_2 from binding to its sixth coordination site. In contrast, the fact that the coupled oxidation reaction of the heme in the H63V mutant is arrested at the verdoheme stage cannot be easily explained by the coordination of ferrous verdoheme by a ligand originating from the polypeptide. Furthermore, the electronic

spectrum originating from the verdoheme complex of the H63V mutant (Fig 4a) is identical to that reported for ferrous pyridine verdohemochrome [22], where the band at 660 nm strongly suggests that the ferrous verdoheme in H63V is hexacoordinated. The two axial ligands are likely to be His-39 (proximal) and possibly H_2O or OH^- in the distal site. By comparison, the electronic spectra of ferrous pentacoordinated verdoheme and ferric verdohemes (pentacoordinated and hexacoordinated) display distinct bands between 690 and 700 nm [30]. It is noteworthy that OH^- has been postulated as a distal ligand for verdoheme in heme oxygenase. The coordination of OH^- to ferrous verdoheme has been explained on the basis of one of the two resonance structures of verdoheme that possesses a formal positive charge on the iron, which is thought to impart this molecule with appreciable ferric characteristics [31]. This idea is supported by the fact that the ferrous verdoheme complex of myoglobin is known to bind cyanide and azide with stability that is comparable to or higher than those observed for the corresponding met-myoglobin complexes [31]. Moreover, the association constant for the formation of ferrous verdoheme-CO complex has been shown to be more than 10^4-fold weaker than that measured for the formation of a ferrous heme-CO complex [32]. It is therefore likely that the stability exhibited by verdoheme in the H63V mutant stems from the inability of O_2 to displace the distal ligand on verdoheme (presumably OH^-). An analogous mechanism of inhibition has been proposed for the conversion of ferrous verdoheme to iron-biliverdin in the presence of strongly coordinating ligands [33]. For example, the conversion of the ferrous pyridine verdohemochrome to iron-biliverdin does not take place unless pyridine is replaced by 2-picoline. In the presence of 2-picoline verdoheme is rapidly converted into iron-biliverdin. It has been postulated that the bulky methyl group next to nitrogen in 2-picoline pulls the iron below the heme plane, hence

diminishing the stability of the second picoline ligand, which in turn results in a more accessible site to coordinate oxygen [33]. Evidently, the structural reasons in H63V that are responsible for arresting the coupled oxidation reaction at the verdoheme stage are not clear yet. Additional research in this area is currently being pursued in our laboratory.

iii). Regioselectivity of the Coupled Oxidation Reaction

Ortiz de Montellano and coworkers reported that the regioselectivity observed for the oxidation of heme by HO appears to be controlled by heme-electronic factors and not simply by steric interactions in the distal pocket [8, 34, 35]. This conclusion was drawn from the fact that γ-meso-methylmesoheme was oxidized by HO exclusively at the γ-meso position, δ-meso-methylmesoheme was oxidized at the δ- and α- positions, and the β-derivative was found to be a poor substrate [34]. On the other hand, the oxidation of all four isomers of meso-formyl heme is never carried out at the carbon bearing the electron withdrawing formyl group [35]. The idea that the regioselectivity of heme oxygenation observed with HO is dictated by heme-electronic effects is also supported by the ^{1}H-NMR spectroscopic studies performed by La Mar *et al.* with rat and human heme-HO complexes [36, 37]. These investigators observed an unprecedented pattern of isotropic shifts originating from heme substituents in the cyanide-inhibited enzyme [36]. The most interesting aspect of this pattern is that only one of the heme methyl groups displays a chemical shift that is resolved from the diamagnetic envelope of resonances. On the basis of previous studies carried out on model heme complexes [38], it was suggested that this unusual pattern of isotropic shifts, *i.e.* heme electronic structure,

originates from increased spin density at the α- and γ-meso positions of the heme in HO [36].

The regioselectivity observed for the coupled oxidation of the heme in the H63M and H63V mutants of cytochrome b_5, *i.e.* the exclusive attack to the α-meso position in the H63M mutant and the equivalent attack to α- and γ-meso positions in H63V, suggested an electronic control of regioselectivity similar to that proposed for HO. It is therefore conceivable that the efficient coupled oxidation reaction observed with the two mutants of OM cytochrome b_5, as well as the regioselectivity of their coupled oxidation reactions, originates from a heme-electronic structure similar to that reported for HO [36, 37]. In order to explore this idea, NMR spectroscopic studies were performed with the H63V mutant whose heme had been labeled with ^{13}C at strategic positions in order to facilitate the assignment of resonances arising from heme substituents. The results of these studies, summarized in Table 1 and in the ^{1}H spectrum of Fig 10, clearly indicate that the heme electronic structure of the heme in HO and the heme in the H63V mutant of OM cytochrome b_5 are different (see below).

Whereas in the ^{1}H-NMR spectrum of HO the only heme-methyl resonance outside the diamagnetic envelope is that originating from the methyl group located on pyrrole carbon-3 (22.5 ppm) [36, 37], the ^{1}H-NMR spectrum of the H63V mutant displays two methyl groups with large isotropic shifts. These are located on pyrrole carbons 3 and 8 (see Table 1 and Fig 10). In addition, the resonances originating from meso hydrogens α and γ in HO exhibit large upfield shifts (α = -5.10 ppm, γ = 3.84 ppm) with respect to their β and δ counterparts (β = 7.60 ppm, δ = 7.13 ppm). By comparison, the resonances arising from meso hydrogens in the heme corresponding to the H63V mutant exhibit similar shifts regardless of their position (see Table 1). The above

Table I. ^{1}H and ^{13}C resonances arising from the heme group in the H63V mutant of OM cytochrome b_5.

Position	Group	Isomer A		Isomer B	
		^{1}H (ppm)	^{13}C (ppm)	^{1}H (ppm)	^{13}C (ppm)
1	Me	1.18	-12.66	19.16	-39.64
2	V α	NA	NA	24.50	NA
	V β	-2.06	146.66	-7.27	219.08
3	Me	27.29	-59.51	6.46	-25.74
4	V α	21.60	NA	NA	NA
	V β	-2.11, -2.63	190.92	0.27, -0.10	132.16
5	Me	3.04	-16.93	27.03	-53.44
6	P α	NA	NA	14.54	NA
	P β	-0.20, -2.33	72.46	-0.64, -1.20	141.74
7	P α	13.90	NA	NA	NA
	P β	-0.36, -0.47	137.87	-0.20, -2.80	79.43
8	Me	30.36	-59.98	1.86	-13.41
α	meso	-1.35	36.06	-1.35	36.06
β	meso	1.59	9.96	3.07	24.59
γ	meso	3.94	9.38	3.94	9.38
δ	meso	3.07	24.59	1.59	9.96

Abbreviations used: Me, methyl; V, vinyl; P, propionate; NA, resonance not yet assigned.

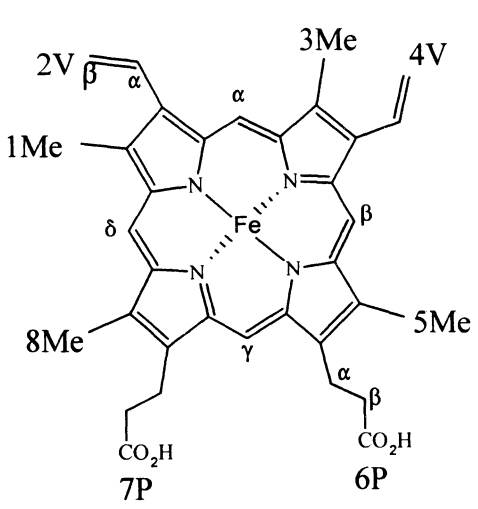

A

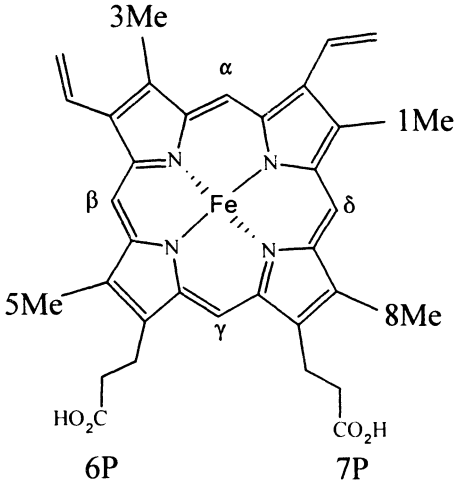

B

observations taken together indicate that the electronic structure of the heme in the H63V mutant is likely to possess a comparable magnitude of spin density among all meso positions. In fact, this idea is strengthened by the fact that the spread of ^{13}C resonances arising from all meso positions is less than 15 ppm (^{13}C spectrum in Fig 9). Since the dipolar contribution to the ^{13}C isotropic shift is expected to be smaller than that provided by the contact mechanism, the relatively small spread observed for the meso-carbon resonances indicates that all meso carbon positions in the H63V heme indeed experience similar spin density. Consequently, heme-electronic control of coupled oxidation regioselectivity does not appear to be consistent with the 50% distribution of α- and γ-verdohemes produced by coupled oxidation of the heme in the H63V mutant.

iv). Steric Control of Regioselectivity in the Coupled Oxidation Reaction Performed by Axial-Ligand Mutants of OM Cytochrome b_5.

In view of the NMR spectroscopic evidence indicating that heme-electronic structure may not play a dominant role in determining the regioselectivity of oxidation of the heme in the axial ligand mutants of cytochrome b_5, the role of steric effects was explored. This was accomplished by the use of the molecular modeling experiments outlined in experimental procedures. Inspection of the results obtained for the H63M mutant (Fig 11A) reveals that the sulfur atom in the side chain of Met-63 (purple) is located between the heme-iron (yellow) and the γ-meso carbon (all meso carbons are shown in red); for reference, the γ-meso carbon is located between the two heme-propionates (pink). It is therefore clear that the side chain of Met-63 protects the γ-meso position from being attacked by the activated oxygen on the heme iron. The same view of the molecule shows that the side chains of Val-61 (blue) and Ala-67 (light blue) are

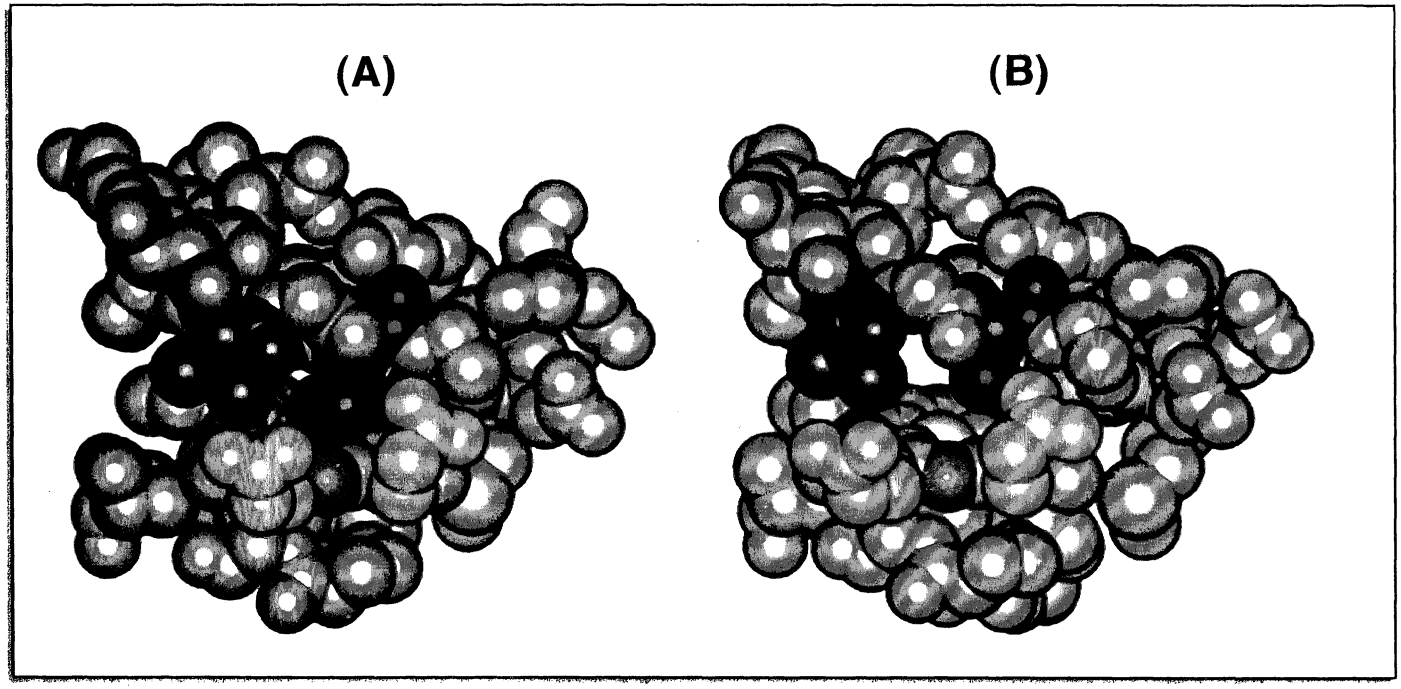

Figure 11. Space filling diagrams of the molecular models of (A) the H63M mutant, and (B) the H63V mutant obtained from the coordinates corresponding to the crystal structure of OM cytochrome b_5. See text for identification of the colored amino acid residues and heme substituents.

located on top of meso positions δ and β, respectively. The methyl groups in the side chains of Val-61 and Ala-57 pack against the δ- and β-meso carbons, thus protecting these positions from being attacked by heme-bound activated oxygen. In contrast, it can be seen that the α-meso position (shown at the far end of the heme) is not protected, hence indicating that this meso position is susceptible to be attacked by activated oxygen. This conclusion is in good agreement with the experimental observations reported above. The results of the calculations performed with the H63V mutant of cytochrome b_5 are shown in Fig 11B. Whereas meso positions δ and β are still protected by the methyl groups in the side chains of Val-61 (magenta) and Ala-67 (light blue), meso positions α and γ are completely unprotected as a result of the shorter Val side chain (purple). These results indicate that an iron-bound activated oxygen molecule can attack the α- and γ-meso position with equal probability, conclusion that is in excellent agreement with the equimolar mixture of α- and γ-verdohemes found as products of the coupled oxidation of the heme in the H63V mutant.

v). Efficiency of the Coupled Oxidation Reaction

The heme environment in the axial ligand mutants of cytochrome b_5 is very similar to that exhibited by HO and myoglobin in that their heme is coordinated by a proximal (non-ionized, non-hydrogen-bonded) histidine and a distal water ligand. This environment is strikingly different from those observed in typical O_2 activating hemoproteins such as cytochrome P450 and peroxidases [39]. The latter react with O_2 to form an activated ferryl oxidizing species, whereas heme oxygenation catalyzed by HO is known to proceed via the formation of a ferric peroxide (Fe-O-O-H) intermediate [7]. Once formed, the ferric peroxide intermediate can follow two divergent

paths: (a) the formation of a ferryl species, thus avoiding heme oxygenation, or (b) a fast reaction with heme resulting in heme oxygenation. The fact that heme oxygenation has been observed with several hemoproteins, *i.e.* myoglobin and hemoglobin, albeit in a slower manner, underscores the existence of two competing pathways. The existence of these competing pathways implies that proteins involved in heme catabolism (*e.g.* HO) have evolved to favor the reaction between the ferric peroxide intermediate and the heme. Consequently, it is important to carry out research aimed at understanding the relevant structural motives responsible for channeling oxygen activation toward heme oxygenation. Axial ligand mutants of cytochrome b_5 perform the heme oxygenation reaction relatively fast and with controlled regioselectivity, thus providing a good model system to probe structural aspects related to heme oxygenation by hemoproteins. Two important structural aspects possessed by these mutants are likely to contribute to their efficient heme oxidation activity: (a) the lack of distal ligand capable of forming a hydrogen bond with the iron-bound hydroperoxo intermediate and (b) the presence of an open (water accessible) heme environment. These are discussed below.

It has been proposed that the formation of hydroxyheme catalyzed by heme oxygenase occurs via the binding of O_2 to its ferrous heme iron, followed by the addition of a second electron to this complex that results in the formation of a ferric-peroxo intermediate [8] (Figure 12). The presence of a distal ligand whose orientation permits the formation of a hydrogen bond to the activated ferric-peroxo intermediate may accelerate the rate of heterolytic cleavage to form the oxyferryl species shown in Scheme I, hence protecting the heme group from the highly reactive ferric-hydroperoxo intermediate. In contrast, the absence of a distal ligand impairs the rate of heterolytic oxygen cleavage of the ferric-hydroperoxo intermediate, thus permitting enough time for

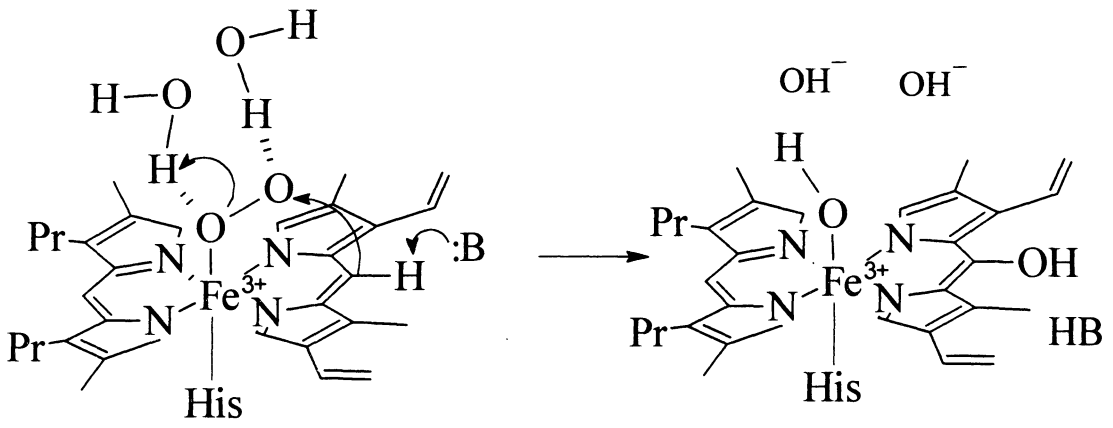

Figure 12. Schematic representation of the possible role of a heme binding pocket highly accessible to the aqueous environment. The β- and δ-meso positions in the heme structure are omitted for clarity.

the latter to react with the heme. Moreover, if the heme binding pocket provides relatively high accessibility to water, the increased polarity of the heme environment may increase the electrophylicity of the peroxo intermediate, thus making it more susceptible to nucleophylic attack by a meso carbon, as shown in Figure 12. Consistent with this idea, the reaction of hydrogen peroxide with sperm-whale myoglobin and some of its derivatives in which the distal histidine (His-64) was mutated [40], showed that in the absence of this amino acid, a ferric-peroxo complex is accumulated. The accumulation of the ferric peroxo intermediate stems from the fact that the rate of heterolytic cleavage to form the oxyferryl species is slowed down. Interestingly, the accumulation of the ferric-peroxo intermediate in the His-64 mutants of sperm-whale myoglobin eventually resulted in the formation of verdoheme [40]. These authors concluded that an important role played by a distal histidine residue in globins and peroxidases is to prevent the accumulation of a reactive ferric-peroxo complex that might otherwise damage the prosthetic group. Additional evidence implicating the role of the polarity of the heme pocket in accelerating heme oxygenation has been reported by Hildebrand *et al.* [41], who reported that the V67A/V68S mutant of horse heart myoglobin is more efficient at oxygenating its heme than the wild-type protein. These authors suggested that increased polarity of the distal pocket crated by the double mutation is responsible for the increased rate of coupled oxidation exhibited by the double mutant.

Conclusions

The lack of a three-dimensional structure of HO has provoked a great deal of speculation regarding the role played by residues in the heme pocket in the coupled oxidation reaction. The fact that heme oxidation occurs regardless of the presence

of a protein environment, *i.e.* the coupled oxidation of the pyridine hemochrome, clearly indicates that the reaction is not conditioned to occur only in a hemoprotein. Nevertheless, the obvious differences in heme oxidation efficiency and regioselectivity observed for the pyridine hemochrome and several heme-containing proteins, are a clear testimony of the influence that the heme plays in accelerating the reaction and in dictating the regioselectivity of oxidation. The present study provides experimental evidence supporting the idea that the regioselectivity of coupled oxidation exhibited by the H63V and H63M mutants of OM cytochrome b_5 is likely dictated by steric interactions between the activated ferric peroxo intermediate and residues in the distal pocket. Furthermore, the isotropic shift patterns exhibited by the H63V mutant indicate that electronic factors are likely not to be involved in dictating the regioselectivity of heme oxygenation, although similar studies carried out with the cyano complex of the mutants will certainly aid to corroborate our results.

It is known that the heme environment in cytochrome b_5 is unusually polar for a heme-containing protein [15, 24] as a result of the large accessibility of water to its heme cavity. The efficiency of heme oxygenation observed with the axial ligand mutants of OM cytochrome b_5, therefore, is likely to originate from the large accessibility of water to their heme environment. This idea is supported by the fact that the recently solved X-ray crystal structure of HO revealed a heme environment that is largely accessible to water [16]. Furthermore, studies performed with other heme containing proteins indicate that the coupled oxidation reaction is accelerated for site-directed mutants possessing a more polar distal pocket [40, 41]. Consequently, investigating the heme oxidation reaction performed by axial ligand mutants of OM cytochrome b_5 seems to offer an interesting alternative to shed light on the mechanistic aspects of enzymatic heme catabolism.

Particularly interesting is their unique property to provide a stable environment for the highly reactive verdoheme intermediate. In early work, it was shown that the oxygen atoms contained in biliverdin are incorporated from two distinct O_2 molecules [43], which implies that the conversion of verdoheme into biliverdin occurs as a result of a redox process [4, 33, 42-44]. These results, however, are in clear contrast with experiments showing that biliverdin can also be produced via a hydrolytic mechanism that involves nucleophilic attack of verdoheme by OH^- followed by ring-opening of the macrocycle upon acidification of the solution [33, 45]. If a redox process is required to achieve formation of biliverdin by the axial ligand mutants of OM cytochrome b_5, then the arrest of the reaction at the verdoheme-protein complex stage may be related to the following possibilities. (1) An unusually negative redox potential of the protein-verdoheme complex, or (2) An usually strongly coordinated sixth ligand bound to verdoheme, which does not permit the binding of O_2, hence inhibiting the oxidation of verdoheme to iron-biliverdin. On the other hand, if a hydrolytic process is required for completion of the entire catalytic cycle (*i.e.* conversion of heme into biliverdin or iron-biliverdin), then the unusual stability of the verdoheme intermediate may be related to a poor electrophilic character promoted by peculiarities of the heme pocket topology in cytochrome b_5. Studies that will allow us to discern the redox and ligation states of the verdoheme complexes are the subject of future work to be undertaken in our laboratory.

References

1. Tenhunen, R., Marver, H., S. and Schmid, R. (1969) *J. Biol. Chem.* 244, 6388.
2. Verma, A., Hirsch, D. J., Glatt, C. E., Ronnett, G. V. and Snyder, S. H. (1993) *Science* 259, 381.
3. Ishikawa, K., Sato, M., Ito, M. and Yoshida, T. (1992) *Biochem. Biophys. Res. Commun.* 182, 981.
4. Wilks, A. and Ortiz de Montellano, P. R. (1993) *J. Biol. Chem.* 268, 22357.
5. Sun, J., Wilks, A., Ortiz the Montellano, P. R. and Loehr, T. M. (1993) *Biochemistry* 32, 14151.
6. Ito-Maki, M., Kazunobu, I., Matera, K. M., Sato, M., Ikeda-Saito, M. and Yoshida, T. (1995) *Arch. Biochem. Biophys.* 317, 253.
7. Wilks, A., Torpey, J. and Ortiz de Montellano, P. R. (1994) *J. Biol. Chem.* 269, 29553.
8. Ortiz de Montellano, P. R. (1998) *Acc. Chem. Res.* 31, 543.
9. Takahashi, S., Ishikawa, K., Takeuchi, N., Ikeda-Saito, M., Yoshida, T. and Rousseau, D. L. (1995) *J. Am. Chem. Soc.* 117, 6002.
10. Fujii, H., Dou, Y., Zhou, H., Yoshida, T. and Ikeda-Saito, M. (1998) *J. Am. Chem. Soc.* 120, 8251.
11. Brown, S. B., Chabot, A. A., Enderby, E. A. and North, A. C. T. (1981) *Nature* 289, 93.
12. O'Carra, P. and Colleran, E. (1969) *FEBS Lett.* 5, 295.
13. Bonnet, R. and McDonagh, A. F. (1973) *J. Chem. Soc. Perkin Trans. 1* 881.
14. Rodriguez, J. C. and Rivera, M. (1998) *Biochemistry* 37, 13082.

15. Rodriguez-Maranon, M. J., Feng, Q., Stark, R. E., White, S. P., Zhang, X., Foundling, S. I., Rodriguez, V., Schilling III, C. L., Bunce, R. A. and Rivera, M. (1996) *Biochemistry* 35, 16378.

16. Ortiz de Montellano, P. R., Schuller, D. J., Wilks, A. and Poulos, T. L. *Heme Oxygenase: Crystal Structure and Mechanism.* In *217th ACS National Meeting.* 1999. Anaheim, CA.

17. Rivera, M., Barillas-Mury, C., Christensen, K. A., Little, J. W., Wells, M. A. and Walker, F. A.(1992) *Biochemistry* 31, 12233.

18. Rivera, M. and Walker, F. A. (1995) *Anal. Biochem.* 230, 295.

19. Rivera, M., Qiu, F., Bunce, R. A. and Stark, R. E. (1999) *JBIC* 4, 87.

20. Rodriguez, J. C., Desilva, T. and Rivera, M. (1998) *Chem. Lett.* 353.

21. Antonini, E., and Brunori, M. In *Hemoglobin and Myoglobin in their Reactions with Ligands*; Neuberger, A., and Tatum, E. L., Eds.; North Holland Publishing Co.: Amsterdam, 1971; pp 13-39.

22. Lagarias, J. C. (1982) *Biochim. Biophys. Acta* 717, 12.

23. Murakami, T., Morishima, I., Toshitaka, M., Ozaki, S.-i., Hara, I., Yang, H.-J. and Watanabe, Y. (1999) *J. Am. Chem. Soc.* 121, 2007.

24. Rivera, M., Seetharaman, R., Ghirdhar, D., Wirtz, M., Zhang, X., Wang, X. and White, S. (1998) *Biochemistry* 37, 1485.

25. Biel, S. W. and Biel, A. J. (1990) *J. Bacteriol.* 172, 1321.

26. Harris III, W. F., Burkhalter, R. S., Lin, W. and Timkovich, R. (1993) *Bioorg. Chem.* 21, 209.

27. Keller, R. M. and Wüthrich, K. (1980) *Biochim. Biophys. Acta* 621, 204.

28. LaMar, G., N., Burns, P. D., Jackson, J. T., Smith, K. M., Langry, K. C. and

Strittmatter, P. (1981) *J. Biol. Chem.* 256, 6075.

29. Shokhirev, N. V. and Walker, F. A. (1998) *JBIC* 3, 581.

30. Liu, Y., Moënne-Loccoz, P., Loehr, T. M. and Ortiz de Montellano, P. R. (1997) *J. Biol. Chem.* 272, 6909.

31. Takahashi, S., Matera, K. M., Fujii, H., Zhou, H., Ishikawa, K., Yoshida, T., Ikeda-Saito, M. and Rousseau, D. L. (1997) *Biochemistry* 36, 1402.

32. Migita, C. T., Matera, K. M., Ikeda-Saito, M., Olson, J. S., Fujii, H., Yoshimura, T., Zhou, H. and Yoshida, T. (1998) *J. Biol. Chem.* 273, 945.

33. Saito, S. and Itano, H. A. (1982) *Proc. Natl. Acad. Sci. USA* 79, 1393.

34. Torpey, J., Lee, D. A., Smith, K. M. and Ortiz de Montellano, P. R. (1996) *J. Am. Chem. Soc.* 1118, 9172.

35. Torpey, J. and Ortiz de Montellano, P. R. (1997) *J. Biol. Chem.* 272, 22008.

36. Hernandez, G., Wilks, A., Paolesse, R., Smith, K. M., Ortiz de Montellano, P. R. and La Mar, G. N. (1994) *Biochemistry* 33, 6631.

37. Gorst, C. M., Wilks, A., Yeh, D. C., Ortiz de Montellano, P. R. and La Mar, G. N. (1998) *J. Am. Chem. Soc.* 120, 8875.

38. Tan, H., Simonis, U., Shokhirev, N. V. and Walker, F. A. (1994) *J. Am. Chem. Soc.* 116, 5784.

39. Marnett, L. J. and Kennedy, T. A. In *Cytochrome P450: Structure, Mechanism, and Biochemistry*; Ortiz de Montellano, P. R. Ed.; Plenum Press: New York, 1995; p 49.

40. Brittain, T., Baker, A. R., Butler, C. S., Little, R. H., Lowe, D. J., Greenwood, C. and Watmough, N. J. (1997) *Biochem. J.* 326, 109.

41. Hildebrand, D. P., Tang, H.-L., Luo, Y., Hunter, C. L., Hunter, M. S., Brayer, G.

D. and Mauk, A. G. (1996) *J. Am. Chem. Soc.* 118, 12909.

42. Brown, S. B. and King, R. F. G. J. (1976) *Biochem. Soc. Trans.* 4, 197.

43. Yoshida, T., Noguchi, M., and Kikuchi, G. (1980) *J. Biol. Chem.* 255, 4418.

44. Sano, S., Sano, T., Morishima, I., Shiro, Y., and Maeda, Y. (1986) *Proc. Natl. Acad. Sci. USA* 83, 531.

45. Koerner, R., Latos-Grazynski, L., and Balch, A. L. (1998) *J. Am. Chem. Soc.* 120, 9246.

CHAPTER IV

REDUCTIVE DEHALOGENATION OF CARBON TETRACHLORIDE BY SODIUM DITHIONITE

Introduction

Halogenated aliphatic hydrocarbons, such as carbon tetrachloride (CCl_4), have been widely recognized as persistent ground-water and air pollutants and the search for methods aimed at their safe elimination has become an area of notable interest in contemporary environmental science. The reductive dehalogenation of carbon tetrachloride has been actively investigated because of its relatively high solubility in water (800 mg/L at 20°C) and for its well known properties as a potent hepatotoxin. The chronic toxicity of carbon tetrachloride is due to destruction of cytochrome P450, protein acylation, lipid peroxidation, and altered intracellular calcium distribution [1]. An important feature of CCl_4 is its special susceptibility to undergo reductive dehalogenation reactions, which are facilitated by the electrophilic character of the carbon due to its four electronegative chlorine substituents. For this reason a number of reductive dehalogenation methods have been portrayed as alternatives to transform carbon tetrachloride into environmentally friendly compounds. Several studies in this area have concluded that enzymes [2], coenzymes [3], porphyrin rings [4], corrinoids [5,6],

electrodes [7], mineral surfaces [8-10], zero valent metals [11-15], and semiconductor photocatalysts [16,17] can be successfully used to reductively dehalogenate halocarbons. Unfortunately, enzyme lability, reactivity of metals with water [13] and low quantum yields of photocatalysts [18], are factors that still compromise the efficiency of those methods.

In this study, sodium dithionite ($Na_2S_2O_4$) was investigated as an alternative to carry out the reductive dehalogenation of aqueous solutions of carbon tetrachloride [51]. The utilization of sodium dithionite to dehalogenate carbon tetrachloride appears to offer a simple solution to the problem of water contaminated with such persistent halocarbon.

i). Sodium Dithionite in Reductive Dehalogenation Studies

The half-cell reaction for the anaerobic oxidation of dithionite ($S_2O_4^{2-}$) to sulfite (SO_3^{2-}) (Equation 1), provides a good indication of the reducing strength of dithionite. This property together with its easy availability is the main reason why dithionite has long been used in different industrial and research applications.

$$2\ SO_3^{2-} + 2\ H_2O + 2\ e^- \rightleftharpoons S_2O_4^{2-} + 4\ OH^- \quad E° = -1.12\ V \qquad (1)$$

Previous reports on dehalogenation reactions by dithionite include the studies by Chung and Hu [19], who reported that the dehalogenation of α-haloketones carried out with $Na_2S_2O_4$ in either, aqueous or aqueous-DMF solutions, yields the corresponding parent ketones. Reductive dehalogenation experiments in which DDT was converted to DDD with 8% efficiency were reported by Miskus *et al.* [20]. These experiments demonstrated the remarkable ability of $Na_2S_2O_4$ to partially dehalogenate DDT.

Sodium dithionite has also been utilized to reduce enzymes and cofactors for their

subsequent use in the catalysis of reductive dehalogenation reactions in solution [21,22], and in toxicologic studies employing microsomal preparations [23-25]. For example, Wolf *et al.* [23] reported the formation of carbon monoxide in anaerobic incubations containing sodium dithionite, rat liver microsomes, and CCl_4. Carbon monoxide was identified as a reaction product in these microsomal preparations. Control experiments performed (a) in the absence of CCl_4 and (b) with acid-denatured microsomes, resulted in undetectable concentrations of CO. Subsequently, Ahr and coworkers [24] confirmed the production of CO (detected as ^{14}CO) in anaerobic reaction mixtures containing rat-liver microsomes, sodium dithionite and $^{14}CCl_4$. Noteworthy is the fact that small amounts of CO were produced after 1 h of reaction in control experiments consisting only of $Na_2S_2O_4$ (0.8 mg/mL) and $^{14}CCl_4$ [24]. In addition, small amounts of $^{14}CHCl_3$ were also found upon reaction of sodium dithionite with $^{14}CCl_4$.

Similar experiments carried out with systems consisting of rat liver microsomes incubated with CCl_4 and $Na_2S_2O_4$ were found to be very effective in producing trichloromethyl radical ($\cdot CCl_3$) [26]. The formation of $\cdot CCl_3$ radicals was attributed due to the one-electron reduction of carbon tetrachloride by cytochrome P450. The role of sodium dithionite in these reactions has been thought to be exclusively the reduction of cytochrome P450.

It is therefore interesting that, despite the extensive use of sodium dithionite in enzymatic and toxicologic reductive dehalogenation studies, studies aimed at determining the extent with which sodium dithionite participates in the reductive dehalogenation of carbon tetrachloride have not been undertaken.

Experimental Procedures

i). Reagents

Carbon tetrachloride (99.9 %) and chloroform (99.9 %) were purchased from Sigma (St. Louis, MO). Sodium dithionite (purity ~ 85%), sodium bisulfite and sodium thiosulfate were purchased from Aldrich (1001 West St. Paul Ave., Milwaukee, WI) and were stored in a desiccator under vacuum. All chemicals were used without further purification.

ii). Reductive Dehalogenation Experiments

All experiments were conducted in 70 mL threaded-mouth glass reaction vessels (diameter = 3.4 cm; length = 12 cm) equipped with a teflon stopcock in a sidearm. Gastight sealing of the system was achieved with a teflon "mininert" valve (Alltech, Deerfield, IL). The reductive dehalogenation of carbon tetrachloride was assayed in 65 mL buffered reaction mixtures consisting of saturated aqueous solutions of CCl_4 (0.8 mg/mL at 20 °C) and 1.1 mmol of $Na_2S_2O_4$. Phosphate buffers (0.10 M) were prepared with deionized water (18 MΩ·cm, Nanopure; Barnstead). Because impurities from commercial sodium dithionite (sodium sulfite, Na_2SO_3 and sodium thiosulfate, $Na_2S_2O_3$) are also reducing agents, control experiments containing 2.2 mmol of sodium bisulfite or 1.1 mmol of sodium thiosulfate instead of sodium dithionite, were carried out under the same experimental conditions.

Saturated aqueous solutions of carbon tetrachloride for reductive dehalogenation were prepared as follows: Prior to the addition of the halocarbon, buffer solutions (0.10

M phosphate pH = 7.5) were bubbled with argon for 5 min. The reaction vessels were then sealed with a "mininert" valve and 33 μL of carbon tetrachloride was injected through the valve's septum with the aid of a Hamilton microliter syringe. The resulting heterogeneous solution was then stirred with a magnetic bar until complete dissolution of the hydrocarbon was achieved. All experiments were carried out at room temperature. The initial concentration of CCl_4 was determined by gas chromatography-mass spectrometry (GC-MS) before addition of sodium dithionite (See Sampling and Methods of Analysis).

Solutions of the reducing agent ($Na_2S_2O_4$, $NaHSO_3$ or $Na_2S_2O_3$) were prepared as follows: A 10 mL glass vessel provided with a side arm and a stopcock was connected to a Schlenk line. A weighed amount of reducing agent was placed into the empty glass vessel while a gentle stream of argon was allowed to flow through the vessel in order to maintain an anaerobic atmosphere and a slight positive pressure of argon in the system. The container was immediately sealed with a rubber septum. One mL of 0.5M NaOH was injected through the septum with the aid of a Hamilton gas-tight syringe and the solution stirred until the solid had dissolved completely. Dehalogenation reactions were initiated by addition of a freshly prepared solution of reducing agent to the aqueous solution saturated with CCl_4.

iii). Experiments with sonication

Saturated mixtures of carbon tetrachloride in phosphate buffer (pH 7.5) were prepared as described above. Dissolution of the halocarbon, however, was accelerated by sonication of the mixture in a 50-60 Hz ultrasonic cleaner (Bransonic, Branson

Ultrasonics Corporation, Danbury, CT). Intervals consisting of 20 s of sonication followed by stirring with a magnetic bar were repeated in order to facilitate homogenization. Similar experiments were also carried out with reaction mixtures containing 1.1 mmol of sodium dithionite in addition to the halocarbon.

iv). Sampling and Methods of Analysis

The concentration of carbon tetrachloride in aqueous solution was monitored by GC-MS. Sampling of the liquid phase was typically carried out by direct immersion of a 100 μm polydimethylsiloxane SPME fiber (Solid Phase Microextraction fiber; Supelco, Bellefonte, PA) into the reaction mixture for 5 min. The SPME fiber was subsequently transferred into the injection port of a Hewlett Packard GC (HPG 1800A) equipped with an electron impact ionization-mass spectrometer detector. The detector was operated in the scanning mode between m/z of 10 to 425. The GC column was a 30 m x 0.25 mm i.d. HP-5 capillary column. Split injections were performed with the following GC conditions: helium carrier gas; column flow = 0.5 ml/min, split flow = 7.5 ml/min, split ratio = 15, injector temperature = 250 °C, column temperature = 50 °C for the initial 4 min, and then ramped to 200 °C at 20 °C/min, where it was held for 1 min.

Identification of the analytes was carried out by comparison of the mass spectra corresponding to the molecules in the eluting chromatographic peaks with those stored in the instrument's library. Standard solutions of carbon tetrachloride or chloroform were prepared by adding a weighed amount of the halocarbon to 66 mL of 0.1 M phosphate buffer, pH 7.5. Calibration curves for CCl_4 and $CHCl_3$ were constructed by plotting the abundances of the signals in the mass spectrum at m/z = 117 for CCl_4 (fragment CCl_3^+)

and at m/z = 83 for $CHCl_3$ (fragment $CHCl_2^+$) *vs* the corresponding standard halocarbon concentration expressed in ppm.

Volatile products were analyzed by direct sampling (1 μL) of the headspace followed by GC/MS analysis. The following chromatographic conditions were utilized: detector operated in the scanning mode between m/z of 10 to 200; column, 15 m x 0.32 mm i.d. Gaspro capillary column (Alltech); injector temperature = 100 °C; column temperature = 25 °C for the initial 3 min, and then ramped to 200 °C at 20 °C/min where it was held for 1 min.

v). Chloride Ion Determination

Chloride ion concentration was determined with the aid of a combination chloride-selective electrode (Orion, Boston, MA). The determination was carried out at the end of the dehalogenation reaction (5 h). Calibration of the chloride-selective electrode was accomplished with the aid of standards prepared by dilution of a commercial standard solution of sodium chloride (0.1000 M, Orion). Aliquots of 10 mL were analyzed and interferences caused by reducing agents remaining in the reaction mixture were eliminated by oxidation with a 0.1M $NaBrO_3$ solution. Readings were made 3 min after the addition of the oxidizing solution in order to avoid oxidation of the analyte. A control sample consisting of phosphate buffer pH 7.5, 1.1 mmol of $Na_2S_2O_4$ and 600 ppm of NaCl was run to monitor the validity of the analysis. Chloride was also determined by ion chromatography with the aid of Dionex-100 ion chromatograph.

vi). NMR spectroscopy

Reductive dehalogenation with sodium dithionite was carried out as described above, except that $^{13}CCl_4$ (99%, Cambridge Isotope Laboratories) was utilized in the reaction. The concentration of $^{13}CCl_4$, $^{13}CHCl_3$ and ^{13}CO was monitored by GC/MS as described in the Experimental Section. At the end of the reaction (5 h), a 500 μL aliquot of the resultant solution was mixed with D_2O to produce a solution containing 10% D_2O in order to obtain a ^{13}C-NMR spectrum. The spectrum was obtained with the aid of a Varian *Inova 400* spectrometer operating at a ^{13}C frequency of 100.6 MHz. The spectrum was acquired with a spectral width of 24.14 kHz, 2.0 s acquisition time, 96576 data points, a relaxation delay of 500 ms and WALTZ decoupling.

Results

i). Reductive Dehalogenation of CCl_4 carried out with $Na_2S_2O_4$

The disappearance of carbon tetrachloride upon addition of sodium dithionite to aqueous solutions of the halocarbon in phosphate buffer at pH 7.5 is depicted in Fig 1. Reduction of CCl_4 to concentrations below 2 ppm was achieved after 2.5 h of reaction at room temperature and undetectable amounts resulted after 4-5 h. Carbon dioxide and sulfur dioxide were detected in the headspace of reaction mixtures analyzed after acidification with 1 mL of 3M H_2SO_4. Control experiments indicated, however, that the observation of carbon dioxide is mainly due to HCO_3^- formed upon dissolution of CO_2 in the phosphate buffer and was not originated as a reaction product. Sulfur dioxide is formed from SO_3^{2-} and $S_2O_4^{2-}$ upon acidification of the solution.

It has been previously reported [27] that compounds commonly used in the preparation of buffer solutions may behave as radical scavengers. The possible effect of

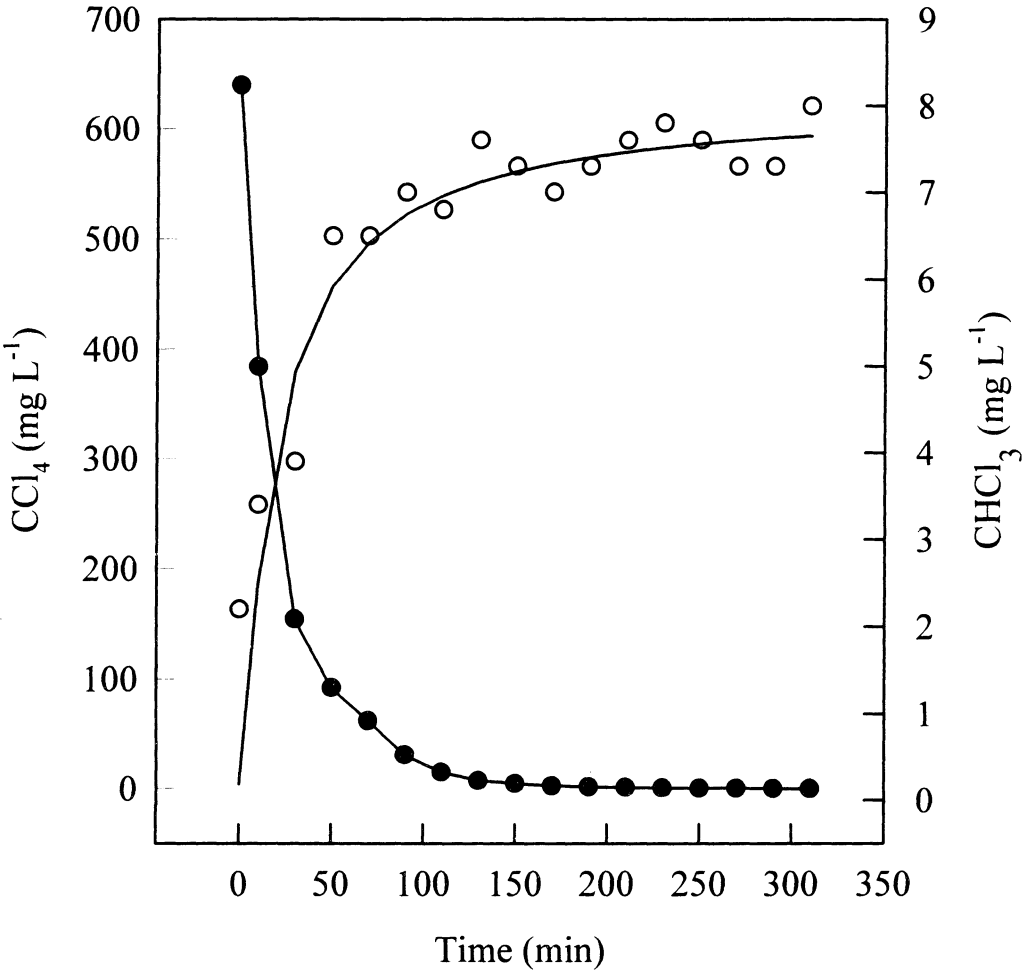

Figure 1. Time course of the reaction between CCl_4 and $Na_2S_2O_4$ as monitored by GC-MS. (●) CCl_4, (○) $CHCl_3$.

phosphate on the reductive dehalogenation of CCl_4 by sodium dithionite was tested by performing the reductive dehalogenation experiments in several different buffer solutions. Experiments performed in carbonate buffer, pH 8.1; borax buffer, pH 9.2 and in TRIS buffer, pH 7.5, displayed the same behavior observed in experiments performed with phosphate buffered solutions.

Headspace analysis of reaction mixtures in which $^{13}CCl_4$ was reductively dehalogenated with sodium dithionite clearly indicated that ^{13}CO is not formed during the reaction. This was evident from the absence of a peak at m/z = 29 in the mass spectrum obtained upon analysis of the volatiles, as described in experimental procedures. Analysis of the solution resulting from reacting $^{13}CCl_4$ and sodium dithionite by ^{13}C-NMR spectroscopy resulted in a spectrum displaying only one resonance with a chemical shift δ = 112 ppm (Fig 2). Since this NMR spectrum was obtained at the end of the reaction when $^{13}CCl_4$ was no longer detectable by GC-MS, it is possible to conclude that this resonance corresponds to the main carbon-containing reaction product. The ^{13}C-NMR spectrum was also acquired with the proton decoupler turned off in order to observe the multiplicity of the carbon signal due to ^{1}H-^{13}C coupling. The resulting spectrum was identical to that shown in Fig 2, thus indicating that the observed resonance corresponds to a quaternary carbon.

The concentration of chloride ion in reaction mixtures was found to be 28 % ± 2% of the expected concentration to be produced if all the chlorine from CCl_4 was converted to Cl^-. The small amounts of chloroform detected were found to have practically no effect on the chlorine balance estimated at the end of the experiments. It is important to mention that the same percentage of chloride was found with two different analytical techniques, namely, chloride ion-selective electrode and ion chromatography.

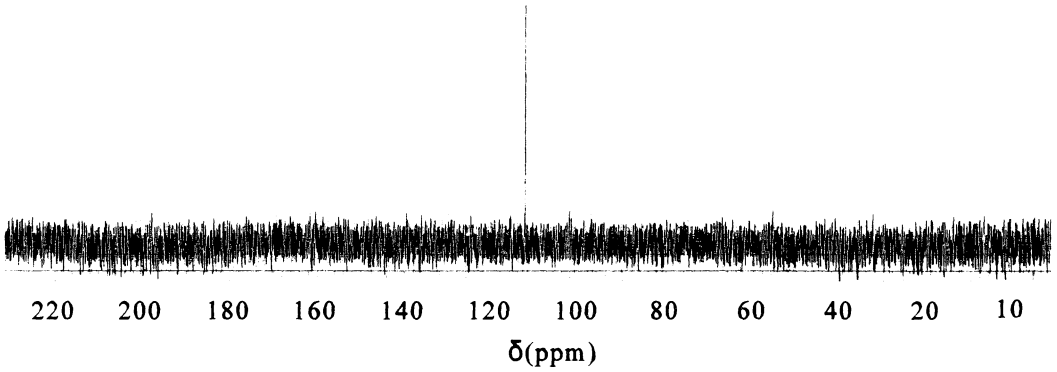

Figure 2. ^{13}C-NMR spectrum of the product of the reaction between $^{13}CCl_4$ and $Na_2S_2O_4$. The chemical shift was referenced to a solution consisting of 30% dioxane in D_2O through the peak at 66.67 ppm.

ii). Reductive Dehalogenation carried out with Na_2SO_3 and $Na_2S_2O_3$.

Sodium sulfite and sodium thiosulfate are two commonly used reducing agents. Furthermore, these compounds are found as impurities in commercial preparations of sodium dithionite [28]. When tested, sodium thiosulfate showed to be unreactive toward carbon tetrachloride in experiments performed at pH 7.5 in phosphate buffer solutions. The concentration of CCl_4 remained practically unchanged during the 4 hours of the experiment. When CCl_4 was treated with Na_2SO_3, on the other hand, traces of chloroform were formed at pH 7.5 and 9.5 but not at pH 5.5 (Fig 3). The formation of chloroform was found to be directly related to the pH of the solution, as higher apparent rates of formation occurred under more alkaline conditions.

Discussion

i). Radical anion $SO_2^{\cdot-}$ as the reactive species in reductive dehalogenation reactions carried out with $S_2O_4^{2-}$.

It is well known that the dithionite anion ($S_2O_4^{2-}$) disproportionates in aqueous solutions to the bisulfite (HSO_3^-) and thiosulfate ($S_2O_3^{2-}$) anions, as shown in Equation 2 [29]. Decomposition of $S_2O_4^{2-}$ by this reaction has been shown to occur rapidly in acidic media [30, 31]. On the other hand, sodium dithionite in alkaline solutions has been shown to be relatively more stable if maintained under anaerobic conditions [28, 32, 33].

$$2\ S_2O_4^{2-} + H_2O \rightleftharpoons 2\ HSO_3^- + S_2O_3^{2-} \qquad (2)$$

Moreover, in alkaline solutions, sodium dithionite is also known to be in equilibrium with

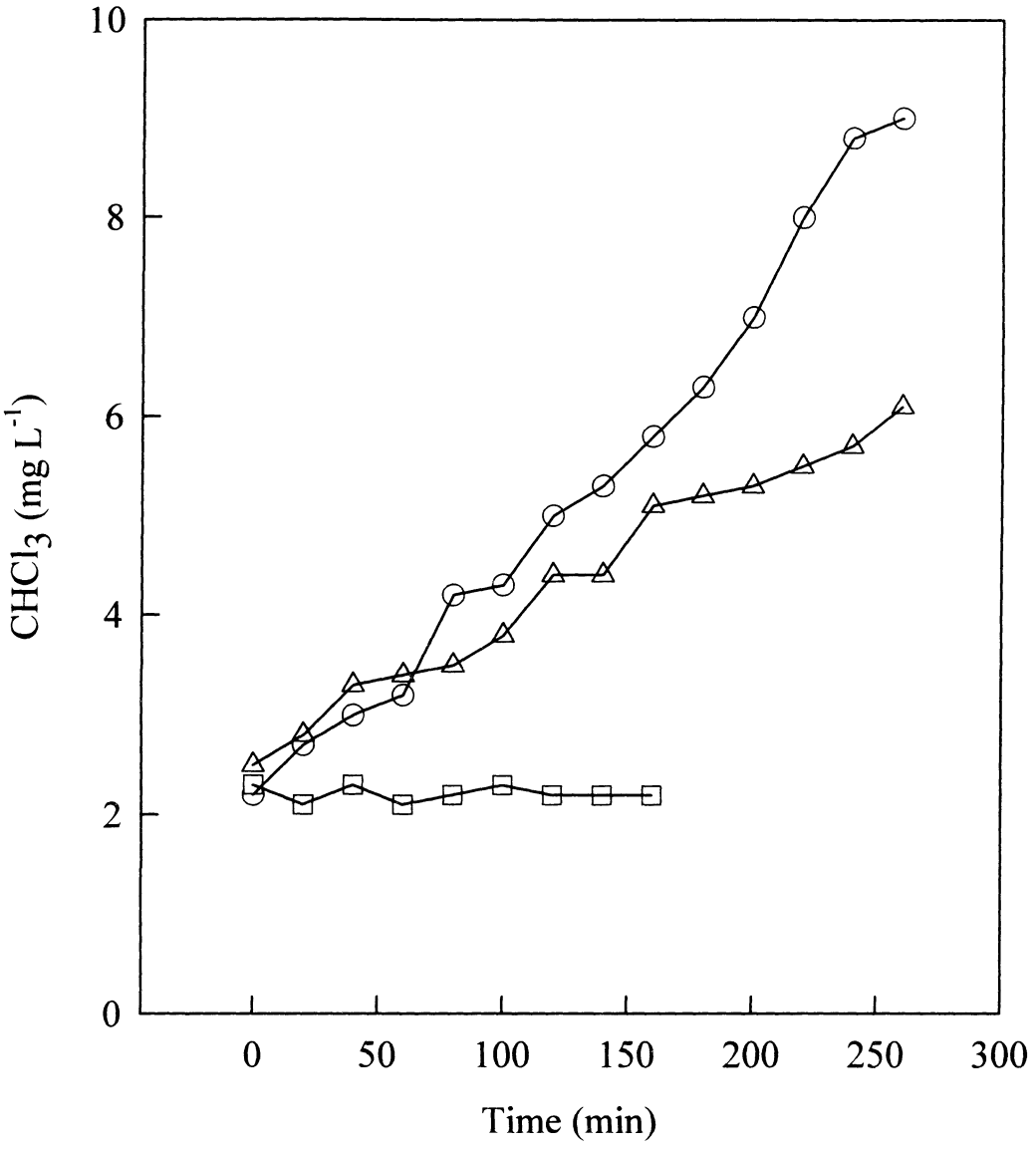

Figure 3. Formation of chloroform in reaction mixtures consisting of 2.2 mmol of Na_2SO_3 and 33 μL of CCl_4 in 65 mL phosphate buffer at pH 5.5 (square), pH 6.5 (triangle), and pH 7.5 (circle).

the sulfonyl anion radical ($SO_2\cdot^-$), as indicated by Equation 3. Evidence for this equilibrium comes from electron paramagnetic resonance (EPR) experiments [34, 35]. The equilibrium constant for the homolytic dissociation of $S_2O_4^{2-}$ to $SO_2\cdot^-$ has been determined by EPR spectroscopy under several conditions. The value more relevant to the studies reported here is $K = 8.5 \times 10^{-10}$, which was obtained in phosphate buffer at μ = 0.30 M and pH = 7.25 [34].

$$S_2O_4^{2-} \rightleftharpoons 2\ SO_2\cdot^- \qquad (3)$$

Mechanisms for the reduction of electron-transfer proteins and metal complexes by sodium dithionite have been proposed based on kinetic studies [34, 36-48]. In these studies, reductions carried out by dithionite have been proposed to occur via transfer of one electron from $SO_2\cdot^-$, or stepwise two-electron-transfer from $S_2O_4^{2-}$, to the electron acceptor, depending on the concentration of dithionite [36-43]. Other studies, however, have concluded that $SO_2\cdot^-$ is the only species participating in the reduction process regardless of the concentration of dithionite in solution [45-48]. The fact that $SO_2\cdot^-$ is a more reactive species than $S_2O_4^{2-}$ seems to argue in favor of the latter scenario. Electron-transfer reactions in which the radical anion $SO_2\cdot^-$ is the electron-donor occur with the concomitant formation of one neutral SO_2 molecule. In addition, hydration of sulfur dioxide has been reported to readily occur in aqueous solutions with the subsequent formation of bisulfite or sulfite, depending on the pH of the solution.

ii). Identification of the Major Reaction Product

Scheme I was constructed to aid in explaining the rationale followed for the identification of the major reaction product, and includes compounds typically produced

in reductive dehalogenation reactions of CCl_4 [5, 6, 8, 9, 16, 22, 24]. Because of the high reactivity of the sulfonyl anion radical, it seems likely that the two-electron reduction of carbon tetrachloride proceeds via the initial one-electron reduction of the halocarbon by the radical anion $SO_2\cdot^-$, with the subsequent formation of a trichloromethyl radical, $\cdot CCl_3$ (Reaction 1). Further one-electron reduction of $\cdot CCl_3$ by $SO_2\cdot^-$ can produce either a trichlorocarbanion (Reaction 3) or a dichlorocarbene (Reaction 5). Subsequent protonation of the trichlorocarbanion (Reaction 6) produces chloroform, thus explaining the traces of this compound observed experimentally. The dichlorocarbene, on the other hand, can undergo hydrolysis to produce formate or carbon monoxide (Reactions 8, 9). None of these compounds were found in the analysis of the reaction mixture. Instead, a water-soluble compound, which is non-extractable with the polydimethylsiloxane SPME fiber, was detected in the ^{13}C NMR spectrum obtained from a sample originally containing $^{13}CCl_4$. The ^{13}C chemical shift of this compound is 112 ppm, and a spectrum acquired with the ^1H decoupler turned off resulted in a singlet, thus indicating that the carbon atom giving rise to this resonance is quaternary. Furthermore, the value of this chemical shift is strongly indicative of electronegative substituents being attached to the quaternary carbon. The ^{13}C NMR spectrum obtained from reaction mixture containing $^{13}CCl_4$ and sodium dithionite in TRIS buffer was identical to that obtained when the experiment was performed in phosphates buffer. This result provides convincing evidence that the substituents in the main reaction product do not originate from the reaction buffer. In addition, the concentration of chloride ion found in the reaction mixtures indicates that a single chlorine atom was reductively eliminated as chloride ion from the CCl_4 molecule, thus suggesting that three chlorine atoms remain attached to the quaternary carbon. It should be pointed out that the formation of chlorinated inorganic

Scheme I

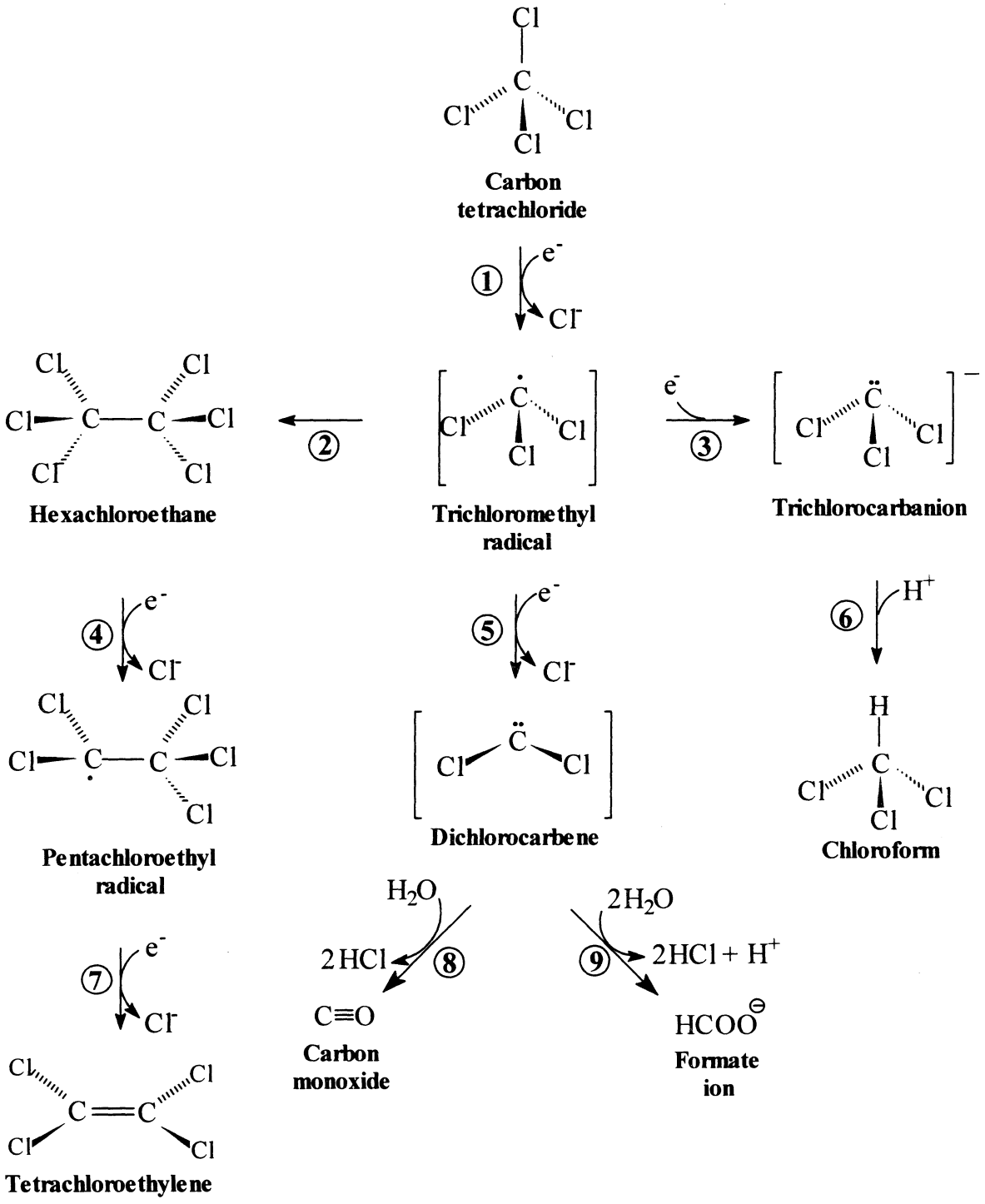
Carbon tetrachloride
Hexachloroethane
Trichloromethyl radical
Trichlorocarbanion
Pentachloroethyl radical
Dichlorocarbene
Chloroform
Tetrachloroethylene
Carbon monoxide
Formate ion
2HCl
2HCl + H+

species such as hypochlorite and chlorite was discarded on the basis of anion chromatography.

In summary, the above experimental evidence indicates that the major product of the reaction between sodium dithionite and carbon tetrachloride is a compound with characteristics that are consistent with a soluble ionic species composed of a single-carbon atom bound to four electronegative substituents. Moreover, since the substituents do not originate from the reaction buffer, and given that the chlorine balance calculated at the end of the reaction was nearly 25%, it is likely that three of the substituents are chlorine atoms. These characteristics taken together and considering the fact that the ^{13}C-NMR spectrum reported for $CCl_3SO_2^-$ shows a single peak at δ = 112 ppm [49], the product of the reaction between sodium dithionite and carbon tetrachloride is identified as the trichloromethane sulfinate anion ($CCl_3SO_2^-$). The formation of $CCl_3SO_2^-$ may arise from the combination of two radical species as shown in Equations (4) and (5) [51].

$$CCl_4 + SO_2\cdot^- \rightleftharpoons \cdot CCl_3 + SO_2 + Cl^- \quad (4)$$

$$\cdot CCl_3 + SO_2\cdot^- \rightleftharpoons CCl_3SO_2^- \quad (5)$$

Recently, an interesting initiator system for the polymerization of methyl methacrylate consisting of N-benzyl quinolinium chloride (BQ^+Cl^-)-$Na_2S_2O_4$-CCl_4 was reported [50]. The polymerization reaction in this system was proposed to occur via the formation of N-benzyl-1,4-dihydroquinoline-4-sulfinate (BQ-sulfinate) upon reaction between BQ^+Cl^- and $Na_2S_2O_4$. BQ-sulfinate is subsequently transferred to the organic phase where it reacts with CCl_4 to form BQ^+ and $Cl_3C\cdot$, which initiates the polymerization [50]. In light of the evidence presented in this report for the direct

reaction between CCl_4 and $Na_2S_2O_4$ to produce $Cl_3C\cdot$, this mechanism may be open to reinterpretation.

iii). Effects of Sonication

When the dissolution of CCl_4 was accelerated by sonicating the aqueous suspension of the halocarbon, analysis of the solution demonstrated the presence of traces of hexachloroethane and tetrachloroethylene. These compounds were produced regardless of the presence of sodium dithionite whenever sonication was employed to accelerate the dissolution of carbon tetrachloride. It is important to stress, however, that hexachloroethane and tetrachloroethylene were not observed when the reductive dehalogenation of CCl_4 was carried out by sodium dithionite in the absence of sonication. These observations clearly indicate that reaction 2 in Scheme I does not play an important role in the reductive dehalogenation of carbon tetrachloride under the experimental conditions reported here.

It is also important to point out that when experiments were performed with sonication in the presence of dithionite, the traces (< 10 ppm) of hexachloroethane formed upon sonication disappeared gradually with time until the compound was no longer detectable by GC-MS (Fig 4). By comparison, the concentration of tetrachloroethylene in solution increased gradually and it leveled off when the concentration of hexachloroethane was no longer detectable. This observation strongly suggested that dithionite reacts with hexachloroethane to produce tetrachloroethylene. This hypothesis was tested by reacting a supersaturated solution of hexachloroethane with sodium dithionite in aqueous phosphate solutions. This reaction may proceed via

the initial one-electron reductive elimination of chloride by $SO_2\cdot^-$ in order to produce a pentachloroethyl radical species (Reaction 4, Scheme I). Subsequent one-electron reductive dehalogenation of the radical species by $SO_2\cdot^-$ results in the formation of tetrachloroethylene (Reaction 7). Tetrachloroethylene, on the other hand, is not reductively dehalogenated by sodium dithionite because this unsaturated halocarbon accumulates as hexachloroethane is reduced (Fig 5).

iv). Sulfite (SO_3^{2-}) and thiosulfate ($S_2O_3^{2-}$) are poor reducing agents for the reductive dehalogenation of carbon tetrachloride.

It has been mentioned that the reducing agents SO_3^{2-} and $S_2O_3^{2-}$ occur as impurities in commercial preparations of sodium dithionite. Experiments aimed at probing the potential role of sulfite and thiosulfate as reducing agents in the reductive dehalogenation of CCl_4 produced the following results. Sodium thiosulfate did not react with carbon tetrachloride. By comparison, when CCl_4 was incubated with sodium sulfite, traces of chloroform were slowly produced at neutral and alkaline conditions, but not under acidic conditions (Fig 3). The concentration of CCl_4 remained practically constant throughout these experiments. The dependence on pH observed for the reaction of CCl_4 with sodium sulfite can be readily explained on the basis of the acid dissociation constant for the deprotonation of HSO_3^- to form SO_3^{2-} ($pK_a = 7.18$) and the reduction potentials reported for both anions (Equations 6 and 7) [29].

$$SO_4^{2-} + 4\,H^+ + 2\,e^- \rightleftharpoons H_2SO_3 + H_2O \qquad E^\circ = 0.17\ V \qquad (6)$$

$$SO_4^{2-} + H_2O + 2\,e^- \rightleftharpoons SO_3^{2-} + 2\,OH^- \qquad E^\circ = -0.93\ V \qquad (7)$$

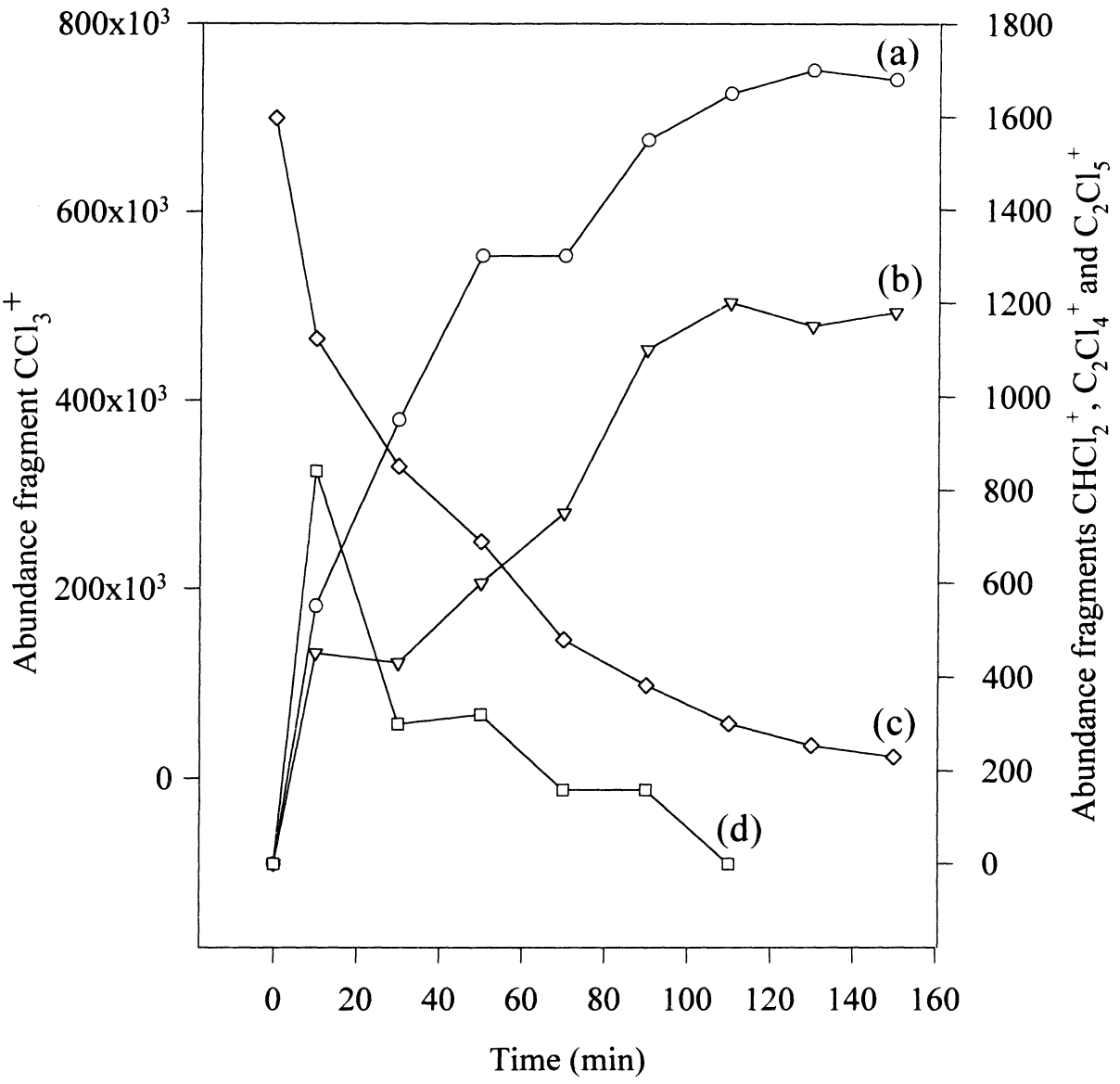

Figure 4. Formation of halogenated compounds upon sonicating reaction mixtures containing sodium dithionite and carbon tetrachloride. The values of the relative abundances corresponding to fragments of (a) chloroform ($CHCl_2^+$; m/z = 83), (b) tetrachloroethylene ($C_2Cl_4^+$; m/z = 166), and (d) hexachloroethane ($C_2Cl_5^+$; m/z = 201) are shown on the right-hand side ordinate axis. The relative abundance corresponding to the fragment arising from (c) carbon tetrachloride (m/z = 117) is shown on the left-hand side ordinate axis.

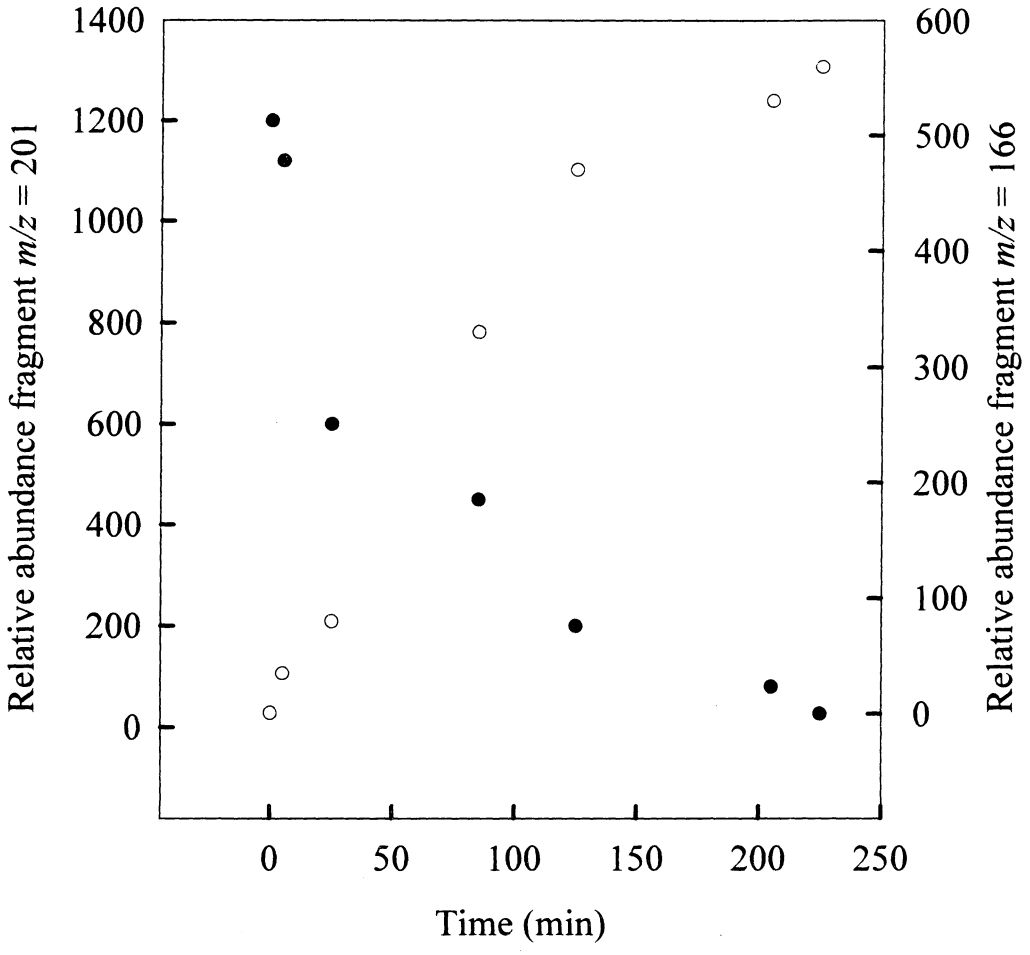

Figure 5. Formation of tetrachloroethylene (○) upon reaction of hexachloroethane (●) with sodium dithionite in 65 mL phosphate buffer pH 7.5.

Under acidic conditions (pH = 5.5), the principal species is the HSO_3^- anion, which is a poor reducing agent, whereas at pH of 7.5 and above, the predominant species is the stronger reducing agent, SO_3^{2-}. Finally, a comparison of the reducing strengths of the sulfite and dithionite anions (Equations 1 and 7) clearly indicates that the larger reducing strength of the dithionite anion accounts for its reductive dehalogenation properties.

Conclusions

The results of this study indicate that sodium dithionite reductively dehalogenates carbon tetrachloride to produce the trichloromethane sulfinate anion ($CCl_3SO_2^-$) as major product, and traces of chloroform. The reaction likely occurs via the direct attack of the sulfonyl radical anion to CCl_4, thus producing the trichloromethyl radical species and chloride ion. The formation of $CCl_3\cdot$ is followed by the combination of this radical species and $SO_2\cdot^-$ to render the major reaction product $CCl_3SO_2^-$. Moreover, hexachloroethane is partially dehalogenated by sodium dithionite producing tetrachloroethylene, although the latter is unaffected by $Na_2S_2O_4$. Because the majority of the species produced by the reaction between $Na_2S_2O_4$ and CCl_4 are ionic in nature, a method involving sodium dithionite can be envisioned for eliminating carbon tetrachloride from water by an ion-exchange process.

References

1. Testa, B. In *Biochemistry of Redox Reactions*; Academic Press: London, 1995; pp 407-410.
2. Castro, C. E., Wade, R. S. and Belser, N.O. (1985) *Biochemistry* 24, 204.
3. Gantzer, C. J. and Wackett, L. P. (1991) *Environ. Sci. Technol.* 25, 715.
4. Klecka, G. M. and Gonsior, S. J. (1984) *Chemosphere* 13, 391.
5. Assaf-Anid, N., Hayes, K. F. and Vogel, T.M. (1994) *Environ. Sci. Technol.* 28, 246.
6. Lewis, T. A., Morra, M. J. and Brown, P. D. (1996) *Environ. Sci. Technol.* 30, 292.
7. Kulikov, S. M., Plekhanov, V. P., Tsyganok, A. I., Schlimm, C. and Heitz, E. (1996) *Electrochim. Acta* 41, 527.
8. Kriegmann-King, M. R. and Reinhard, M. (1992) *Environ. Sci. Technol.* 26, 2198.
9. Kriegmann-King, M.R. and Reinhard, M. (1994) *Environ. Sci. Technol.* 28, 692.
10. Hooker, P. D. and Klabunde, K. J. (1994) *Environ. Sci. Technol.* 28, 1243.
11. Matheson, L. J. and Tratnyek, P. G. (1994) *Environ. Sci. Technol.* 28, 2045.
12. Muftikian, R., Fernando, Q. and Korte, N. (1995) *Wat. Res.* 29, 2434.
13. Boronina, T., Klabunde, K. J. and Sergeev, G. (1995) *Environ. Sci. Technol.* 29, 1511.
14. Helland, B. R., Alvarez, P. J. J. and Schnoor, J. (1995) *J. Hazardous Materials* 41, 205.
15. Warren, K. D., Arnold, R. G., Bishop, T. L., Lindholm, L. C. and Betterton, E. A. (1995) *J. Hazardous Materials* 41, 217.

16. Choi, W. and Hoffmann, M. R. (1995) *Environ. Sci. Technol.* 29, 1646.

17. Choi, W. and Hoffmann, M. R. (1996) *J. Phys. Chem.* 100, 2161.

18. Sun, L. and Bolton, J. R. (1996) *J. Phys. Chem.* 100, 4127.

19. Chung, S. and Hu, Q. (1982) *Synth. Commun.* 12, 261.

20. Miskus, R. P., Blair, D. P. and Casida, J. E. (1965) *J. Agr. Food. Chem.* 13, 481.

21. Li, S. and Wackett, L. P. (1993) *Biochemistry* 32, 9355.

22. Krone, U. E. and Thauer, R. K. (1989) *Biochemistry* 28, 4908.

23. Wolf, C. R., Mansuy, D., Nastainczyk, W., Deutschmann, G. and Ullrich, V. (1977) *Mol. Pharmacol.* 13, 698.

24. Ahr, H. J., King, L. J., Nastainczyk, W. and Ullrich, V. (1980) *Biochem. Pharmacol.* 29, 2855.

25. DeWeerd, K. A. and Suflita, J. M. (1990) *Appl. Environ. Microbiol.* 56, 2999.

26. Janzen, E. G., Stronks, H. J., Dubose, C. M., Poyer, J. L. and McCay, P. B. (1985) *Environ. Health Perspectives* 64, 151.

27. Singh, D. K., Sharma, R. N. and Srivastava, R. D. (1978) *AIChE J.* 24, 232.

28. McKenna, C. E., Gutheil, W. G. and Song, W. (1991) *Biochim. Biophys. Acta* 1075, 109.

29. Cotton, F. A. and Wilkinson, G. *Advanced Inorganic Chemistry*; John Wiley & Sons: New York, 1988; Chapter 13.

30. Lyons, D. and Nickless, G. In *Inorganic Sulfur Chemistry*; Nickless, G., Ed.; Elsevier: Netherlands, 1968; Chapter 14.

31. Camacho, F., Paez, M. P., Blázquez, G., Jimenez, M. C. and Fernández, M. (1995) *Chem. Eng. Sci.* 50, 1181.

32. Dixon, M. (1971) *Biochim. Biophys. Acta* 226, 241.

33. Burleigh, B. D., Foust, G. P. and Williams, C. H. (1969) *Anal. Biochem.* 27, 536.

34. Lambeth, D. O. and Palmer, G. (1973) *J. Biol. Chem.* 248, 6095.

35. Pemberton, R. S., Depew, M. C., Heitner, C. and Wan, J. K. S. (1995) *J. Wood Chem. Technol.* 15, 65.

36. Creutz, C. and Sutin, N. (1973) *Proc. Natl. Acad.. Sci. U.S.A.* 70, 1701.

37. Mayhew, S. G. (1978) *Eur. J. Biochem.* 85, 535.

38. Chien, J. C. W. and Dickinson, L. C. (1978) *J. Biol. Chem.* 253, 6965.

39. Halm, A. J. (1979) *Phys. Chem.* 83, 2553.

40. Pinnel, D. and Jordan, R. B. (1979) *Inorg. Chem.* 18, 3191.

41. Scaife, C. W. and Wilkins, R. G. (1980) *Inorg. Chem.* 19, 3244.

42. Mehrotra, R. N. and Wilkins, R. G. (1980) *Inorg. Chem.* 19, 2177.

43. Jones, G.D., Jones, M. G., Wilson, M. T., Brunori, M., Colosimo, A. and Sarti, P. (1983) *Biochem J.* 209, 175.

44. Hintz, M. J. and Peterson, J. A. (1980) *J. Biol. Chem.* 255, 7317.

45. Kazmi, S. A., Shorter, A. L. and McArdle, J. V. (1982) *J. Inorg. Biochem.* 17, 269.

46. Johnson, J. L., Tolley, A. M., Erickson, J. A. and Watt, G. D. (1996) *Biochemistry* 35, 11336.

47. Curtis, G. P. and Reinhard, M. (1994) *Environ. Sci. Technol.* 28, 2393.

48. Hua, I. and Hoffmann, M. R. (1996) *Environ. Sci. Technol.* 30, 864.

49. Allmann, R., Hanefeld, W., Krestel, M., and Spangenberg, B. (1987) *Angew. Chem. Intl. Eng.* 26, 1113.

50. Shimada, S., Obata, Y., Nakagawa, K., and Tabuchi, K. (1993) *Polymer J.* 25, 169.

51. Rodriguez, J. C. and Rivera, M. (1997) *Chem. Lett.* 1133.

VITA

JUAN CARLOS RODRIGUEZ-QUINTERO

Candidate for the Degree of

Doctor of Philosophy

Thesis: DESIGN AND CHARACTERIZATION OF AXIAL-LIGAND MUTANTS OF OUTER MITOCHONDRIAL CYTOCHROME b_5 WITH HIGHLY EFFICIENT HEME OXYGENATION ACTIVITY

Major Field: Chemistry

Biographical:

Personal Data: Born in Guadalupe Victoria, Baja California, Mexico, April 25, 1969, the son of Jose Rodriguez and Esther Quintero.

Education: Graduated from Colegio de Bachilleres, Guadalupe Victoria, Baja California Mexico in 1986; received Bachelor Science Degree in Chemistry from the Universidad Autonoma de Guadalajara, Guadalajara, Mexico, in December 1990; completed requirements for the Doctor of Philisophy Degree at Oklahoma State University in August, 1999.

Professional Experience: August, 1995 to present, graduate research and teaching assistant, Oklahoma State University.